U.PORTO
FEUP FACULDADE DE ENGENHARIA
UNIVERSIDADE DO PORTO

Optimal use of ultra-thin plies in composite structures

Carolina Furtado Pereira da Silva

Supervisor:
Prof. Dr. Pedro P. Camanho

A Thesis submitted for the degree of
Master of Science in Mechanical Engineering
to the Faculty of Engineering, University of Porto

Porto, June 2015

Acknowledgements

I take this opportunity to express my gratitude to Prof. Dr. Pedro P. Camanho for the opportunity to participate in this project, for taking the time to share his expertise and for all the support and encouragement without which this dissertation would not have been possible. I would also like to thank him for the support throughout my MSc course, for all the advice, opportunities and for always expecting the best of me.

To Albertino Arteiro, PhD candidate, for all his help and availability during this work, for taking the time to teach me the tricky aspects of experimental testing and for providing me the knowledge and tools needed to complete this work.

To Ing. Miguel Figueiredo and Ing. Rui Silva, for the help and patience during the experimental work and to Dr. José Xavier, from the Center of Research and Technology of Agro-Environmental and Biological Sciences, for making it possible to use digital image correlation during the experimental program.

I must also thank my work colleagues, Albertino Arteiro, Cláudia Cardoso, Giuseppe Catalanotti, Hélder Mata and Ricardo Pinto for the valuable breaks and for being an example of hard work.

I acknowledge Chomarat, Oxeon and Hexcel, for providing the material used in the experimental program carried out on this thesis.

A special thanks to all my friends, in particular, João Sottomayor, Pedro Cavaleiro and Rodrigo Furtado, for taking this journey alongside me, for all the support and advice in the most joyful and tiresome moments. To Rodrigo Tavares for accompanying me during this work and for all the tip sharing breaks that helped me overcome inevitable punctual frustrations. Finally, I would also like to thank my family for the unconditional support and for acknowledging my own little successes, which has always given me the motivation to complete the sometimes overwhelming challenges I have in hand and yet the will to keep on looking for more.

Abstract

Thin-ply composites are a new generation of composite materials made of plies with fibre areal weight lower than 100 g/m^2 and as low as 25 g/m^2. These materials offer a large set of advantages over conventional ones in terms of mechanical performance because they are able to suppress delamination and delay damage onset. However, this delay may lead to premature, brittle failure of notched structures loaded in tension, since it inhibits stress redistribution in the vicinity of the notches. This disadvantage, together with the higher manufacturing costs, have been the main obstacles to the market penetration and ways to overcome it have been sought out.

The concept of ply hybridization, which is the combination of both thin and thick plies of the same material system in the same laminate, is introduced in this work. The consequences of ply hybridization in quasi-isotropic laminates loaded in tension were analysed by comparing the experimental results obtained for the hybrid lay-ups with those of thin and thick lay-ups with equivalent in-plane properties. Unnotched tension, open-hole tension tests and open-hole fatigue tests were performed to analyse the unnotched and notched behaviour of the laminates under static and dynamic loadings and double edge crack tests were performed to obtain the R-curve of the laminates.

Combining thin plies with thicker plies of all fibre orientations resulted in a hybrid laminate with an intermediate notched and unnotched resistance. Combining thin an thicker 0^{o} plies in the same laminate, resulted in equivalent unnotched strength to the thin lay-up, enhanced notched strength compared to the thick lay-up and in intermediate fatigue resistance when compared with thin and thick laminates. This means that ply-hybridization, when designed to trigger specific damage mechanics can result in the global enhanced behaviour, thus overcoming the main disadvantage of thin-ply composites.

Analytical models, if physically-based, are able to deliver fast and accurate prediction and, therefore, gather all the conditions to be used as preliminary design and optimization tools. This is the case of the finite fracture mechanics model and, therefore, in this work, the predictions obtained with this model taking the R-curve into account were compared with the experimental test results. The predictions were in good agreement with the experimental results for the laminates and geometries tested and can, therefore, be used to predict failure for different geometries and to create design charts.

An algorithm based on classical lamination theory and the finite fracture me-

chanics model able to calculate a laminate's unnotched and notched strength having only the ply elastic, strength and fracture properties as input variables is proposed. Its accuracy could not yet be accessed, but, given its potential to yield good results when applied to thin-ply laminates, it can be the base of an optimization algorithm able to select an appropriate lay-up for a specific application.

Contents

List of Figures

List of Tables

Chapter 1

Introdution

1.1 Motivation and Objective

Since the early 1960s, the mechanical potential of fibrous composite materials has been exploited and investigated. These materials have been replacing metal alloys in several high-performance applications and they have been the material of choice when high mechanical performance and low weight are the main requirements.

Recently, a new generation of composite materials has been introduced in the market: the thin-ply composites. These materials are made of plies as thin as 0.02 mm, almost six times thinner that those used in conventional composites. Thin-ply composites offer a large set of advantages over conventional ones both in terms of design space and mechanical performance and offer the possibility of producing lighter structures, which has always been one of the main concerns of the aeronautical industry. Moreover, even tough the production technique of thin-ply prepregs is different than that of conventional prepregs, the fabrication procedure, i.e, stacking and curing procedures, does not involve major modifications. This means that the established manufacturing processes of conventional laminates can still be used.

The enhanced mechanical performance of thin-ply composites is mainly due to the delayed onset of damage exhibited by this materials. In general, thin-ply composites exhibit an enhanced unnotched strength, compressive notched strength and better resistance to fatigue. However, this delay of the damage onset has a negative impact in notched structures loaded in tension since it inhibits local stress distribution at the vicinity of the notch leading to premature brittle failure of the structures. This disadvantage, together with the higher manufacturing costs, have been the main obstacles to the market penetration and ways to overcome it have been sought out.

The objective of this work is to study how thin-ply laminates can be used to their full potential in composites structures. To achieve this goal, two lines of research will be explored.

The first is ply hybridization which is the combination of both thin and thick layers of the same material in the a composite structure. This will result in hybrid structures that, if well designed, will combine the advantages of thick and thin-ply composites. The detailed study of the mechanical response of these kind of composite laminates, will enable the understanding of the consequences of ply hybridization. Firstly, a series of mechanical tests were performed to a thin-, a thick- and a hybrid-structure of the same material system. Since the major disadvantage of thin-ply composites is its comparatively lower notched tensile strength, priority was given to study the tensile behaviour of hybrid structures. The mechanical tests performed were unnotched tension, open-hole tension and open-hole fatigue and specimens with different sizes were tested so that the size effect could be accounted for. Since the effective use of composite materials in structural applications relies on the ability to predict their behaviour accurately, an analysis based on finite fracture mechanics was made and the experimental and computational results were compared.

The second research line is based on the development of an algorithm that could possibly be the base of an optimization algorithm capable of selecting an optimal lay-up of thin-ply laminates having open-hole tension and plain strength as design drivers. Open-hole strength can be predicted using Finite Fracture Mechanics and, since, the onset of damage is delayed to the point just before failure, plain strength can be predicted using Classical Lamination Theory. Combining these models the notched strength for a given material and lay-up should be able to be predicted having only the ply elastic, strength and fracture properties as input variables.

1.2 Thesis outline

In chapter 2, a literature review on the mechanical behaviour of thin-ply composites is given based on experimental work performed by Sihn et al [35], Amacher et al. [4] and Arteiro et al. [6].

In chapter 3, a detailed description of the of the material selection, manufacturing, the test plan and test procedures followed is given. In chapter 4 the experimental test results of unnotched tension tests, open-hole tension, open-hole fatigue and double edge crack tests for the NCF T700GC/M21 and STF T700SC/M21 are presented and discussed.

In chapter 5, an analysis based on Finite Fracture Mechanics model is made the results are compared with the experimental open-hole tension test results available for NCF T700GC/M21 and STF T700SC/M21 lay-ups.

In chapter 6, a review on the mechanical performance of composite laminates and analytical models used to predict the unnotched strength, *in-situ* strengths and fracture toughness of composite laminates is given.

In chapter 7, an analytical methodology to calculate the notched strength for a given material and lay-up having only the ply elastic, strength and fracture properties as input variables is proposed.

Chapter 8 presents the main conclusions of this study.

Chapter 2

Thin-ply composites - Literature review

Conventional composite laminates are made of plies with fibre areal weight (FAW) higher than 100 g/m^2. However, a new generation of composite materials has been introduced in the market: thin-ply composites. This type of material is made out of plies with FAW of around 50 or even 25 g/m^2, which corresponds to a ply thickness as low as 0.02 mm. The plies are produced by a method known as spread tow thin-ply technology in which large fibre tows are continuously spread to a flat thinner tape. Since the plies are thinner, the resin flows better between the fibres and, since the bundles are smaller, the fibres are better dispersed throughout the laminate, which results in a more homogeneous material than conventional laminates. A schematic representation of the thin- and thick-ply composite morphology is presented in figure 2.1.

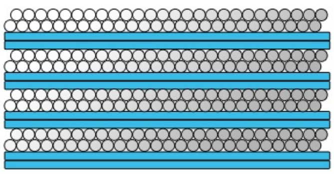

(a)

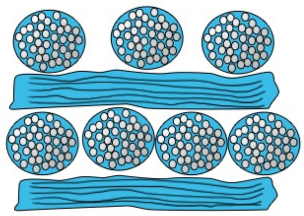

(b)

Figure 2.1: Thin-ply 2.1a and thick-ply 2.1b morphology

The use of thin-plies offers a large set of advantages over conventional composite materials. Firstly, thinner plies offer some advantages in terms of design. On one hand, design constrains such as quasi-isotropy or symmetry can be met with less total laminate thickness and, therefore, weight can be saved. On the other hand, since more plies can be stacked together for the same laminate thickness, the design freedom is improved, and, for example, smaller mismatch angles (angles between adjacent plies) can be used, which is shown to improve the interfacial fracture resistance [5]. This means that, for example, in a 0.9 mm thick laminate, instead of the standard three 0.3 mm thick plies stacking sequence [0/90/0], a more complex stacking sequence of 0.03 mm thin plies as $[0/45/90/\text{-}45/0]_{3s}$ sequence could be used. [4]

Secondly, in terms of manufacturing, thinner plies allow the production of both non-crimp fabrics and weaved fabrics with low crimp angles that offer mechanical performance equivalent to that of unidirectional reinforcement but which are much easier to handle and lay-up.

Thirdly, the use of thinner plies has been proven to have a positive impact on the mechanical performance of the components due to improved design space, better homogenization and to positive size effects that the use of thinner plies represents. On one hand, by reducing of ply thickness in a multidirectional laminate, the *in-situ* effect, which is characterized by an increase of the strength of a ply that is constrained between other plies with different orientations, gains additional importance (fig. 2.2) [13]. This means that, for the same material system and for two different lay-ups with the same in-plane elastic properties, their ultimate strengths will be different because the strength of the plies within a laminate will be higher the thinner the plies used. On the other hand, the use of thin plies scattered throughout the laminate has been proven to reduce stress concentrations at the free-edges, thus avoiding subcritical damage such as transverse cracking and delaying the onset of free-edge delamination as shown in figure 2.3 [4] [35] [6].

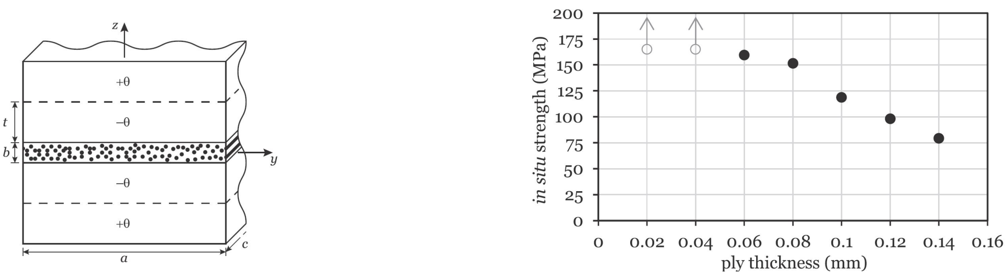

(a) *(b)*

Figure 2.2: The in-situ effect: transverse strength of a 90º ply constrained between two 0º plies as function of its thickness [5]

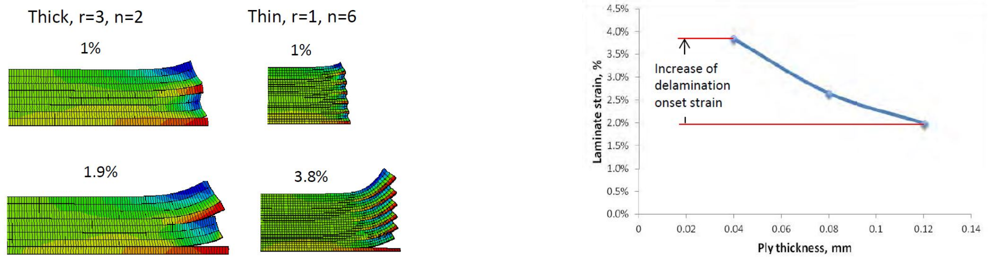

(a) *(b)*

Figure 2.3: Simulation 2.3a and onset 2.3b of free-edge delamination in a thick- and thin-ply composite $[45_r/\text{-}45_r/0_r/90_r]_{nS}$

Various experimental studies were carried out as an attempt to:

- **Compare and quantify the performance of conventional (thick) and thin-ply composite laminates**

  - Sihn et al. [35] performed unnotched tension and open-hole tension tests in both static and fatigue loadings as an attempt to characterize the performance of spread-tow, thin-ply laminates. Two quasi-isotropic CFRP laminates with the same in-plane properties were tested: THIN laminate with ply thickness of 0.04 mm and THICK laminate with ply thickness of 0.20 mm.

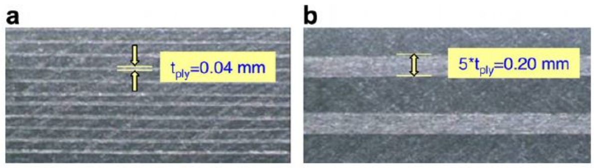

Figure 2.4: THIN (a) and THICK (b) laminates [35]

  - Amacher et al. [4] performed unnotched tension tests, open-hole tensile tests, open-hole fatigue tests, open-hole compression tests and bearing tests to in quasi-isotropic thick-, intermediate- and thin-ply laminates. The different types of laminate were produced with unidirectional prepreg tapes with different fibre areal weights: 30 g/m^2 (thin), 100 g/m^2 (intermediate) 300 g/m^2 (thick)

- **Evaluate the mechanical response of non-crimp fabrics** e.g. Arteiro et al. [6] conducted a series of mechanical tests in two different thin-ply laminates of carbon NCF^{TM} T700/AR-2527 epoxy system prepreg material from Aldida in order to understand the failure mechanisms of thin-ply composites. The lay-ups of both laminates are presented in table 2.1. Lay-up 1 is asymmetric and the mismatch angles between the plies are 45°. Lay-up 2 is symmetric by bi-angle layer but asymmetric by ply: in one half of the laminate, the mismatch angles between two different bi-angle layer is 90° and in the other half it is 0° which means that, in this half, there is ply blocking. This investigation allowed a better insight of why the mechanical performance of thin-ply laminates revealed beneficial.

Table 2.1: Lay-ups of the laminates tested in the experimental program performed in [6]

	Lay-up	Ply thickness [mm]	Nr. of plies	Total thickness [mm]
L 1	$[(0/\text{-}45) \ / \ (90/45)]_{6T}$	0.08	24	2.0
L 2	$[(0/\text{-}45)/(45/0)/(90/45)/(\text{-}45/90)]_S$	0.08	16	1.3

By careful analysis of the numerical and visual results of the tests performed in these studies the benefits of using thin-plies can be better understood, and, therefore, the conclusions drawn in the studies will be presented hereafter.

2.1 Unnotched tension and compression

In general, quasi-isotropic thin-ply laminates show enhanced ultimate plain strength. Unlike thick-ply composites, little severe damage such as delamination or transverse cracking before failure was detected in thin-ply composites. In fact, as reported in [6] and [4], the response of thin-ply laminates loaded in tension remains linear up to failure which indicates that the onset of damage is delayed until the point just before failure, as can be observed in Figure 2.5, which summarizes the results obtained by Amacher et at. [4].

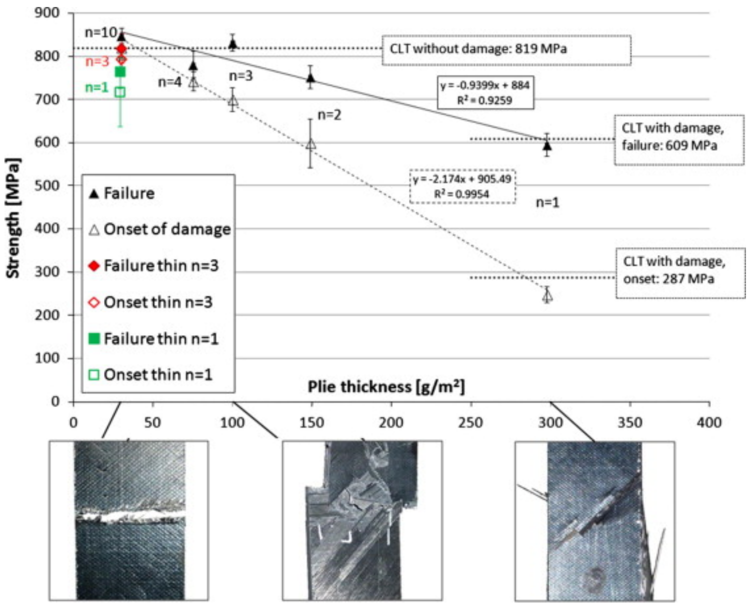

Figure 2.5: Ultimate strength and onset of damage with respect to ply thickness in unnotched quasi-isotropic tests, and failure modes observed for thick, intermediate and thin-ply laminates [4]

In [6], Arteiro at al. compare the behaviour of two different thin-ply lay-ups (table 2.1). The failure stress of both tensile and compressive tests are presented in table 2.2 and figure 2.6 shows the typical fracture surface of lay-up 1 and 2 specimens loaded in tension. It can be concluded that lay-up 1 has a higher strength than lay-up 2 and while lay-up 1 the fracture was catastrophic with practically no visible delamination, lay-up 2 shows pull-out failure mode with splitting and delamination. The different behaviour is explained by the stacking order: lay-up 2 has mismatch angles of 90º between bi-angle layers which means that the interlaminar stresses are higher that in lay-up 1 and, moreover, there is ply-blocking that results in higher stress concentration in adjacent plies and lower *in-situ* strength. Nonetheless, as in [4] both lay-ups exhibited linear response up to failure which means that severe damage before failure is delayed up to the point just before failure.

Since there is less damage near the free-edges, delamination is delayed and so thin-ply composites exhibit an improved fatigue behaviour (Sihn et al. [35] report that after 50000 fatigue cycles, while the strength of thick-ply composites was reduced by 30 %, thin-ply composites maintained their strength).

Table 2.2: Unnotched tension and compression strengths for lay-ups 1 and 2 [6]

Lay-up	X_T^L MPa	STVD	X_C^L MPa	STVD
L 1	800.2	19.0	540.2	11.7
L 2	710.3	13.4	464.5	14.8

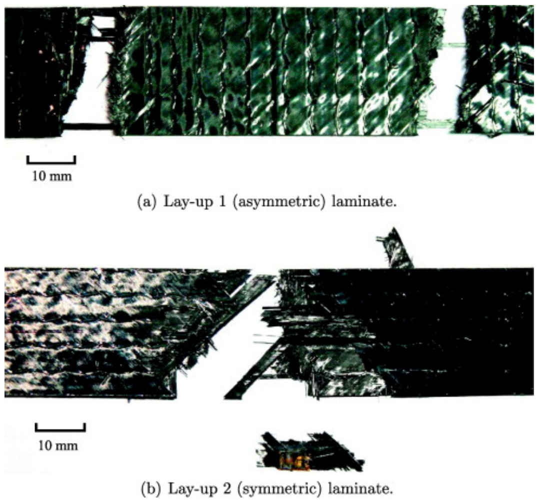

Figure 2.6: Representative unnotched tension specimens after testing [6]

2.2 Open-hole tension

Open-hole tensile tests were also performed and, for this type of geometry and loading (figure 2.7), little damage before failure near the edge of the hole prior to failure is also reported in [35], which means that subcritical damage is suppressed. The experimental results obtained by Amacher et al. [4] show that, while for thick-ply composites the onset of damage in open-hole tensile tests occurred for stresses 50% lower than its failure stress, for thin-ply composites it occurs for stresses near the ultimate stress which confirms that the composite fails without significant damage growth. However, unlike for unnotched laminates, the absence of damage prior to failure in thin-ply composites inhibits the redistribution of local stresses near the hole and leads to premature brittle failure of the laminate. The results for open-hole tensile tests obtained by Amacher et al. [4] are presented in table 2.3.

In general, under fatigue loading, thin-ply composites show enhanced mechanical behaviour since, as subcritical damage is suppressed, damage propagation is slower and less pronounced [4] [35]. Fatigue open-hole tensile tests performed in Amacher et al. [4] and summarized in table 2.3 showed that, while the thick-ply composites tested exhibited progressive propagation of transverse cracks in the 90° plies and shear cracks in the ±45 plies and of delamination, which lead to failure

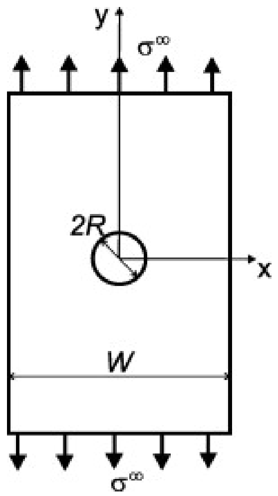

Figure 2.7: Notched laminate under tensile loading [17]

in a reduced number of cycles, the thin-ply composites tested could handle up to 1 million cycles without any degradation of its mechanical properties. This behaviour is clearly reported by Sihn et al. [35] and is shown in figure 2.8 where the severity of damage of quasi isotropic THIN and THICK lay-ups after 100k fatigue cycles at 70% of the laminate's notched strength are shown.

Even tough, in "absolute values" thin-ply composites tested show a clear enhanced performance, it has to be taken into account that the maximum stresses for which its life can be considered nearly infinite (<320 MPa) were below the reported onset of damage stresses (352 MPa), while for the thick-ply composites tested, they were above this value (271 MPa vs 255 MPa). It is clear that the propagation of damage that already exists will be faster than of non-existent damage and this can explain the results. Nonetheless, the two types of materials tested have the same mechanical in-plane properties and were subjected to the same loading conditions, so the enhanced fatigue life of thin-ply composites is valid, even though it might only be a consequence of delayed onset of damage.

Table 2.3: Open-hole onset of damage and failure stresses and open-hole fatigue number of cycles up to failure for different maximum applied stresses [4]

	Static		Fatigue	
	Onset of damage	Final failure	Max. Stress	Number of cycles
Thick	255 MPa	545 MPa	271 MPa	180 k
			316 MPa	20 k
			361 MPa	10 k
Thin	352 MPa	380 MPa	268 MPa	>1 million
			315 MPa	>1 million
			342 MPa	8 k

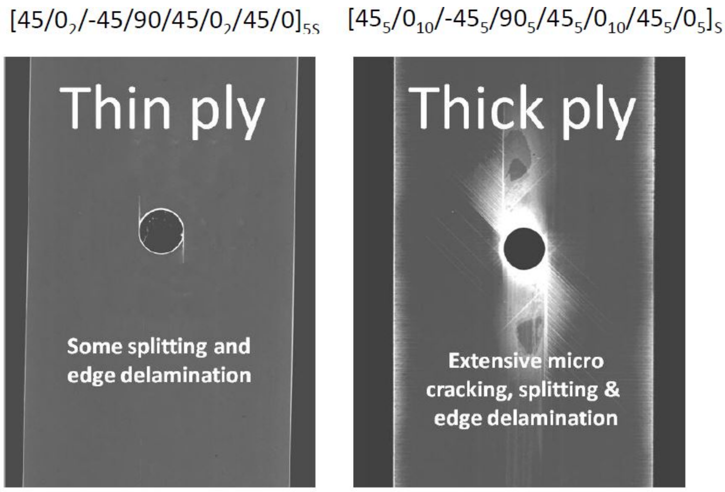

Figure 2.8: Damage in thin and thick specimens after OHT fatigue loading [35]

2.3 Summary

Thin-ply composites offer a large set of advantages over conventional ones both in terms of design space and mechanical performance and offer the possibility of producing lighter structures, which has always been one of the main concerns of the aeronautical industry. The use of thin-plies suppresses the appearance of damage in the free-edges and delays transverse cracking and delamination onset, thus improving the overall behaviour of the composite laminate. In general, thin-ply composites exhibit:

- enhanced unnotched strength
- lower notched tensile strength since there is almost no damage prior to failure and, therefore, redistribution of local stresses is inhibited which leads to premature brittle failure of the laminate
- enhanced fatigue resistance since the onset of damage is delayed and, therefore, damage propagation is slower and less pronounced.

Chapter 3

Experimental Work

The first objective of this work is to evaluate the consequences of ply hybridisation which is the combination of both thin and thick layers of the same material in a composite structure. To do so, experimental tests were performed using thin-, thick- and hybrid- configurations for of the same material system. Some aspects of the material selection, manufacturing, the test plan and test procedures followed during this work will be explained hereafter.

3.1 Material and lay-up selection

Two different carbon-epoxy system prepregs were used in this experimental study:

- NCF T700GC/M21 : Chomarat's C-Ply T700GC non-crimp-fabric (NCF) bi-angle layers with FAW of 75 g/m^2 per layer impregnated with M21 epoxy. C-Ply are made up of two unidirectional layers with different orientations that are sewn together which results in bi-angle layers that have equivalent mechanical performance and are easier to handle than unidirectional prepregs. In this work [0^o/-45^o] and [0^o/+45^o] C-ply were used. The ply nominal thickness is 0.075 mm per ply and, therefore, 0.150 mm per bi-angle layer.

- STF T700SC/M21 : Oxeon's T700SC spread tow fabric (STF) impregnated with M21 epoxy from Hexcel. This fabric is produced by interlacing Spread Tow tapes which results in a nearly crimp-less cross plied fabric with the mechanical properties of a cross plied UD and the handling of a fabric prepreg. Two fabrics were used: 160 g/m^2 with a ply nominal thickness of 0.160 mm and 240 g/m^2 with a ply nominal thickness of 0.240 mm per fabric layer.

The mechanical properties of T700GC/M21 prepreg system are presented in tables 3.1 and 3.2 where, E_1 and E_2 are the longitudinal and transversal Young's modulus, respectively, G_{12} is the shear modulus, ν_{12} is the major Poisson coefficient, X_T and X_C are longitudinal tensile and compressive strengths, respectively, Y_T^{UD} and Y_C^{UD} are transversal tensile and compressive strengths, respectively, S_L is the in-plane shear strength and G_{IC} and G_{IIC} are the mode I and mode II interlaminar fracture toughnesses, respectively. Note that, even though the GC and SC fibre sizings are different, they should not influence the ply's elastic properties. The same might not be true for the fracture as strength properties and, therefore, the properties presented in table 3.1 are only valid for NCF T700GC/M21.

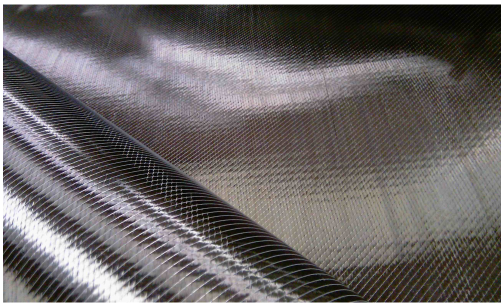

(a)

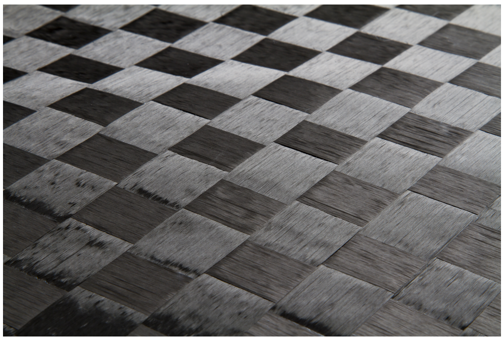

(b)

Figure 3.1: C-Ply from Chomarat 3.1a and Spread Tow Fabric from Oxeon 2.1b morphology

Table 3.1: T700GC/M21 ply elastic properties [ONERA]

E_{11} (GPa)	E_{22} (GPa)	ν_{12}	G_{12} (GPa)
130.0	8.300	0.32	4.500

Table 3.2: T700GC/M21 ply strength and fracture properties [ONERA]

X_T (MPa)	X_C (MPa)	Y_T^{UD} (MPa)	Y_C^{UD} (MPa)	S_L^{UD} (MPa)	S_T^{UD} (MPa)	G_{IC} (N/mm)	G_{IIC} (N/mm)
2000	-1300	76.0	-256	81.0	51.0	0.350	1.500

Three lay-ups for each type of material system were selected: a thin, a thick an a hybrid lay-up. Their selection followed certain design constrains:

- The lay-ups must be symmetry
- Total laminate thickness of between 1.6 mm - 1.9 mm.
- For the same prepreg system, the thickness of the three lay-ups should as similar as possible so that the effect of the thickness of the specimens is not relevant and does not invalidate the comparison between thin, thick and hybrid lay-ups.
- For the same prepreg system, the in-plane elastic properties should be equal.

While for NCF T700GC/M21 , using prepreg with the same areal weight, it is possible to create a thicker ply by overlaying two plies with the same orientation, this is not possible for the STF T700SC/M21 since a layer is composed of an interlaced Spread Tow Tape with two different orientations. In this case, thin plies were made from prepreg with and areal weight of 160 g/m^2 and thick plies were made from prepreg with areal weight of 240 g/m^2.

Using NCF T700GC/M21 :

- the thin layup (hereafter referred to as NCF-THIN) was selected so that there was no ply blocking, i.e. so that all plies have the minimum possible thickness (0.075 mm).
- the thick layup (hereafter referred to as NCF-THICK) was selected so that there was, when possible, ply blocking, i.e. so that all plies have the maximum possible thickness (0.15 mm).
- the hybrid lay-up (hereafter referred to as NCF-HYBRID) was selected so that the thickness of the 90° and 45° plies were minimized (0.075 mm) and the thickness of the 0° plies were maximized (0.15 mm). Assuming that, when loaded in tension, 0° plies of notched structures exhibit split cracking near the notches, the thicker 0° plies were placed close to the center of the laminate in an attempt to confine this type of cracking to the vicinity of the notch and prevent its propagation along the whole specimen.

Using STF T700SC/M21 :

- in the thin layup (hereafter referred to as STF-THIN) all the plies are made from 160 g/m^2 prepreg.
- in the thick layup (hereafter referred to as STF-THICK) all the plies are made from 240 g/m^2 prepreg.
- Using Spread tow fabric, it is not possible to use thicker 0° plies only, since 0° and 90° plies are interlaced and using prepregs with FAW of 240 g/m^2 for thicker plies and with FAW 160 g/m^2 for thinner plies, it is not possible to maintain the quasi-isotropy restriction and maximize the thickness of the 0° (and consequently of the 90°) plies only as in the NCF-HYBRID lay-up, so, for hybrid lay-up (hereafter referred to as STF-HYBRID) all the plies are made from 160 g/m^2 prepreg except two (0°/90°) and two (-45°/45°) plies.

The six layups are presented in table 3.3.

Table 3.3: Selected layups (160 g/m^2 STF; 240 g/m^2 STF)

Laminate ID	Lay-up	Nr. plies	t (mm)
NCF-THIN	$[(90/+45)/(0/-45)]_{3s}$	24	1.8
NCF-THICK	$[(90/+45)/(+45/0)/(0/-45)/(-45/90)/(90/+45)/(0/-45)]_s$	24	1.8
NCF-HYBRID	$[(90/+45)/(0/-45)(90/+45)/(90/-45)/(+45/0)/(0/-45)]_s$	24	1.8
STF-THIN	$[(0/90)/(+45/-45)]_{3s}$	48	1.92
STF-THICK	$[(0/90)/(+45/-45)]_{2s}$	32	1.92
STF-HYBRID	$[((0/90)/(+45/-45))_2/(0/90)/(+45/-45)]_s$	40	2.24

3.2 Manufacturing

Four plates of each material system and lay-up were made, which results in a total of 24 plates, were manufactured as follows:

1. The prepreg was cut in squared plies of 305 mm x 305 mm as shown in figure 3.2
2. The plies were layed-up into plates as shown in figures 3.3, 3.4 and 3.5
3. The plates were cured in an autoclave in groups of three following, when possible the recommendations in HexPly M21 datasheet:
   - Apply full vacuum (1 bar)
   - Apply 4 bar gauge autoclave pressure. The recommended pressure is 7 bar however, the autoclave used did not allow pressure over 4 bar.
   - Reduce vaccum to safety value of -0.2 bar when the autoclave pressure reaches 1 bar gauge.
   - Set heat-up rate from room temperature to 180°C ± 5°C to achieve an actual component heat-up rate between 1-2°C/minute.
   - Hold at 180°C ± 5°C for 120 minutes ± 5 minutes
   - Cool component at an actual cooldown rate of 2-5°C/minute
   - Vent autoclave pressure when the component reaches 60°C or below.

The plates were, afterwards, cut to the specimens' nominal dimensions using a diamond-coated disk as shown in fig. 3.7.

Figure 3.2: Manufacturing: cutting the prepreg

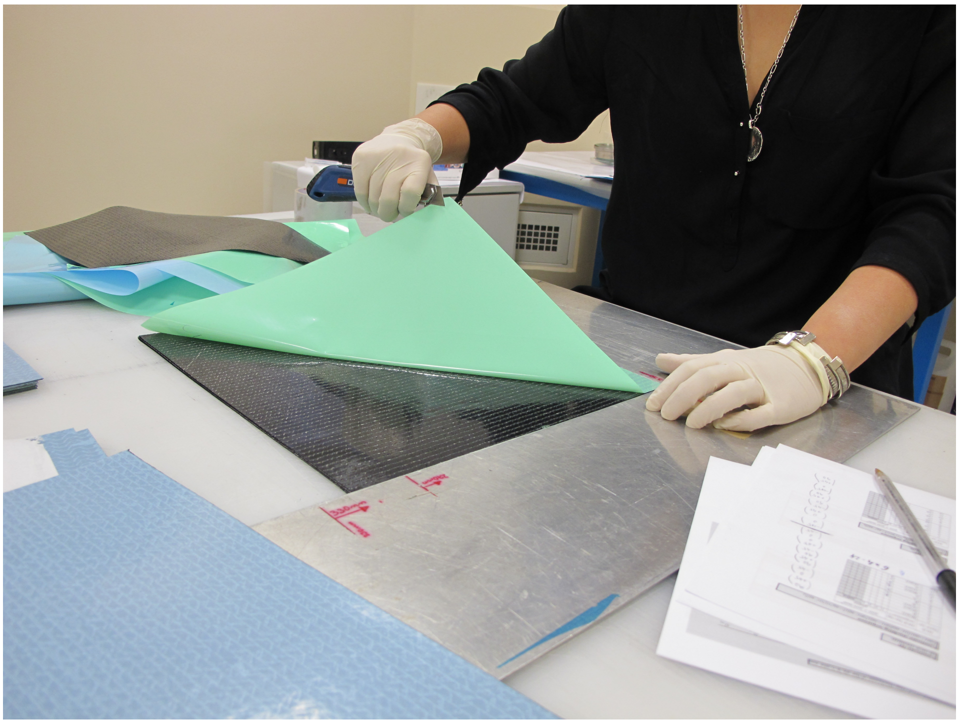

Figure 3.3: Manufacturing: removing the protective layer of the prepreg

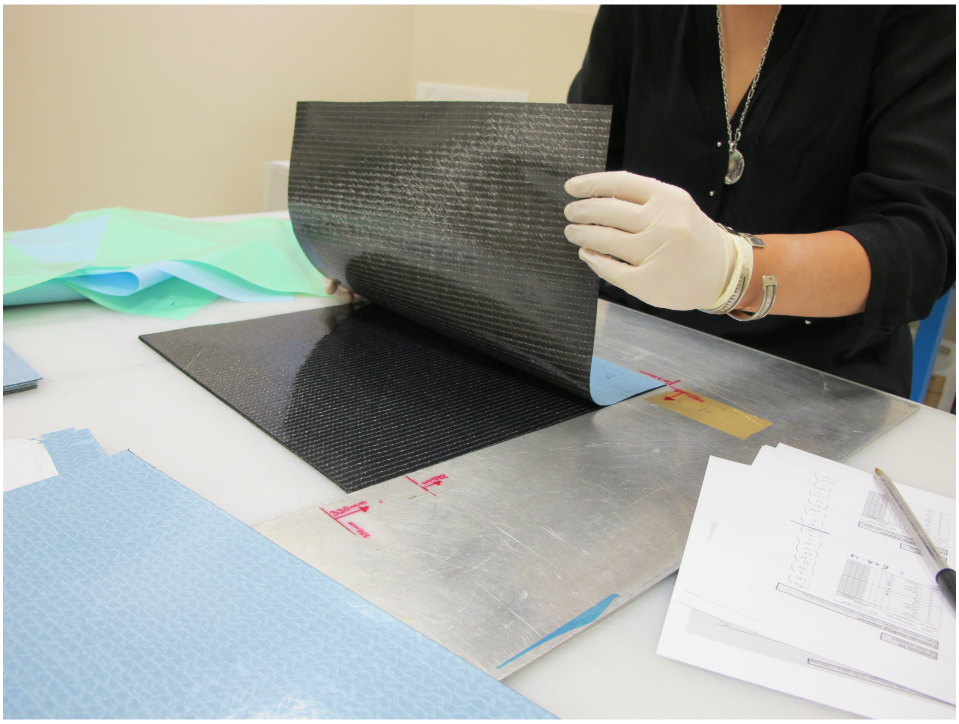

Figure 3.4: Manufacturing: lay-up

Figure 3.5: Manufacturing: removing trapped air between layers

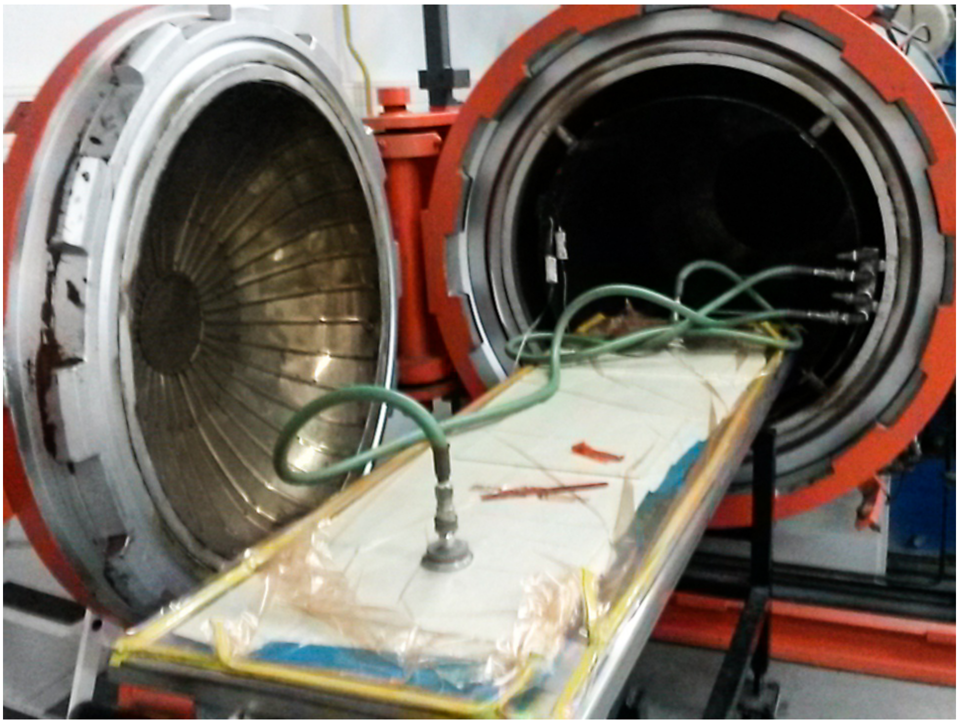

Figure 3.6: Manufacturing: plates before the curing cycle

Figure 3.7: Manufacturing: cutting the plates into specimens

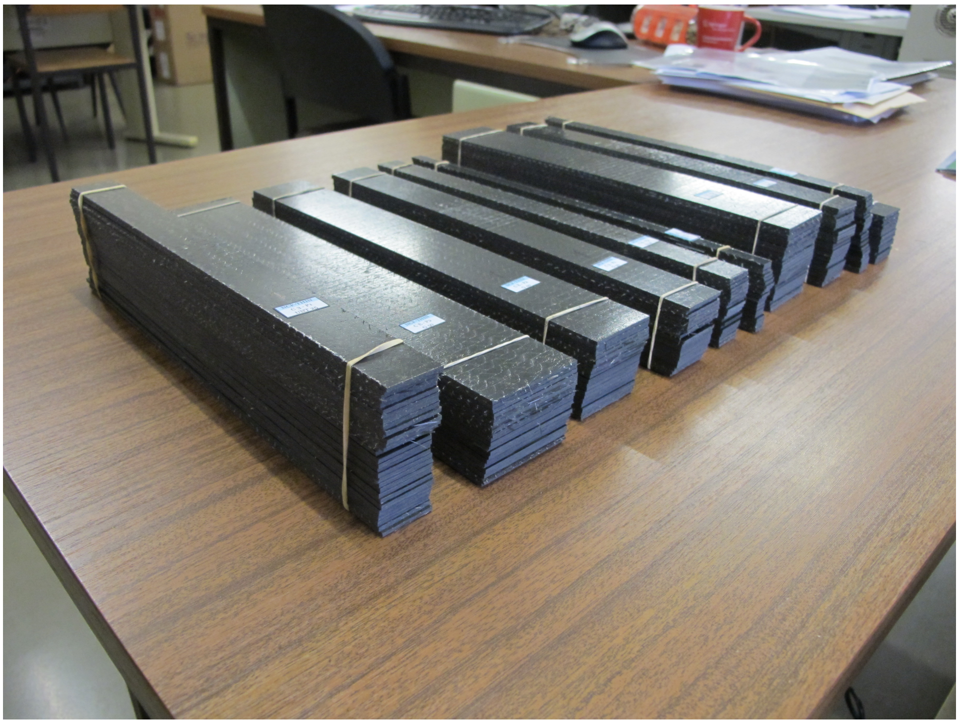

Figure 3.8: Manufacturing: cut specimens before machining

3.3 Digital Image Correlation

Digital image correlation is an optical-numerical full-field displacement measuring technique that can be used to evaluate the displacement and strain fields and to observe damage initiation and propagation [6]. In this work, digital image correlation was used to evaluate the surface displacement and strain field in the surface of some specimens. Before testing, the surface of the specimens was cleaned using sandpaper and acetone and the specimens were sprayed with white and black ink to generate the random distribution of granular dots required by the DIC system. An example of the painted specimens is shown in fig. 3.9.

The ARAMIS DIC-2D v6.0.2 equipped with an 8-bit Baumer 138 Optronic FWX20 camera coupled with a 200 mm Nikkon lens was used. During the test, the optical system was positioned perpendicular to the surface of the specimen and the light system is used to assure an even lightening on the specimen's surface (fig. 3.10). For all specimens, the displacement field was measured in the outer 90^o ply.

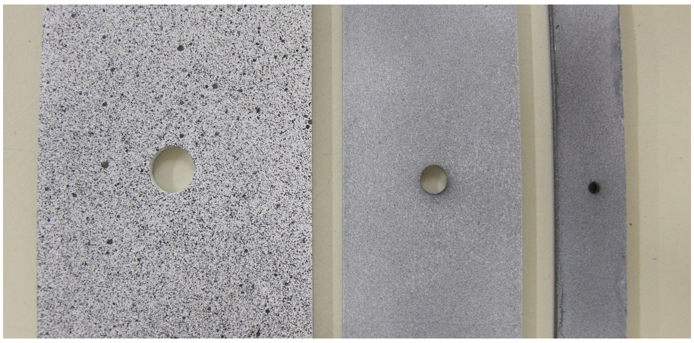

Figure 3.9: Painted specimens for DIC analysis

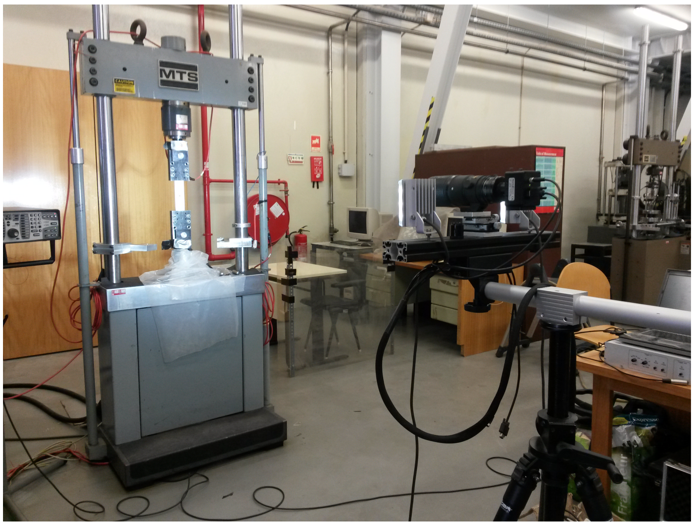

Figure 3.10: Equipment used for digital image correlation

3.4 Test plan and test procedures

A series of mechanical tests were performed to the thin, thick and hybrid laminates of both material systems. Since the major disadvantage of thin-ply composites is its comparatively lower notched tensile strength, priority was given to study the tensile behaviour of hybrid structures.

3.4.1 Plain Strength tests

The unnotched strength is necessary to characterize a composite laminate and, therefore, unnotched tensile tests were performed to the NCF-THIN, NCF-THICK, NCF-HYBRID, STF-THIN, STF-THICK and STF-HYBRID lay-ups following the ASTM D3039 /D3039M standard [1]. The specimens length (L) is 300 mm and its nominal width (W) is 25 mm (table 3.4). The unnotched tensile strength on each specimen is calculated as:

$$X_L^T = \frac{P^{max}}{A} \tag{3.1}$$

where P^{max} is the maximum applied load during the test and A is the cross-sectional area of the specimen. To calculate the A the dimensions of each specimen were measured, instead of using their nominal dimensions.

The tests were performed in displacement control in servo-hydraulic MTS 312.31 testing machine using a 250 kN load cell. Coarse-grain sandpaper was applied between the specimen and the grips to avoid sliding and grips were clamped with a 45 Nm bolt torque.

The DIC technique was used to evaluate the surface displacement and strain field of one test specimen per laminate configuration using a 200mm Nikkon lens. The working distance was 660 mm, the acquisition frequency was 1 Hz and the shutter time was 5.0 ms.

Table 3.4: Unnotched tension test matrix

Test	L (mm)	W (mm)	Nr. specimens/ lay-up	Speed (mm/min)	Acquisition (Hz)
UNT	300	25	5	1	5

3.4.2 Open-hole tension tests

Open-hole tensile tests are used to characterize the resistance of a composite laminate with stress concentrations and to evaluate the effect of size on the laminate strength that is characterized by a decrease in specimen strength as the size of the specimen increases for the same width-to-diameter (W/D) ratio. When a notched structure is loaded, subcritical damage that appears at the vicinity of the notch, and, while for larger specimens, the size of the damaged zone is negligible compared to the specimens in-plane dimensions, for smaller specimens it is not. This explains why, the notched strength tends to the unnotched strength as the specimens size decreases. [14] [30]

The open-hole tensile tests were performed following the ASTM D5766/ D5766M standard [3] and three different sizes with the same width-to-diameter ratio $W/D = 6$ were tested. The dimensions of the specimens are presented in table 3.5. The central open-hole was obtained using a drilling machine.

Open-hole tension tests performed to NCF-THIN, NCF-THICK and NCF-HYBRID specimens were performed in displacement control in servo-hydraulic MTS 312.31 testing machine using a 250 kN load cell. Coarse-grain sandpaper was applied between the specimen and the grips to avoid sliding and grips were clamped with a 45 Nm bolt torque. Open-hole tension tests performed to STF-THIN, STF-THICK and STF-HYBRID specimens were performed in displacement control in an Instron testing machine.

Digital image correlation was used in one specimen of each lay-up and hole diameter configuration to evaluate the surface displacement and strain field. A 200mm Nikkon lens and an acquisition frequency of 1 Hz were used. The specimens were loaded up to 90% of their notched strength and will be inspected using X-ray after testing.

The width and thickness of all specimens were measured and used to calculate the cross-sectional area A. The notched strength $\overline{\sigma}_T^{\infty}$ of each specimen reads:

$$\overline{\sigma}_T^{\infty} = \frac{P^{max}}{A} \tag{3.2}$$

where P^{max} is the maximum applied load during the test.

Table 3.5: Open-hole tension test matrix

Test	L (mm)	W (mm)	D (mm)	Nr. specimens/ lay-up	Speed (mm/min)	Acquisition (Hz)
OHT	300	48	8	4	1	5
OHT	300	30	5	4	1	5
OHT	300	12	2	4	1	5

3.4.3 Open-hole fatigue tests

Open-hole fatigue tests were also performed. The dimensions of the specimens are presented in table 3.6 and followed the ASTM D5766/ D5766M standard [3] , however, as there is no standard to this type of test, the loading conditions were selected as proposed by Amacher et al. [4]: sinusoidal loading in load control with frequency of 2 Hz with peak stress of 70% of the laminate notched strength and a ratio of R=0.1. The specimen's end life was considered reached when its stiffness was reduced by 10% of its initial value. 50k cycles were applied to all specimens. This allows, on one hand, to evaluate the stiffness and residual strength of the specimens after the same number of applied cycles. Also, by analysing the specimen's stiffness during the test, it is possible to access the number of cycles they bear before the failure criterion is reached. For each cycle, the maximum and minimum force and displacement is known and, therefore, the reduction of stiffness can be calculated. The applied stress reads:

$$\overline{\sigma}_T^\infty = \frac{P^{max}}{A} \tag{3.3}$$

where P^{max} is the maximum applied load during the test and A is the cross-sectional area of the specimen. Since they are both constants, the applied stress is also constant. The applied stress can also be calculated as follows:

$$\overline{\sigma}_T^\infty = E\epsilon \tag{3.4}$$

where E is the stiffness and ϵ is the applied strain. The applied stress is constant and therefore

$$\overline{\sigma}_T^\infty{}_i = \overline{\sigma}_T^\infty{}_d \Leftrightarrow E_i\epsilon_i = E_d\epsilon_d \tag{3.5}$$

where the index i refers to properties of the undamaged specimen and the index d refers to properties of the damaged specimen. The reduction of stiffness is given by the ratio E_d/E_i. For the failure criterion used, $E_d/E_i = 90\%$ and therefore, the number of cycles the specimen can withstand before its end life is the number of cycles it can withstand with

$$\epsilon_i = 0.9\epsilon_d \Leftrightarrow \Delta u_d = \frac{\Delta u_i}{0.9} \tag{3.6}$$

The tests were performed in a servo-hydraulic MTS 312.31 testing machine using a 250 kN load cell, coarse-grain sandpaper was applied between the specimen and the grips to avoid sliding and grips were clamped with a 45 Nm bolt torque.

Table 3.6: Open-hole fatigue test matrix

Test	L (mm)	W (mm)	D (mm)	Nr. specimens/ lay-up	Frequency (Hz)	Max. Load	R
OHF	300	30	5	3	2	0.7 $\overline{\sigma}_T^\infty$	0.1

3.4.4 Double edge crack tests

More advanced failure prediction models require not only the material's fracture toughness, but also the material crack resistance curve (R-curve), which is the relation between the increment of crack length resistance and the fracture toughness. Catalanotti et al. [18] proposed a methodology to determine the R-curve of polymer composites reinforced by unidirectional fibres. It is based on the size effect law, which is the relation between the size of the specimens and their notched strength $\overline{\sigma}^\infty(w)$. According to this methodology, the driving force curves G_I at the ultimate remote stress are tangent to the R-curve. This means that the ultimate remote stresses $\overline{\sigma}^\infty$ can be calculated solving the system of equations

$$\begin{cases} G_I(\Delta a) = R(\Delta a) \\ \frac{G_I(\Delta a}{\partial \Delta a} = \frac{R(\Delta a)}{\partial \Delta a} \end{cases} \tag{3.7}$$

According to [9] and [41] the energy release rate in mode I of a two-dimensional orthotropic body for a crack propagating in the x direction is given by:

$$G_I = \frac{1}{\acute{E}} K_I^2 \tag{3.8}$$

where K_I is the mode I stress intensity factor and $\acute{E}$ is the the equivalent modulus which is given by

$$\acute{E} = \left(\frac{1+\rho}{2E_x E_y}\right)^{-1/2} \mu^{1/4} \tag{3.9}$$

with ρ and μ are given by

$$\rho = \frac{(E_x E_y)^{1/2}}{2G_{xy}} - (\nu_{xy}\nu_{yx})^{1/2} \tag{3.10}$$

and

$$\mu = \frac{E_y}{E_x} \tag{3.11}$$

The stress intensity factor K_I is a function of ρ, the notched remote stress σ and of the specimen's dimensions a, w and L and it is given by

$$K_I = \sigma\sqrt{w}\kappa(\alpha, \rho, \zeta) \tag{3.12}$$

where κ is a correction factor that depends on $\zeta = \mu^{-1/4} w/L$, $\alpha = a/w$ and ρ. For $\zeta < 1/2$, κ can be expressed as a function of only κ and ρ [10]. For not highly orthotropic laminates ($0 < \rho < 4$) [10], κ is given by

$$\kappa = f(\alpha)\chi(\rho) \tag{3.13}$$

where χ is the correction factor for the orthotropy of the material

$$\chi(\rho) = 1 + 0.1(\rho - 1) - 0.016(\rho - 1)^2 + 0.002(\rho - 1)^3 \tag{3.14}$$

and ρ is given by 3.10. f is a correction factor that accounts for the geometry of the specimens. For double edge crack specimens it reads [37]

$$f(\alpha) = \sqrt{\pi\alpha}\left[1 + 0.122\cos^4\left(\frac{\alpha\pi}{2}\right)\right]\sqrt{\left(\frac{2}{\alpha\pi}\right)\tan\left(\frac{\alpha\pi}{2}\right)} \tag{3.15}$$

Replacing 3.12 in 3.8, the energy release rate reads

$$G_I(\Delta a) = \frac{1}{\acute{E}} w(\sigma^\infty)^2 \kappa^2(\alpha_0 + \frac{\Delta a}{w}, \rho, \zeta) \tag{3.16}$$

where α_0 is the initial notch length-to-width ratio $\alpha_0 = a_0/w$.

Replacing equation 3.8 in the first equation of 3.7, the $R(\Delta a)$ yields

$$R(\Delta a) = \frac{1}{\acute{E}} w(\overline{\sigma}^\infty)^2 \kappa^2 \tag{3.17}$$

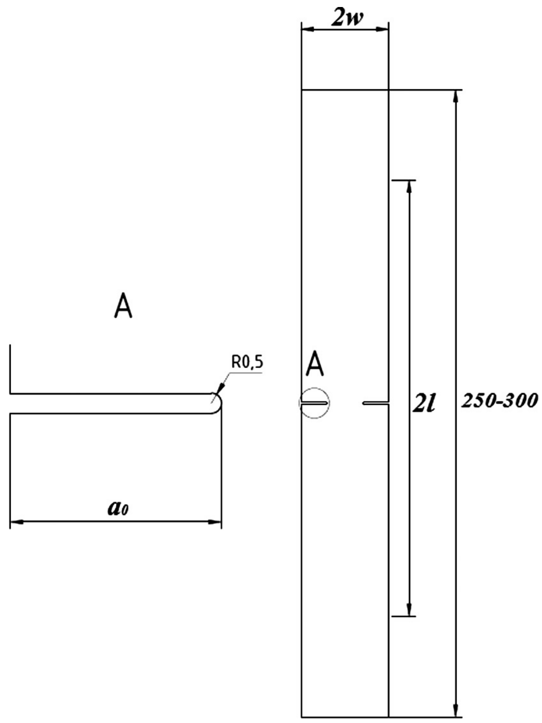

Figure 3.11: Double edge crack specimens [18]

For a constant w/L and a_0/w and knowing that, by definition the R-curve is size independent ($\frac{\partial R}{\partial w} = 0$), differentiating equation 3.17 with respect to w yields:

$$\frac{\partial}{\partial w}(w\overline{\sigma}^{\infty})^2\kappa^2 = 0 \tag{3.18}$$

Given the size effect $\overline{\sigma}^{\infty}(w)$ is know, equation 3.18 can be solved in order of $w(\Delta a)$ which can afterwards be replaced in equation 3.17.

The size effect law can be determined experimentally testing geometrically similar double edge crack specimens, i.e. with the same width-to-crack length $2w/a$ ratio and different width $2w$ as shown in figure 3.11 and applying one of three linear regressions proposed in [12] that best fits the experimental data: i) bilogarithmic regression ii) linear regression I or iii) linear regression II. The regressions and the R-curve parameters (length of the fracture process zone, l_{fpz}, and the fracture toughness at propagation R_{ss}) are shown in 3.7. Note that $\kappa_0 = \kappa(\alpha_0)$ and $\acute{\kappa}_0 = \partial\kappa/\partial\alpha(\alpha_0)$.

It is useful and more convenient to express the R-curve analytically. Catalanotti et al. [18] suggest the following equation

$$R(\Delta a) = R_{ss}\left[1 - (1 - \gamma\Delta a)^{\beta}\right] \tag{3.19}$$

where γ and β are the parameters that best fit the R-curve.

In this study, to obtain the size effect law of the six different lay-ups, tension tests were performed to double edge notched specimens with width w from 5 to 25 mm and width-to-notch length $a/w = 3/5$ (see table 3.8). Three specimens of each

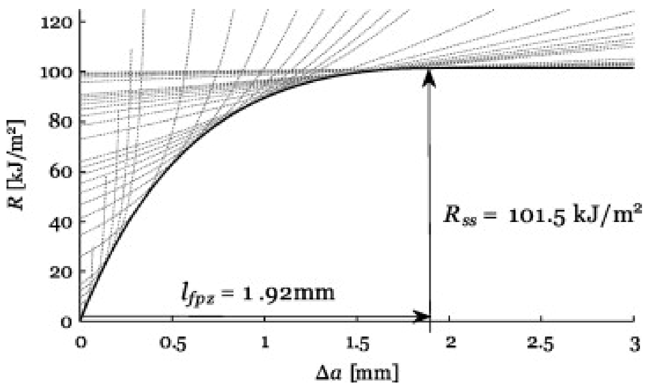

Figure 3.12: Example of a R-curve [18]

Table 3.7: Regressions and the R-curve parameters [18]

Regression	Formula	Fitting parameters	R_{ss}	l_{fpz}
Bilogarithmic	$ln(\overline{\sigma}^{\infty}) = ln\frac{M}{\sqrt{N+w}}$	M, N	$\frac{\kappa_0^2}{\acute{E}}M^2$	$\frac{\kappa(\alpha_0)}{2\acute{\kappa}_0}N$
Linear regression I	$\frac{1}{(\overline{\sigma}^{\infty})^2} = Aw + C$	A, C	$\frac{\kappa_0^2}{\acute{E}}\frac{1}{A}$	$\frac{\kappa(\alpha_0)}{2\acute{\kappa}_0}\frac{C}{A}$
Linear regression II	$\frac{1}{w(\overline{\sigma}^{\infty})^2} = A\frac{1}{w} + C$	A, C	$\frac{\kappa_0^2}{\acute{E}}\frac{1}{C}$	$\frac{\kappa(\alpha_0)}{2\acute{\kappa}_0}\frac{A}{C}$

specimen configuration were tested for each laminate configuration. The double edge cracks were machined in a CNC machine equipped with a 1 mm drill bit. Tests performed to NCF-THIN, NCF-THICK and NCF-HYBRID specimens were performed in displacement control in servo-hydraulic MTS 312.31 testing machine using a 250 kN load cell. Coarse-grain sandpaper was applied between the specimen and the grips to avoid sliding and grips were clamped with a 45 Nm bolt torque. Double edge cracks tests performed to STF-THIN, STF-THICK and STF-HYBRID specimens were performed in displacement control in an Instron testing machine.

Table 3.8: Double edge crack test matrix

Test	L (mm)	2w (mm)	a_0 (mm)	Nr. specimens / lay-up	Speed (mm/min)	Acquisition (Hz)
$G_{1+}(\Delta a)$ A	300	10	3	3	1	5
$G_{1+}(\Delta a)$ B	300	20	6	3	1	5
$G_{1+}(\Delta a)$ C	300	30	9	3	1	5
$G_{1+}(\Delta a)$ D	300	40	12	3	1	5
$G_{1+}(\Delta a)$ E	300	50	15	3	1	5

Chapter 4

Experimental Results

In this chapter, the experimental test results of unnotched tension tests, open-hole tension, open-hole fatigue and double edge crack tests for the NCF T700GC/M21 and STF T700SC/M21 are presented. Since the main goal of this experimental work is to compare the mechanical behaviour of the thin, thick and hybrid laminate configurations of the same material system, the results are presented in two separate sections: section 4.1 is dedicated to the experimental tests results of NCF T700GC/M21 lay-ups and section 4.2 is dedicated to the experimental test results of STF T700SC/M21 lay-ups.

4.1 Experimental results - NCF T700GC/M21

This section presents the experimental tests results of NCF T700GC/M21 lay-ups. To simplify the analysis, the lay-ups are, once again, presented below in table 4.1. Ply blocking is highlighted in red. Note that all plies are symmetric, quasi-isotropic and have the same in-plane properties. In NCF-THIN lay-up, there is no ply-blocking, and, except for the central 45° ply, all plies have nominal thickness of 0.075 mm. NCF-THICK lay-up, two plies with the same orientation are blocked together when possible and therefore, the nominal thickness of most plies is 0.150 mm. NCF-HYBRID lay-up has ply blocking of only two 0° plies near the center of the laminate.

Table 4.1: NCF T700GC/M21 lay-ups

Laminate ID	Lay-up	t (mm)
NCF-THIN	$[(90/+45)/(0/-45)]_{3s}$	1.8
NCF-THICK	$[(90/+45)/(+45/0)/(0/-45)/(-45/90)/(90/+45)/(0/-45)]_s$	1.8
NCF-HYBRID	$[(90/+45)/(0/-45)(90/+45)/(90/-45)/(+45/0)/(0/-45)]_s$	1.8

4.1.1 Unnotched tension test results

The remote stress-displacement relations for plain strength tension of laminates NCF-THIN, NCF-THICK and NCF-HYBRID tests are presented in fig. 4.1. For the unnotched tension tests, all the laminates exhibit linear behaviour up to failure. This suggests that there is little severe transverse cracking before failure which is fibre-dominated.

Representative unnotched tension specimens after testing are shown in figs. 4.2a and a close-up of the fracture planes of the specimens is shown in figures 4.2b and 4.2c. All lay-up NCF-THIN and NCF-THICK and some of the NCF-HYBRID specimens failed in two places, due to catastrophic failure. Lay-up NCF-THIN specimens exhibit brittle net-section failure. In NCF-THICK specimens some delamination can be observed. The different failure modes are related to the stacking sequence. Unlike lay-up NCF-THIN, lay-up NCF-THICK has "ply blocking" i.e. two plies with the same orientation stacked together, which leads to lower in-situ strengths of those plies. This, as reported in [7], triggers delamination onset, pull-out and splitting. NCF-HYBRID specimens revealed a similar fracture plane to NCF-THICK specimens, i.e. some delamination and pull-out failure mode is also observed.

The mean values and standard deviation of the unnotched tension tests for lay-ups NCF-THIN, NCF-THICK and NCF-HYBRID are presented in table 4.2. As reported in [7] and [4], thin-ply structures have higher unnotched tensile strength than thick-ply structures since they are able to delay damage up to the point of final failure. The same is proven here and NCF-THIN specimens show 11.1% higher unnotched tensile strength than NCF-THICK specimens.

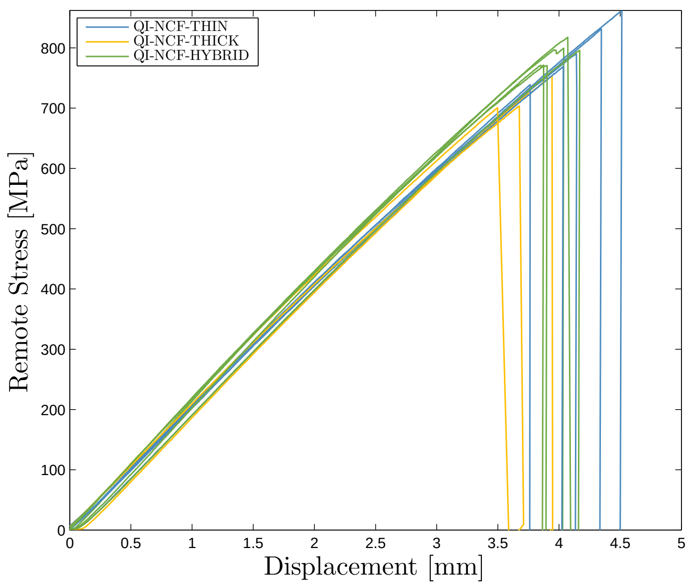

Figure 4.1: Unnotched tension remote stress-displacement relations for NCF-THIN, NCF-THIN and NCF-HYBRID lay-ups.

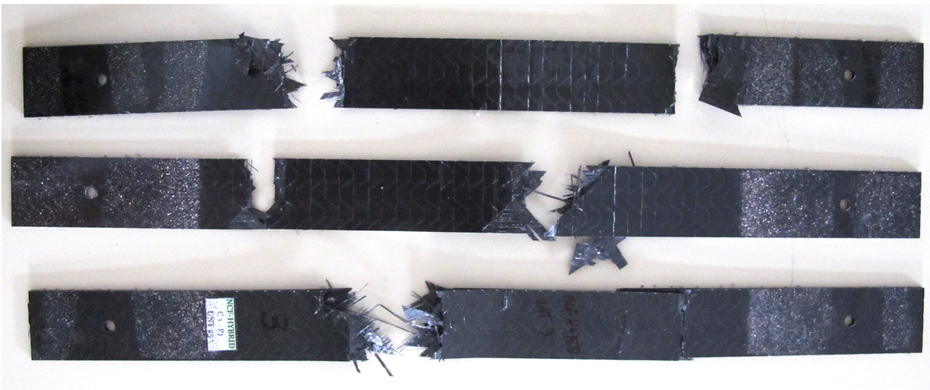

(a) Representative NCF-THIN (above), NCF-THICK (middle) and NCF-HYBRID (below) specimens after testing

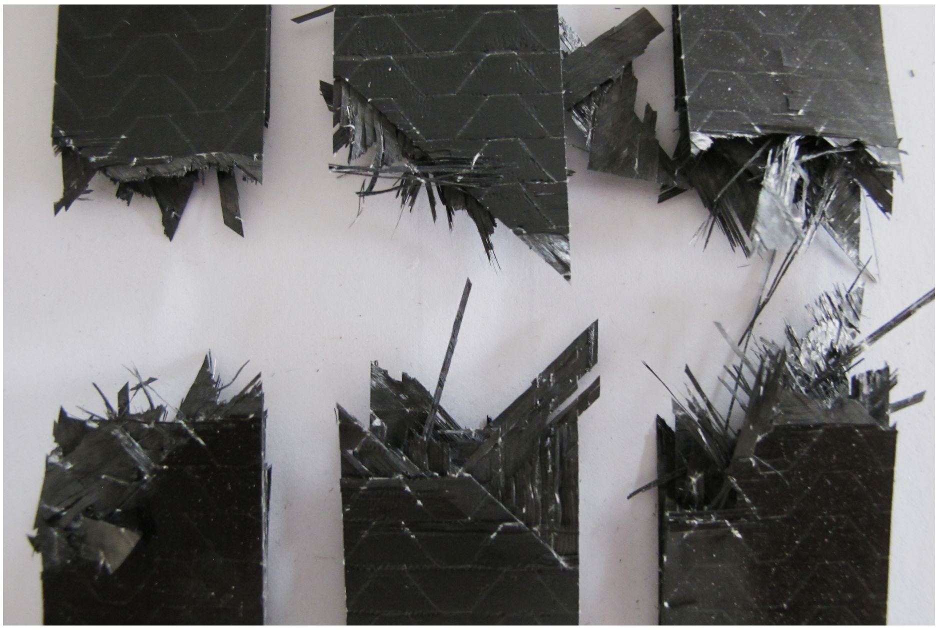

(b) Fracture plane of representative NCF-THIN (left), NCF-THICK (middle) and NCF-HYBRID (right) specimens after testing

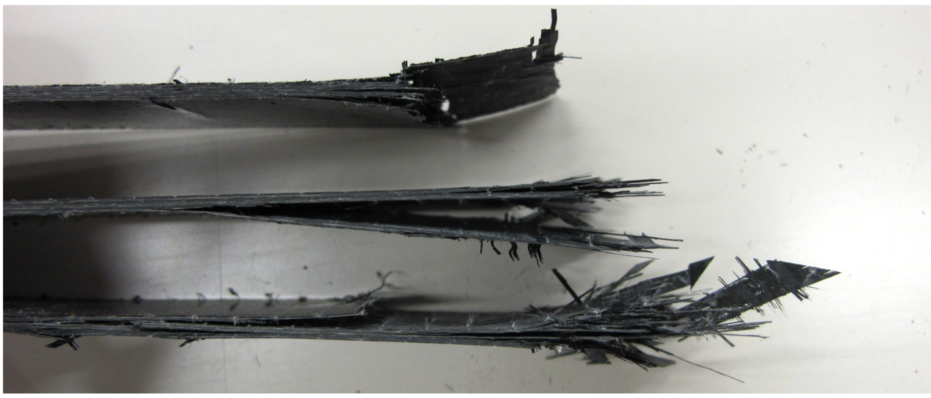

(c) Fracture plane of representative NCF-THIN (above), NCF-THICK (middle) and NCF-HYBRID (below) specimens after testing (side view)

Figure 4.2: Representative NCF T700GC/M21 unnotched tension specimens after testing

NCF-HYBRID specimens presented 10.02% higher unnotched tensile strength than NCF-THICK specimens and 0.93% lower strength than NCF-THIN specimens. The ply's tensile strength in the direction of the fibres X^T in not a function of the ply thickness and, since, ply blocking is limited to 0° plies only, the in-situ strengths of the plies are not significantly affected when compared to the NCF-THIN lay-up which explains the similar unnotched test results between the two lay-ups.

Table 4.2: Unnotched tension results for lay-ups NCF-THIN, NCF-THICK and NCF-HYBRID

Property	Type	Nr valid tests	Mean Value [MPa]	STDV
	NCF-THIN	5	798.68	53.27
X_T^L	NCF-THICK	3	719.17	29.43
	NCF-HYBRID	5	791.24	20.21

Digital image correlation was used during one unnotched tension test per laminate configuration to monitor the the strain field and access the formation of transverse cracks in the surface of the specimens. Figures 4.3a, 4.3b and 4.3c show the surface longitudinal strain fields just before failure for lay-up NCF-THIN, NCF-THICK and NCF-HYBRID, respectively obtained using digital image correlation. Note that the specimens were loaded in the horizontal direction. The bottom right image shows the longitudinal strain along two lines parallel to the free edge of the specimens, positioned as shown in the left bottom images. Figures 4.3a, 4.3b and 4.3c evince that no free edge transverse cracking in the outer 90° ply appears before failure, since there is no discontinuity in the longitudinal strain along the two lines. Although no transverse cracks appear before failure in NCF-THICK lay-up, the strain field along the edges for this laminate is less homogeneous than in NCF-THIN lay-up and more points of strain concentration are visible which might be the reason why the specimen's final failure is triggered at a lower remote stress than NCF-THIN specimens.

The elastic properties of each laminate were calculated using the Classical Lamination Theory and the results are presented in table 4.3.

Table 4.3: Elastic properties of NCF-THIN, NCF-THICK and NCF-HYBRID calculated using the Classical Lamination Theory

Laminate	E_y [GPa]	E_x [GPa]	ν_{xy}	G_{xy} [GPa]
NCF-THIN	49.78	49.78	0.311	18.98
NCF-THICK	49.78	49.78	0.311	18.98
NCF-HYBRID	49.78	49.78	0.311	18.98

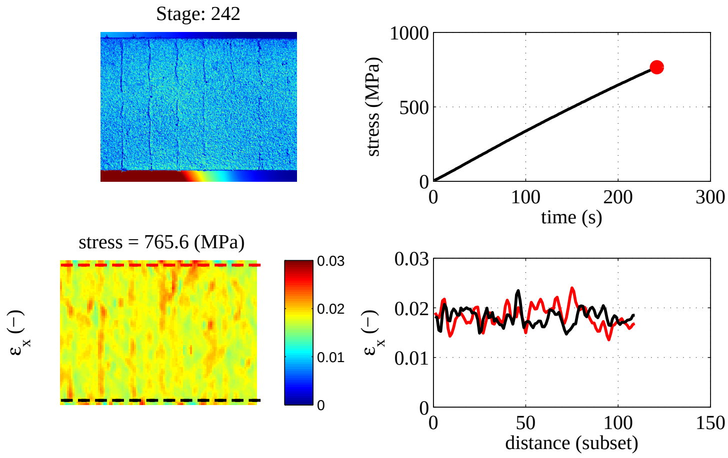

(a) NCF-THIN

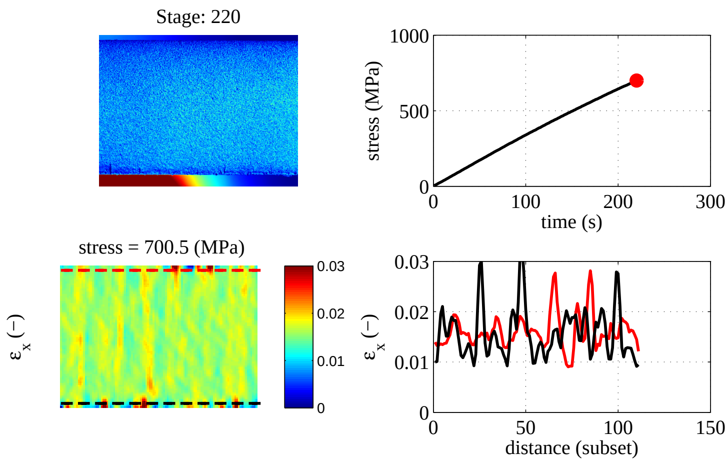

(b) NCF-THICK

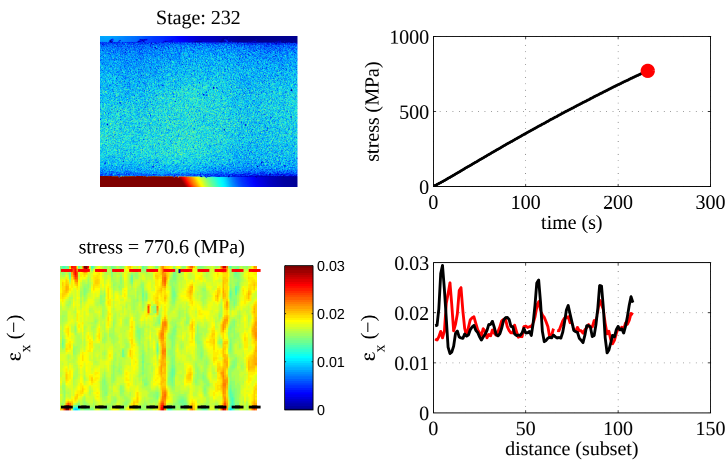

(c) NCF-HYBRID

Figure 4.3: Longitudinal strain field of NCF T700GC/M21 unnotched tension specimens just before failure

4.1.2 Open-hole tension test results

Open-hole tensile tests were performed to evaluate the laminate's resistance in the presence of stress concentrations and to evaluate the size effect of a laminate which is, in general, characterized by a reduction in the specimen's resistance with the increase of its in-plane dimensions, for the same W/d ratio. In this study, and as mentioned in chapter 3, the notched strength of three lay-ups of NCF T700GC/M21 (NCF-THIN, NCF-THICK and NCF-HYBRID) was accessed by testing specimens with hole diameters of $d = 2mm$, $d = 5mm$ and $d = 8mm$ and with the hole diameter-to-width ratio of $d/W = 1/6$. The experimental results of the open-hole tension tests performed will be presented hereafter. Although three tests per laminate configuration and per geometry were planned, some specimens failed within the grips and were for this reason, were not considered valid. The results obtained for these specimens will not be addressed.

The remote stress-displacement relations for open-hole tension tests of laminates NCF-THIN, NCF-THICK and NCF-HYBRID are presented in fig. 4.7a, 4.5 and 4.6. For open-hole tension tests, all the laminates exhibit linear behaviour up to failure with some load drops that do not affect the specimen's stiffness significantly.

Representative open-hole tension specimens after testing are shown in figs. 4.7a, 4.7b and 4.7c. Lay-up NCF-THIN specimens exhibit brittle net-section failure, with less delamination than NCF-THICK and NCF-HYBRID specimens. Some pull-out is observed in lay-ups NCF-THICK and NCF-HYBRID.

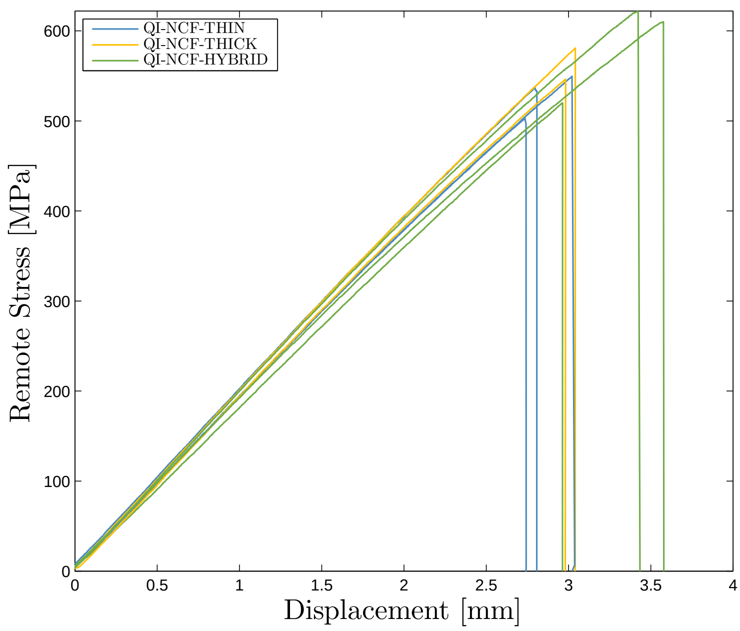

Figure 4.4: Open-hole tension remote stress-displacement relations for $d = 2mm$ for NCF-THIN, NCF-THIN and NCF-HYBRID lay-ups.

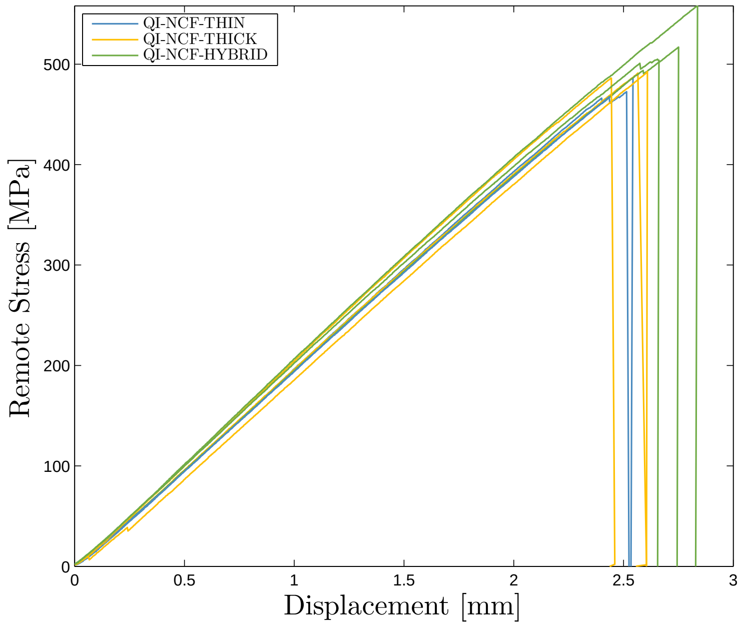

Figure 4.5: Open-hole tension remote stress-displacement relations for d = 5mm for NCF-THIN, NCF-THIN and NCF-HYBRID lay-ups.

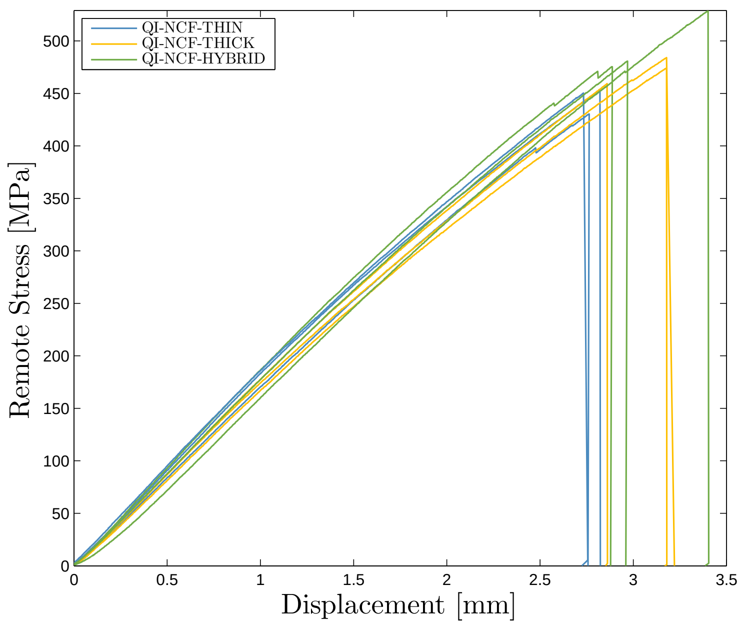

Figure 4.6: Open-hole tension remote stress-displacement relations for d = 8mm for NCF-THIN, NCF-THIN and NCF-HYBRID lay-ups.

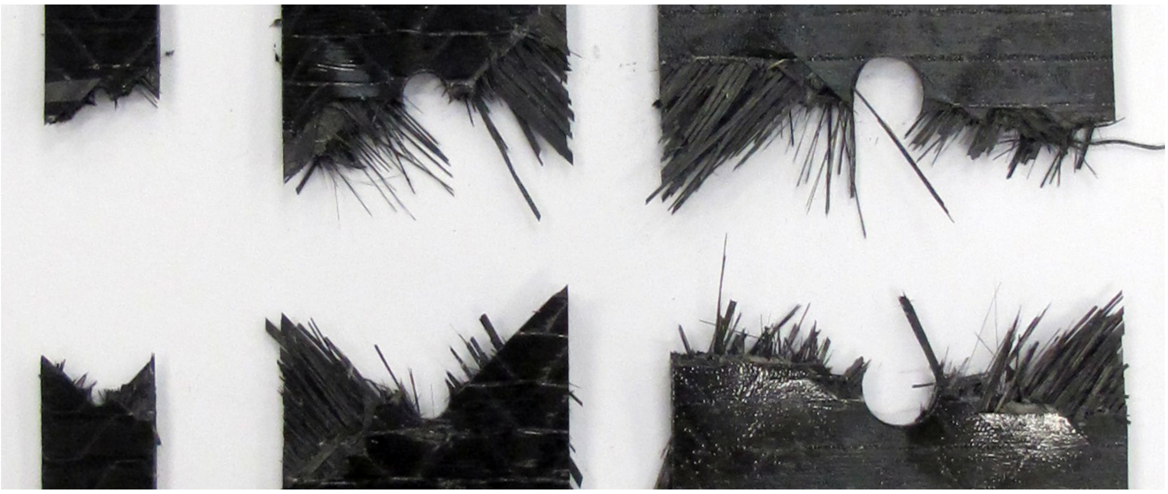

(a) NCF-THIN

(b) NCF-THICK

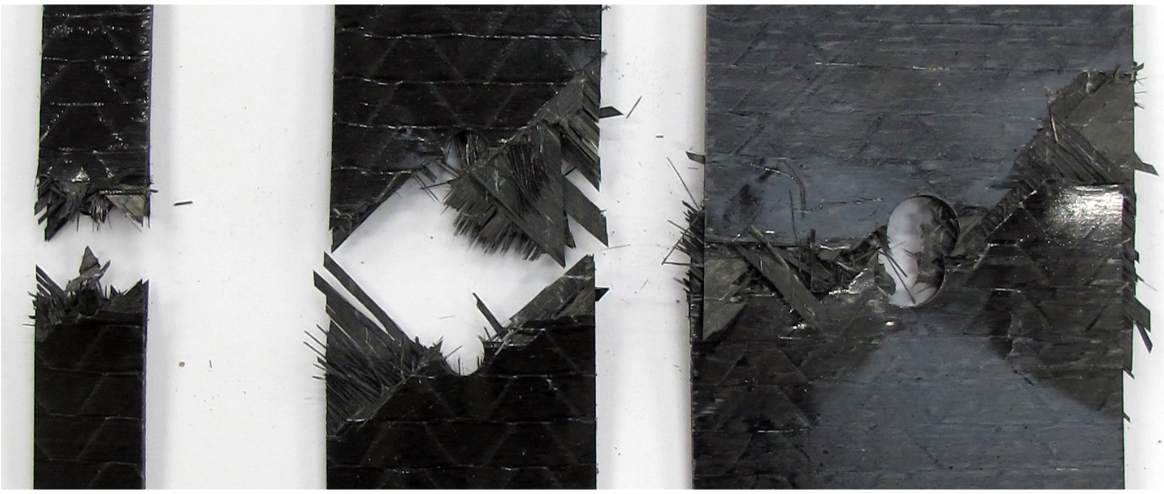

(c) NCF-HYBRID

Figure 4.7: Representative NCF T700GC/M21 open-hole specimens after testing

The mean values and standard deviation of the strengths measured in the open-hole tests are presented in table 4.4 and fig. 4.8. As expected, thin-ply laminates have lower notched strength than thick-ply laminates because, as damage onset is delayed up to the point just before failure, redistribution of stresses at the vicinity of the notch is inhibited leading to premature and brittle failure of the structure. NCF-THIN specimens exhibited 5.94%, 2.21% and 5.91% lower strength than NCF-THICK specimens for d=2mm, d=5mm and d=8mm, respectively. In general, the selected hybrid lay-up revealed to have higher nothed strength than both thin and thick lay-ups:

- For d=2mm, NCF-HYBRID specimens exhibited 10.13% and 3.59% higher notched strength that NCF-THIN and NCF-THICK specimens, respectively.
- For d=5mm, NCF-HYBRID specimens exhibited 9.83% and 7.40% higher notched strength that NCF-THIN and NCF-THICK specimens, respectively.
- For d=8mm, NCF-HYBRID specimens exhibited 11.39% and 4.81% higher notched strength that NCF-THIN and NCF-THICK specimens, respectively.

It appears that, by ply-blocking the 0^o plies, fibre splitting is triggered while damage in the 45^o and 90^o is suppressed. This type of damage allows the redistribution of stresses near the hole, which reduces the stress concentration and, at the same time, as the damage is alligned with the loading direction, limits the damage to vicinity of the notch, which explains the enhanced notched strength in open-hole tension tests.

Table 4.4: Open-hole test results for lay-ups NCF-THIN, NCF-THICK and NCF-HYBRID

Property	Type	d [mm]	Nr valid tests	Mean Value [MPa]	STDV
	NCF-THIN	2	3	530.68	23.90
$\overline{\sigma}_T^\infty$	NCF-THICK	2	2	564.25	24.1
	NCF-HYBRID	2	3	584.48	55.82
	NCF-THIN	5	2	479.76	9.29
$\overline{\sigma}_T^\infty$	NCF-THICK	5	3	490.62	3.38
	NCF-HYBRID	5	3	526.92	27.86
	NCF-THIN	8	3	444.76	12.3
$\overline{\sigma}_T^\infty$	NCF-THICK	8	3	472.68	12.55
	NCF-HYBRID	8	3	495.41	29.50

Analysing table 4.4 and fig. 4.8 it can be concluded that the notched strength of the specimens increases with the decrease of the hole diameter. For the three types of lay-up, a reduction in hole diameter from 8 mm to 2 mm results in an increase of around 19% of the notched strength. When a notched structure starts developing damage, a fracture process zone near the notch is created which redistributes stresses and reduces stress concentration. The smaller the in-plane dimensions of the specimen, the less negligible the size of the damage zone at the vicinity of the notch is and, therefore, smaller specimens will exhibit a more ductile behaviour than larger specimens. This type of response was expected and is taken into account in

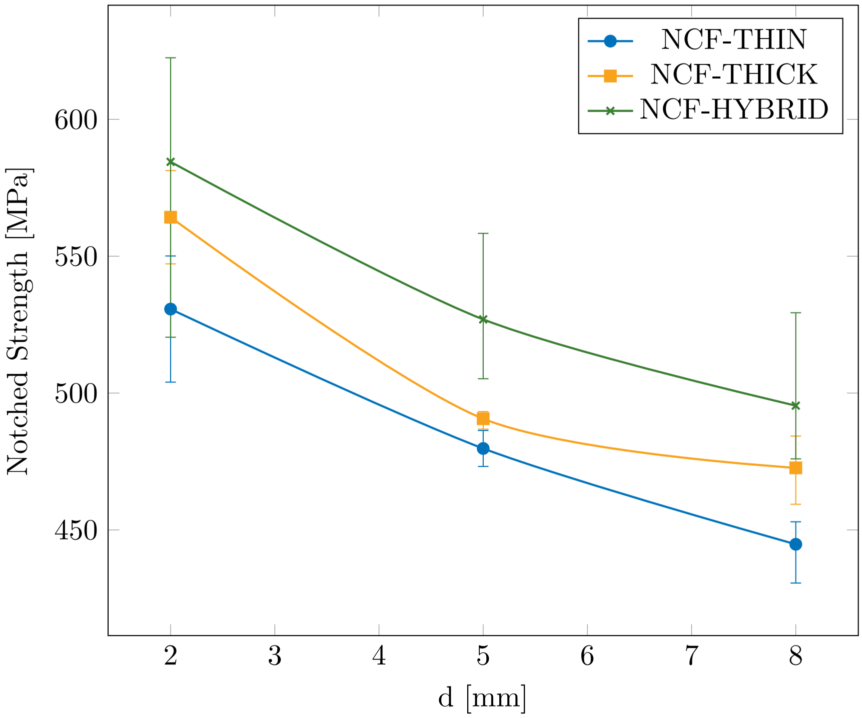

Figure 4.8: Notched strength vs hole diameter for lay-ups NCF-THIN, NCF-THICK and NCF-HYBRID

the analytical models used to predict the notched strength of composite structures, as the Finite Fracture Mechanics Model, explained in section 5.1 [17].

Digital image correlation was used during testing of one specimen of each lay-up and hole diameter configuration to access the differences in damage evolution. The specimens were loaded up to 90% of their notched strength. Figures 4.9, 4.10 and 4.11 show the longitudinal strain at the surface of NCF-THIN, NCF-THICK and NCF-HYBRID specimens loaded at 90% of their notched strength. The bottom right images show the longitudinal strain along two lines positioned near the hole. Since no discontinuity of the strain field along those lines can be identified, it can be concluded that 90% of the specimen's strength revealed to be insufficient to allow the formation of cracks at the vicinity of the hole. In general, the strain concentration near the hole is higher on smaller specimens. Although no free edge transverse cracks appeared in any monitored specimen, smaller specimens exhibit higher strain concentrations and are, therefore, more likely to develop transversal cracks. No relevant differences are visible between NCF-THIN, NCF-THICK and NCF-HYBRID lay-ups.

In general, as reported in [17], for the same d/W ratio, the larger the hole diameter, the more notch sensitive the specimen is. The same conclusion can be taken from this study analysing fig. 4.12 where the normalized notched strength defined as $\overline{\sigma}_N = \overline{\sigma}_T^\infty / X^L$ for the three lay-ups and hole diameters is shown. In this figure, two different types of behaviour are are pointed out in black: notch sensitivity which corresponds to a brittle behaviour where the normalized notched

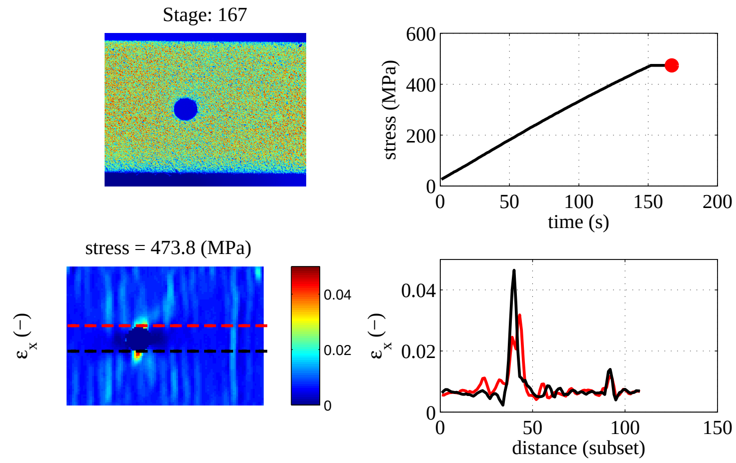

(a) NCF-THIN d=2mm

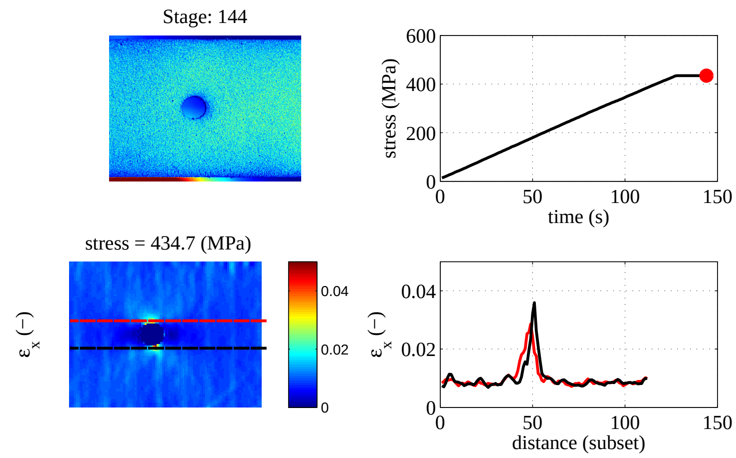

(b) NCF-THIN d=5mm

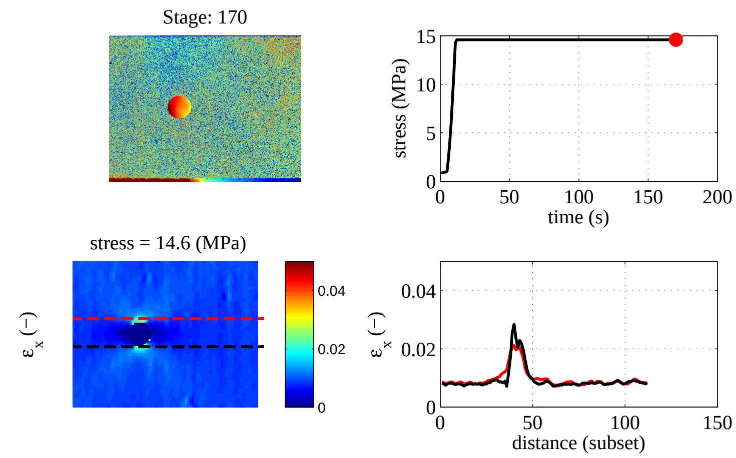

(c) NCF-THIN d=8mm

Figure 4.9: Longitudinal strain field of NCF-THIN specimens at 90% of their failure stress

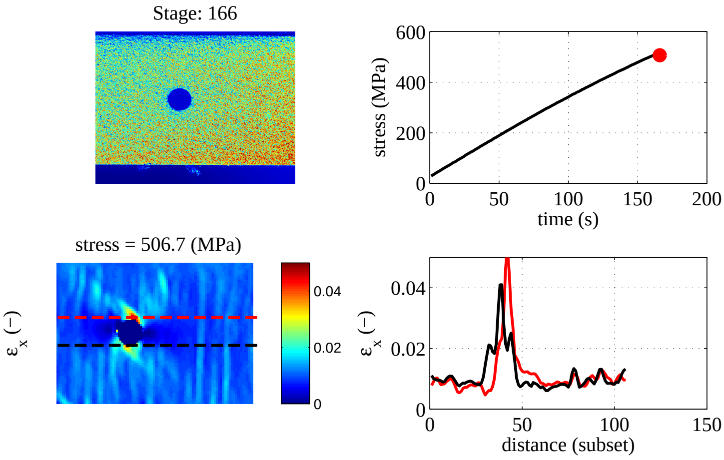

(a) NCF-THICK d=2mm

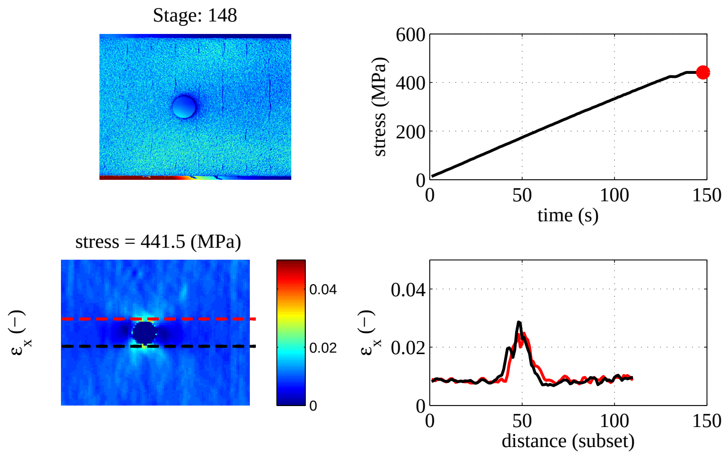

(b) NCF-THICK d=5mm

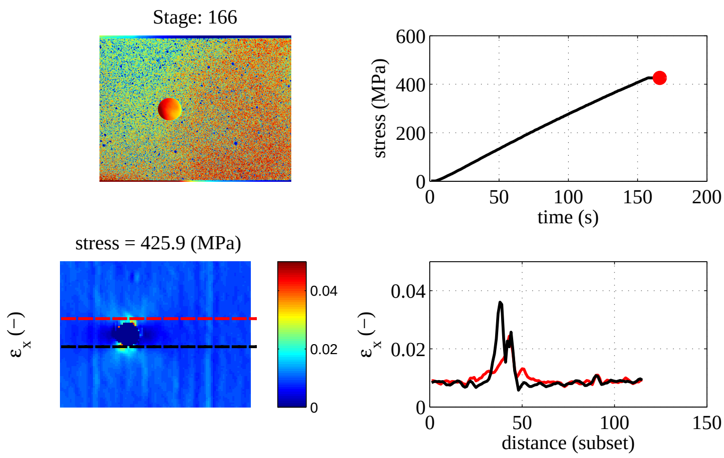

(c) NCF-THICK d=8mm

Figure 4.10: Longitudinal strain field of NCF-THICK specimens at 90% of their failure stress

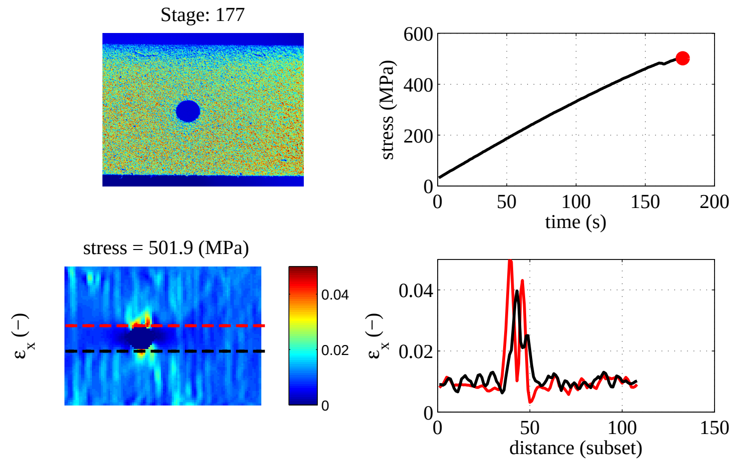

(a) NCF-HYBRID d=2mm

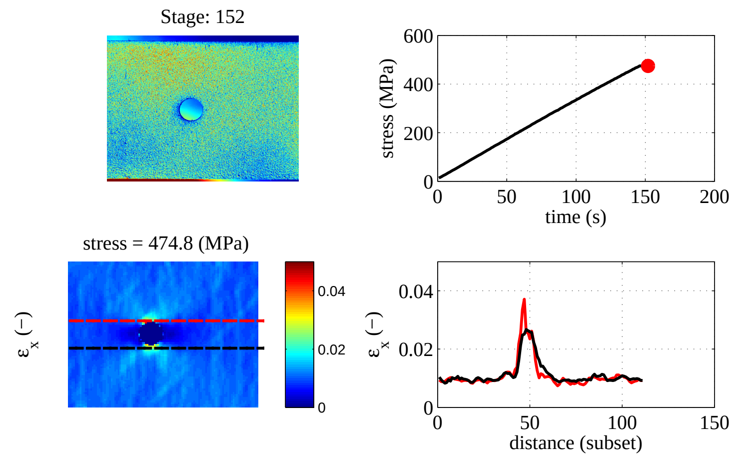

(b) NCF-HYBRID d=5mm

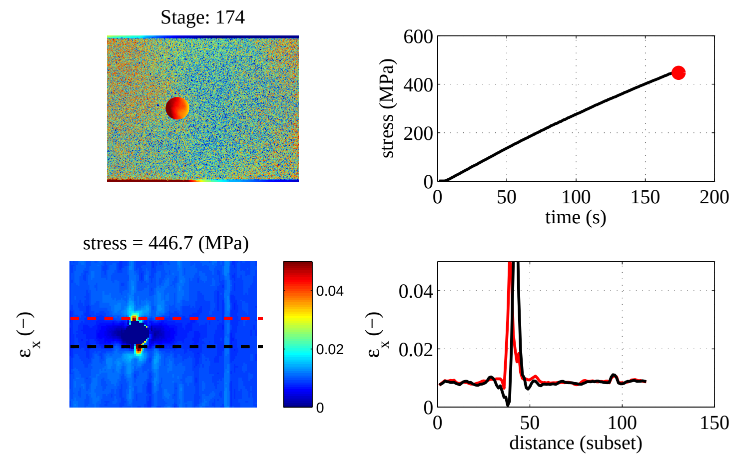

(c) NCF-HYBRID d=8mm

Figure 4.11: Longitudinal strain field of NCF-HYBRID specimens at 90% of their failure stress

strength is defined as $\overline{\sigma}_N = 1/K_T$ and notch insensitivity which corresponds to a ductile behaviour and where the normalized notched strength of the laminate is defined as $\overline{\sigma}_N = 1 - 2R/W$. In this case, for $d/W = 1/6$, and for a quasi-isotropic lay-up ($K_T^{\infty} = 3$), K_T yields:

$$K_T = K_T^{\infty} R_K = 3 \left(\frac{3(1 - d/W)}{2 + (1 - d/W)^3} \right)^{-1} = 3.0944$$

The normalized notch strengths is therefore $\overline{\sigma}_N = 1/K_T = 0.32316$ for notch sensitivity and $\overline{\sigma}_N = 1 - 2R/W = 0.8333$ for notch insensitivity. Analysing fig. 4.12 it can be accessed that NCF-THIN lay-up exhibits a more brittle response that both NCF-THIN and NCF-HYBRID lay-ups. These results will be addressed with more detail in chapter 5.

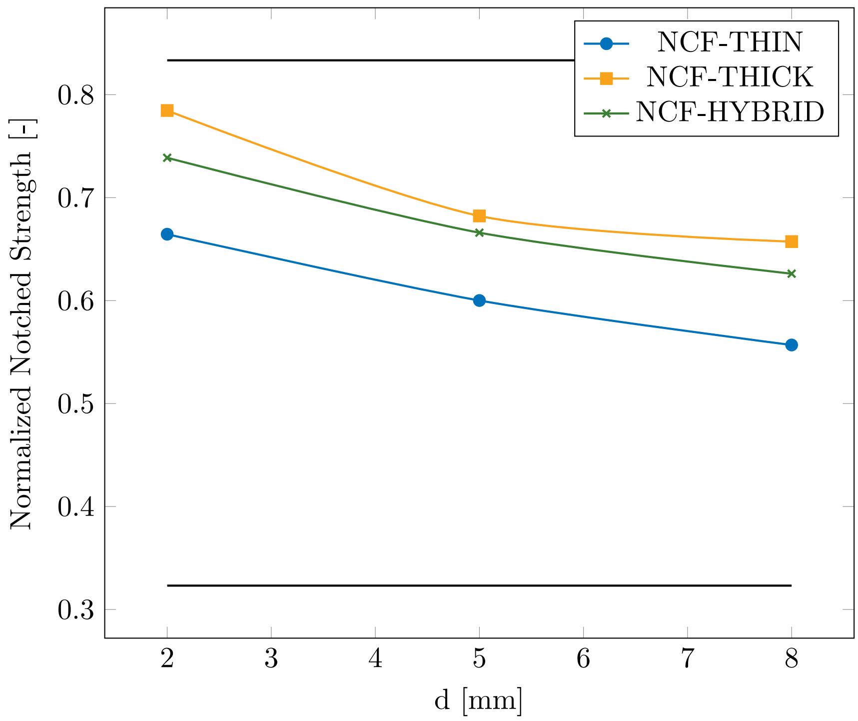

Figure 4.12: Normalized notched strength vs hole diameter for lay-ups NCF-THIN, NCF-THICK and NCF-HYBRID

4.1.3 Open-hole fatigue test results

Open-hole fatigue tests were performed to three lay-ups of NCF T700GC/M21 to compare the evolution of damage in the three lay-ups. The specimen's hole diameter is $d = 5mm$ and $d/w = 1/6$ as shown in table 3.6. Although, three tests per laminate configuration were planned, only one was performed due to schedule problems. For this reason, the results presented hereafter, serve only as preliminary results, that should, in the future, be complemented with more experimental data.

The reduction of stiffness during the tests is shown in figure 4.13. As presented in table 4.5 NCF-THIN, NCF-THICK and NCF-HYBRID specimens suffered a stiffness reduction of 2.486 %, 5.196 % and 3.231%, respectively.

Table 4.5: Open-hole fatigue test results for lay-ups NCF-THIN, NCF-THICK and NCF-HYBRID

Type	$\overline{\sigma}_T^\infty$ [MPa]	$\sigma^{max} = 0.7\overline{\sigma}_T^\infty$ [MPa]	Nr valid tests	Modulus reduction after 50k cycles
NCF-THIN	479.76	335.83	1	2.486%
NCF-THICK	490.62	343.43	1	5.196%
NCF-HYBRID	526.92	368.84	1	3.231 %

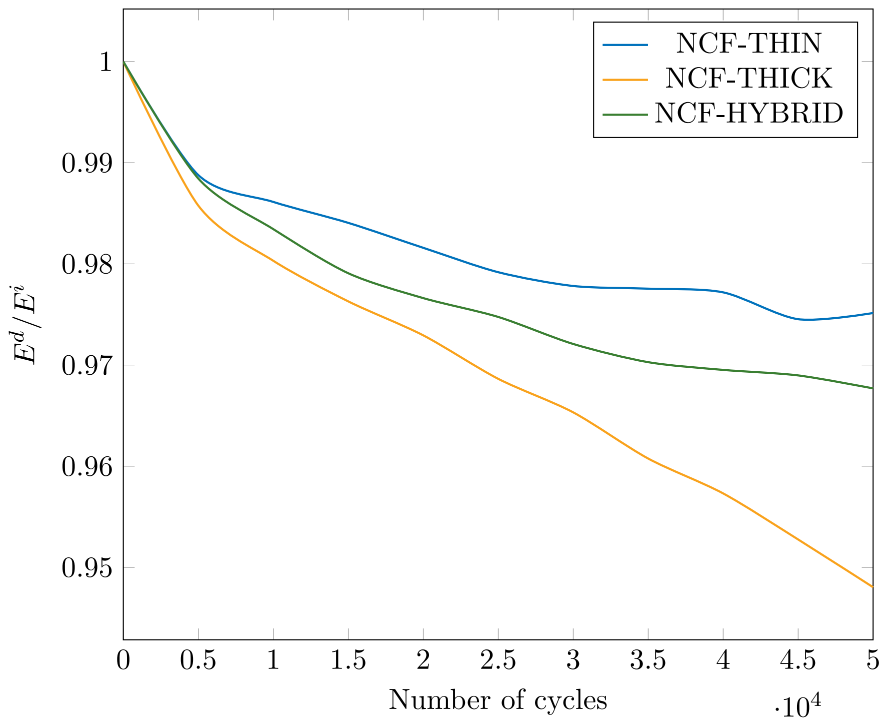

Figure 4.13: Reduction of stiffness during the open-hole fatigue tests to NCF-THIN, NCF-THICK and NCF-HYBRID specimens

While NCF-THIN specimen exhibit no visible damage on the surface, in NCF-THICK and NCF-HYBRID specimens a part of one of the outer 90° ply delaminated near the hole. The surface of the NCF-THICK and NCF-HYBRID specimens after testing are shown in figures 4.14 and 4.15, respectively. The specimens will be inspected after testing using X-ray, so that, a better insight of the extent and type of damage present in each specimen can be accessed.

As expected, NCF-THIN specimen show enhanced resistance to fatigue loadings compared to NCF-THICK specimen because they exhibit less subcritical damage prior to failure and therefore, damage propagation is slower and less pronounced. NCF-HYBRID, exhibited an intermediate response to fatigue loading.

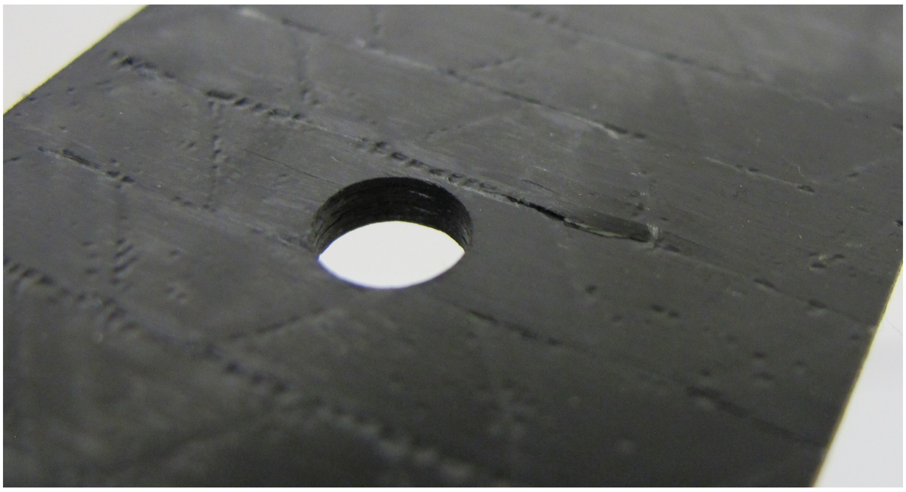

Figure 4.14: NCF-THICK specimen after fatigue loading

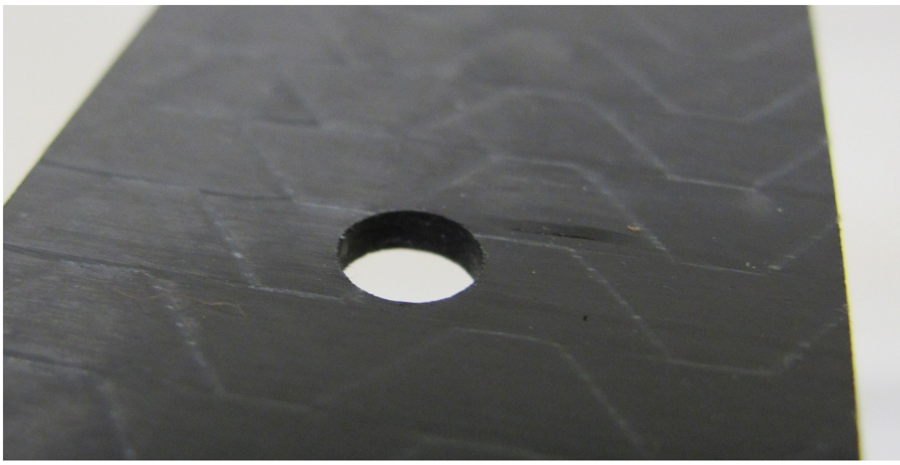

Figure 4.15: NCF-HYBRID specimen after fatigue loading

4.1.4 Double edge crack test results

Double edge crack tests with widths of $w = 5mm$, $w = 10mm$, $w = 15mm$, $w = 20mm$ and $w = 25mm$ and notch length-to-width of $a/w = 3/5$ (see table 3.8) were performed to three lay-ups of NCF T700GC/M21 in order to characterize the size effect law required to obtain the crack resistance curve of the three lay-ups. Three specimens per geometry per laminate configuration were planned, however, some failed within the grips and, were therefore, considered invalid and were disregarded.

The remote stress-displacement relations for double edge crack tests of laminates NCF-THIN, NCF-THICK and NCF-HYBRID are presented in fig. 4.16, 4.17, 4.18, 4.19 and 4.20. Specimens with width $2w = 10mm$ and $2w = 20mm$ exhibit linear behaviour up to failure. Specimens with $2w = 30mm$, $2w = 40mm$ and $2w = 50mm$ exhibit linear behaviour with some load drops before final failure with negligible impact on the specimen's stiffness. Representative double edge notch specimens are shown in figures 4.21a, 4.21b and 4.21c.

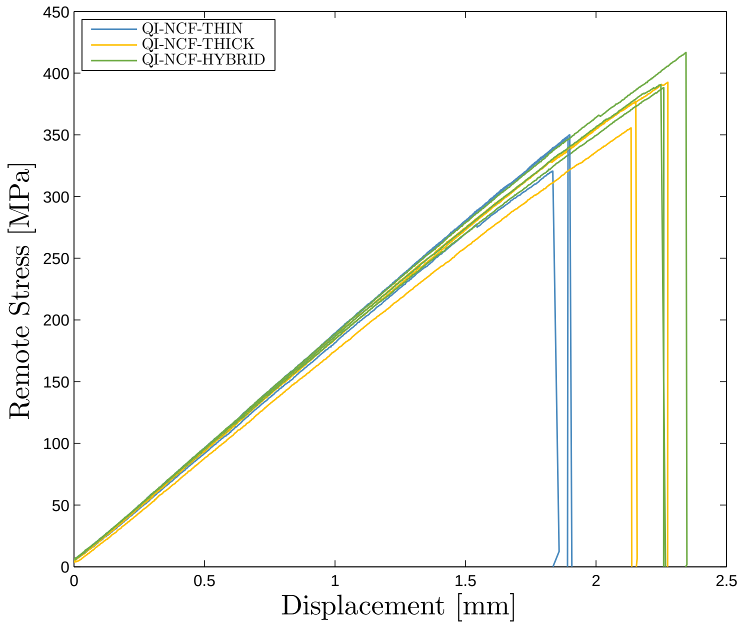

Figure 4.16: Double edge crack remote stress-displacement relations for $2w = 10mm$ for NCF-THIN, NCF-THIN and NCF-HYBRID lay-ups.

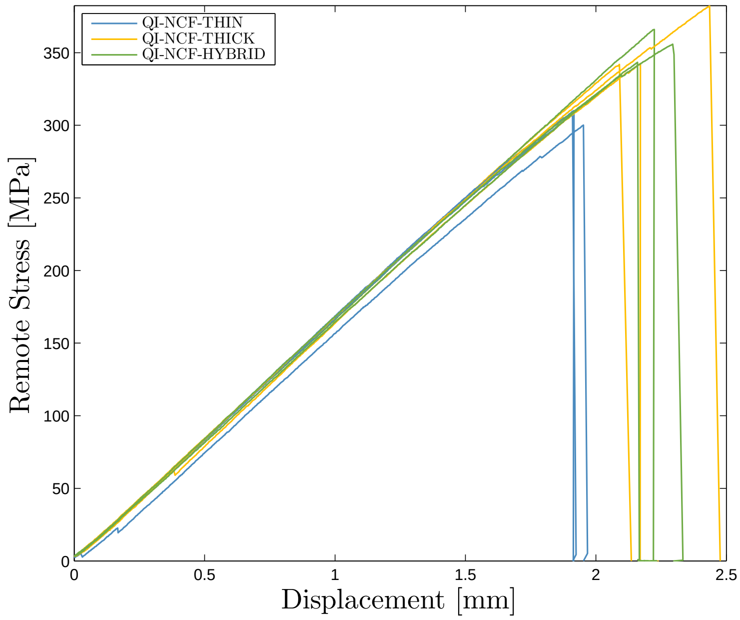

Figure 4.17: Double edge crack remote stress-displacement relations for $2w = 20mm$ for NCF-THIN, NCF-THIN and NCF-HYBRID lay-ups.

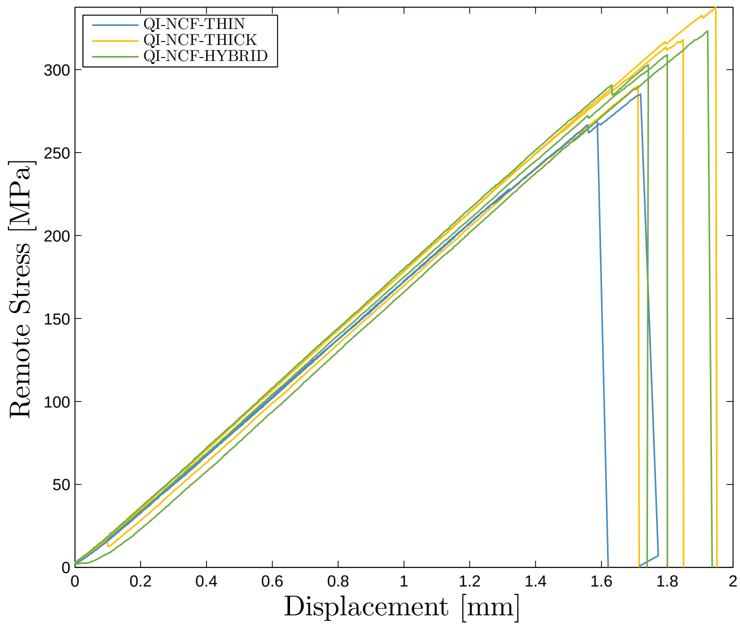

Figure 4.18: Double edge crack remote stress-displacement relations for $2w = 30mm$ for NCF-THIN, NCF-THIN and NCF-HYBRID lay-ups.

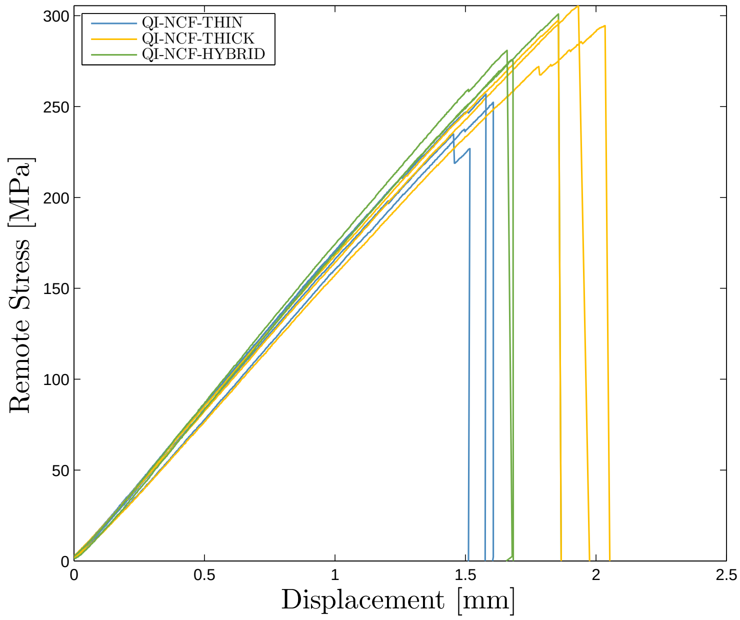

Figure 4.19: Double edge crack remote stress-displacement relations for $2w = 40mm$ for NCF-THIN, NCF-THIN and NCF-HYBRID lay-ups.

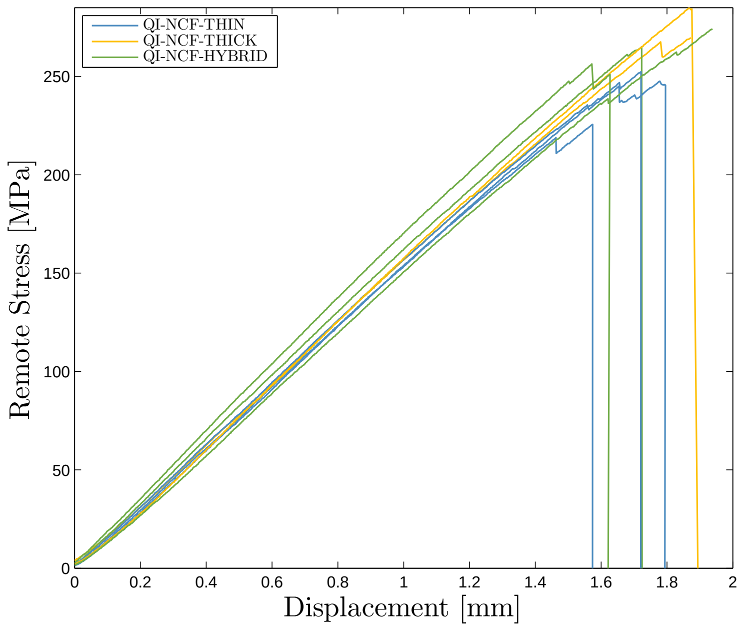

Figure 4.20: Double edge crack remote stress-displacement relations for $2w = 50mm$ for NCF-THIN, NCF-THIN and NCF-HYBRID lay-ups.

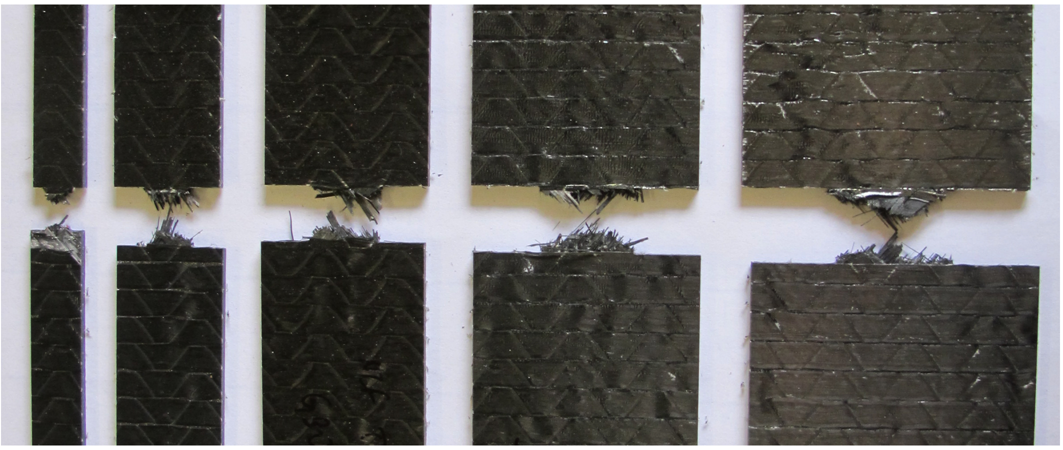

(a) NCF-THIN

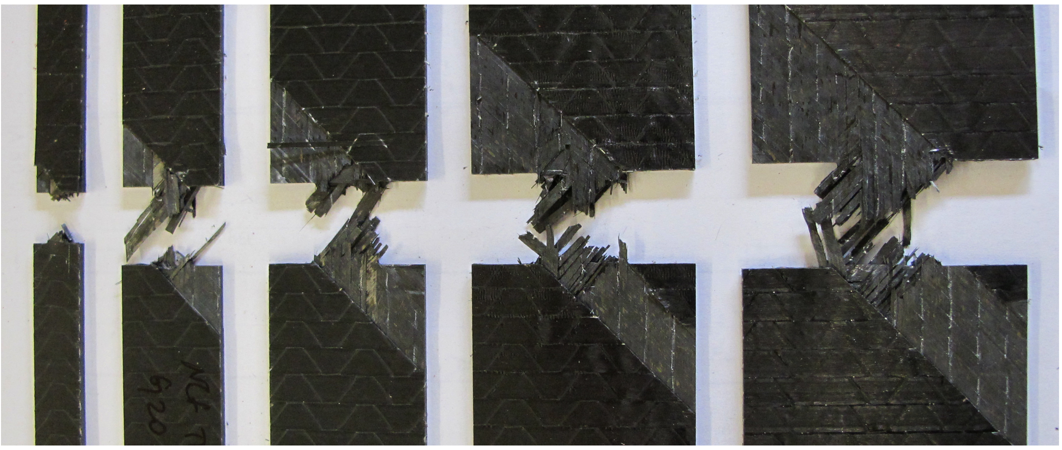

(b) NCF-THICK

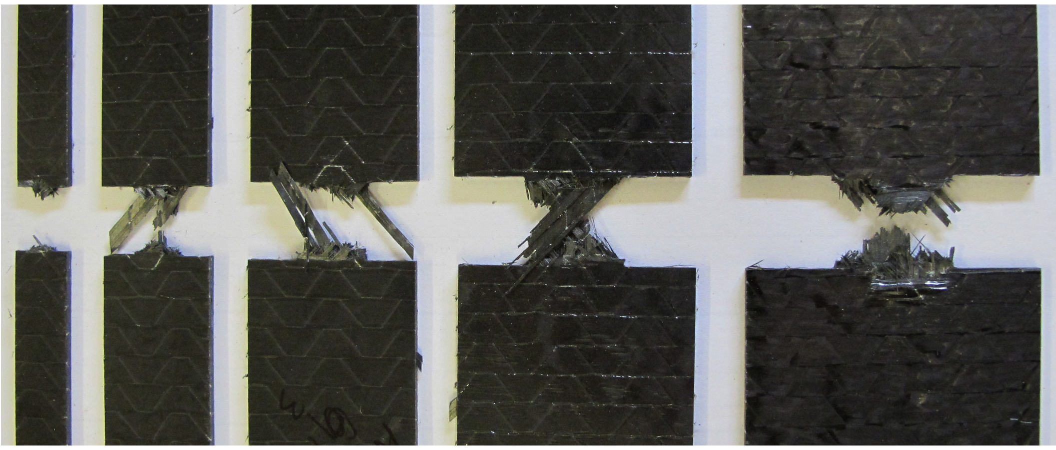

(c) NCF-HYBRID

Figure 4.21: Representative NCF T700GC/M21 double edge crack specimens after testing

The mean values and standard deviation of the double edge crack tests are presented in table 4.6 and fig. 4.22. Between the linear regression I and linear regression II [12] (see section 3.4.4), the regression which best fits the experimental data was determined for each laminate configuration. The two regressions are presented in figures 4.23 and 4.24. The size effect that best fits the experimental data is the linear regression I for lay-ups NCF-THIN and NCF-THICK and the linear regression II for lay-up NCF-HYBRID. The fitting parameters are shown in table 4.7. As explained in section 3.4.4, knowing the size effect law and the elastic properties of the laminate, the steady-state value of the R-curve R_{ss} and the length of the fracture process zone l_{fpz} can be calculated as shown in table 3.7. The elastic properties of the laminate were calculated using the Classical Lamination Theory and are presented in table 4.3. The R-curve parameters and the for lay-ups NCF-THIN, NCF-THICK and NCF-HYBRID are shown in table 4.8 and the R-curves are presented in fig. 4.25. Note that:

$$R(\Delta a) = R_{ss}\left[1 - (1 - \gamma \Delta a)^{\beta}\right] \tag{4.1}$$

Table 4.6: Double edge crack test results for lay-ups NCF-THIN, NCF-THICK and NCF-HYBRID

Property	Type	2w [mm]	Nr valid tests	Mean Value [MPa]	STDV
	NCF-THIN	10	3	340.07	16.47
$\overline{\sigma}_T^{\infty}$	NCF-THICK	10	3	371.36	19.15
	NCF-HYBRID	10	3	399.12	15.58
	NCF-THIN	20	3	306.14	5.09
$\overline{\sigma}_T^{\infty}$	NCF-THICK	20	3	356.08	23.12
	NCF-HYBRID	20	3	355.35	11.26
	NCF-THIN	30	2	277.54	11.4
$\overline{\sigma}_T^{\infty}$	NCF-THICK	30	3	315.68	24.06
	NCF-HYBRID	30	3	312.00	10.65
	NCF-THIN	40	3	248.30	11.52
$\overline{\sigma}_T^{\infty}$	NCF-THICK	40	3	295.54	11.00
	NCF-HYBRID	40	3	286.18	13.30
	NCF-THIN	50	3	242.13	14.23
$\overline{\sigma}_T^{\infty}$	NCF-THICK	50	3	280.28	5.13
	NCF-HYBRID	50	3	263.54	11.78

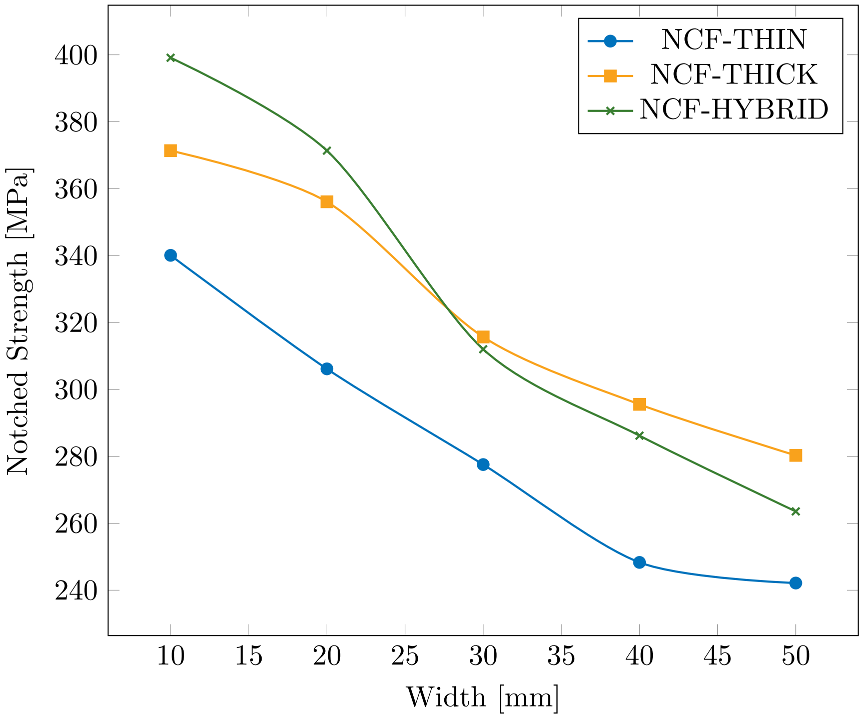

Figure 4.22: Notched strength vs width for for lay-ups NCF-THIN, NCF-THICK and NCF-HYBRID

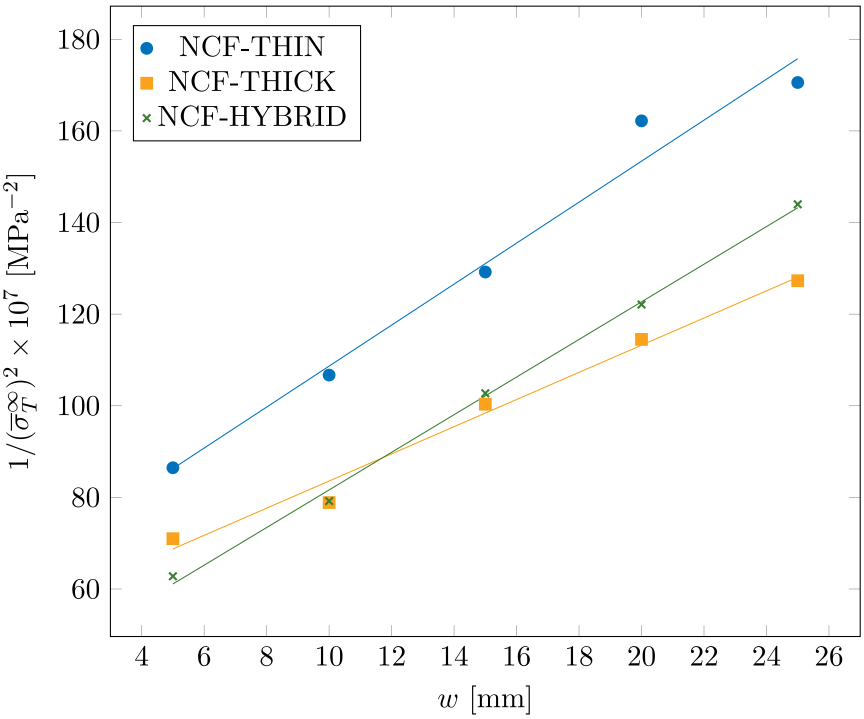

Figure 4.23: Size effect law: Experimental results and linear regression I fitting for NCF-THIN, NCF-THICK and NCF-HYBRID laminates

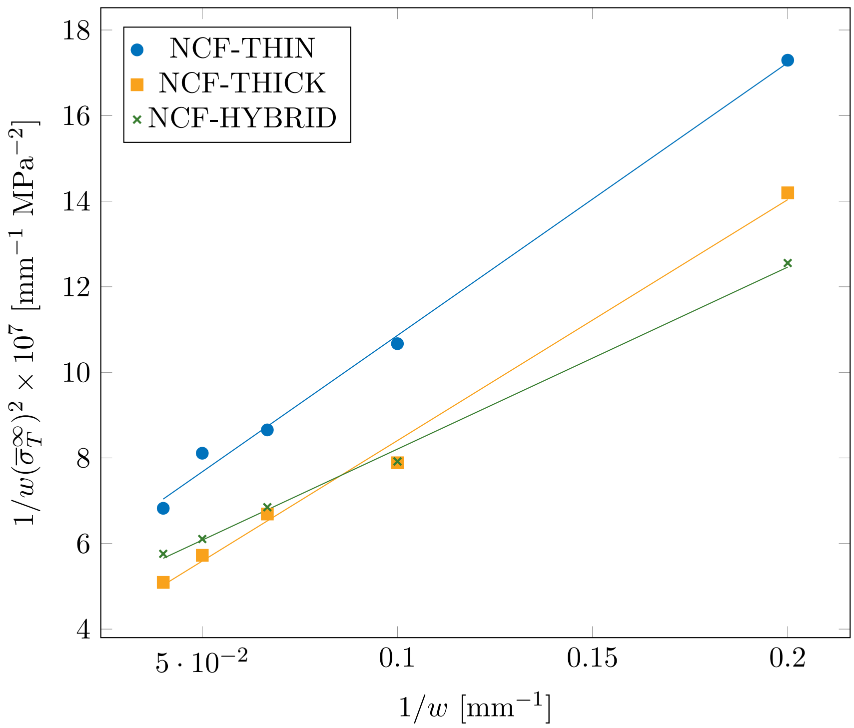

Figure 4.24: Size effect law: Experimental results and linear regression II fitting for NCF-THIN, NCF-THICK and NCF-HYBRID laminates

Table 4.7: Best fitting parameters of the size effect law for NCF-THIN, NCF-THICK and NCF-HYBRID lay-ups

Laminate	Best fitting	A [MPa^{-2} mm^{-1}]	C [MPa^{-2}]	R^2
NCF-THIN	LR I	4.474×10^{-7}	6.404×10^{-6}	0.9785
NCF-THICK	LR I	2.965×10^{-7}	5.392×10^{-6}	0.9852
Laminate	Best fitting	A [MPa^{-2}]	C [MPa^{-2} mm^{-1}]	R^2
NCF-HYBRID	LR II	4.253×10^{-6}	3.952×10^{-7}	0.9965

Table 4.8: Parameters of the R-curve lay-ups NCF-THIN, NCF-THICK and NCF-HYBRID lay-ups

Laminate	R_{ss} [kJ/m^2]	$l_{fpz}[mm]$	γ [mm^{-1}]	β
NCF-THIN	127.22	4.686	0.1681	4.151
NCF-THICK	191.95	5.9523	0.1302	4.237
NCF-HYBRID	144.02	3.5228	0.2274	4.064

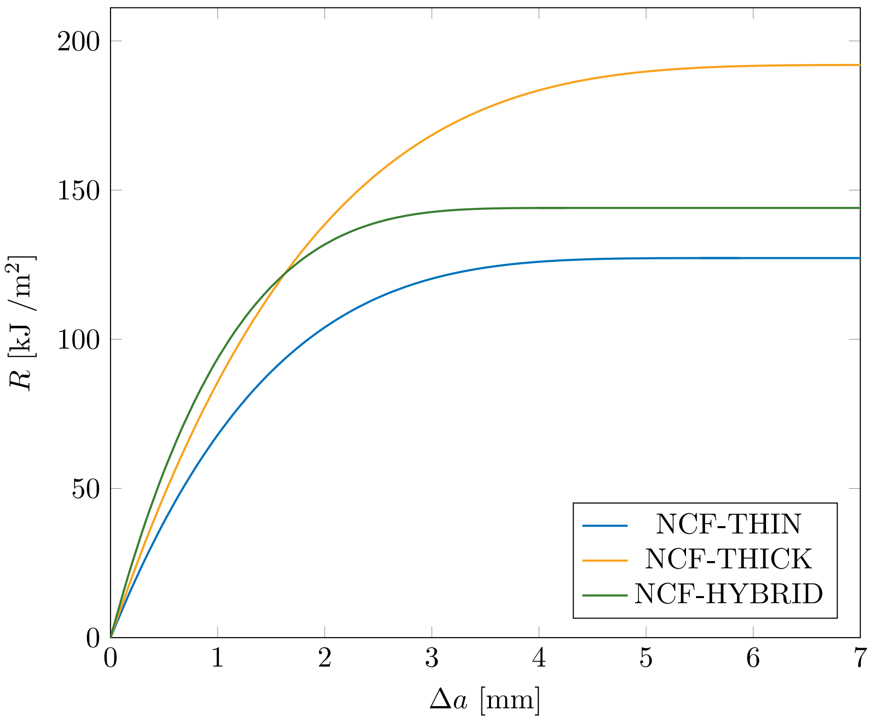

Figure 4.25: R-curve for NCF-THIN, NCF-THICK and NCF-HYBRID lay-ups

4.1.5 Concluding Remarks

Analysing the experimental results, it can be concluded that, when loaded in tension, NCF-THIN structures show enhanced unnotched tensile strength and enhanced fatigue resistance, but lower failure loads of notched structures loaded in tension. In NCF-THICK structures, the opposite behaviour is observed: they exhibit enhanced performance in notched structures loaded in tension but lower unnotched strength and less resistance to damage propagation in tensile fatigue loadings. This is explained by the stacking sequence: unlike for NCF-THIN lay-up, in NCF-THICK lay-up almost all plies are clustered together with one other ply with the same orientation, which results in plies with double the thickness. The thinner the plies, the higher the in-situ strengths and, therefore, the higher the applied stress has to be so that damage onset is triggered. This delay in damage onset is beneficial in unnotched structures loaded in tension and in fatigue loadings but leads to premature failure of notched structures since stress redistribution in the vicinity of the notches is inhibited.

NCF-HYBRID lay-up has only ply blocking of two 0^o plies near the center of the laminate. The experimental study conducted showed that, this type of ply-hybridization, results in enhanced unnotched and notched strengths. In fact, NCF-HYBRID exhibited a reduction of only 0.93 % in unnotched strength when compared to NCF-THIN laminate which is the one that exhibits higher unnotched strength between the two non-hybrid lay-ups. The ply's tensile strength in the direction of the fibres X^T in not a function of the ply thickness and, since, ply blocking is limited to 0^o plies only, the in-situ strengths of the plies are not significantly affected when compared to the NCF-THIN lay-up which explains the similar unnotched test results between the two lay-ups. At the same time, NCF-HYBRID showed 3.59%, 7.47% and 4.81% higher notched strength for d=2mm, d=5mm and d=8mm, respectively, when compared with NCF-THICK laminate which is the one that exhibits higher notched strength between the two non-hybrid lay-ups. The experimental study suggests that, by ply-blocking the 0^o plies, fibre splitting is triggered while damage in the 45^o and 90^o is suppressed. This type of damage allows the redistribution of stresses near the hole, which reduces the stress concentration and, at the same time, as the damage is aligned with the loading direction, limits the damage to vicinity of the notch, which explains the enhanced notched strength in open-hole tension tests.

NCF-HYBRID lay-up showed 37.8% higher and 29.98 % lower resistance to damage propagation in open-hole fatigue tests than NCF-THICK and NCF-THIN structures, respectively. This intermediate behaviour was expected, since there is more extensive subcritical damage than in NCF-THIN laminated but, since the damage is aligned with the loading direction, its propagation will be slower and less pronounced than in NCF-THICK laminates. However, these are only preliminary results and should be complemented with more experimental data because:

1. only one specimen per laminate was tested due to schedule problems

2. the specimens were only subjected to 50k cycles which revealed insufficient to reach the defined failure criteria: reduction of 10% in the specimen's stiffness. In fact, NCF-THIN, NCF-THICK and NCF-HYBRID specimens only suffered a stiffness reduction of 2.486 %, 5.196 % and 3.231%, respectively, after 50k cycles. The remaining specimens should be tested until the failure criteria is reached, so that a more valid comparison between lay-ups can be made.

3. the load and displacement peaks in each cycle were obtained using the information provided by the testing machine's LVDT and therefore, the accuracy of the results might be compromised since sliding might not have been successfully avoided using sandpaper. This does not invalidate the comparison because all the specimens were subjected to the same gripping method and loading conditions but can, however, suggest that the specimens are more damaged than they actually are. The remaining open-hole fatigue specimens should be instrumented with strain gages, so that, the test results are more accurate.

4. only one specimen geometry was planned. It would be interesting to analyse the size effect not only in open-hole tension tests but also in open-hole fatigue tests.

4.2 Experimental results - STF T700SC/M21

This section is dedicated to the experimental tests results of STF T700SC/M21 lay-ups. To simplify the analysis, the lay-ups are, once again, presented below in table 4.9. Note that all plies are symmetric, quasi-isotropic and have the same in-plane properties.

All plies of STF-THIN lay-up have nominal ply thickness of 0.08 mm (0.160 per bi-angle layer). All plies of NCF-THICK lay-up have nominal thickness of 0.120 mm (0.240 mm per bi-angle layer). NCF-HYBRID lay-up has thicker central layers than the outer layers: there are two (0°/90°) and two (45°/-45°) 0.240 mm thick layers and four (0°/90°) and four (45°/-45°) 0.160 mm thick layers.

Table 4.9: STF T700SC/M21 lay-ups (160 g/m² STF; 240 g/m² STF)

Laminate ID	Lay-up	t (mm)
STF-THIN	$[(0/90)/(+45/\text{-}45)]_{3s}$	1.92
STF-THICK	$[(0/90)/(+45/\text{-}45)]_{2s}$	1.92
STF-HYBRID	$[((0/90)/(+45/\text{-}45))_2/(0/90)/(+45/\text{-}45)]_s$	2.24

4.2.1 Unnotched tension test results

The remote stress-displacement relations for plain strength tension of laminates STF-THIN, STF-THICK and STF-HYBRID tests are presented in fig. 4.26. All specimens exhibited linear response up to failure. This suggests that there is little severe transverse cracking before failure and that failure is fibre-dominated.

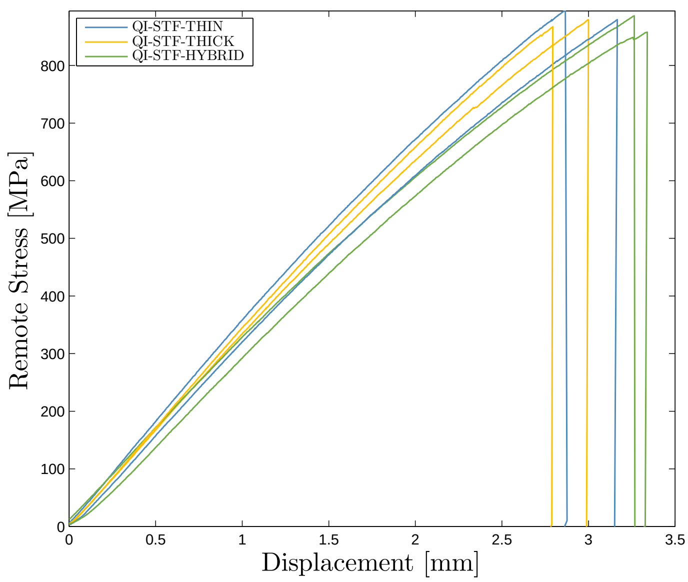

Figure 4.26: Unnotched tension remote stress-displacement relations for STF-THIN, STF-THIN and STF-HYBRID lay-ups.

Representative unnotched tension specimens after testing are shown in figs. 4.27 and 4.28. Some specimens failed in two places due to catastrophic failure characteristic of CFRP. STF-THIN specimens exhibit brittle net-section failure and the failure section is perpendicular to the loading direction. STF-THICK and STF-HYBRID specimens exhibit a pull-out failure mode with some splitting and delamination. The different failure modes are related to the ply thickness of the fabric used each lay-up. While lay-up NCF-THIN is from 160 g/m^2 STF, NCF-THICK is made from 240 g/m^2 STF. The plies in-situ strengths are, therefore, lower in NCF-THICK lay-up which triggers delamination onset, splitting and pull-out.

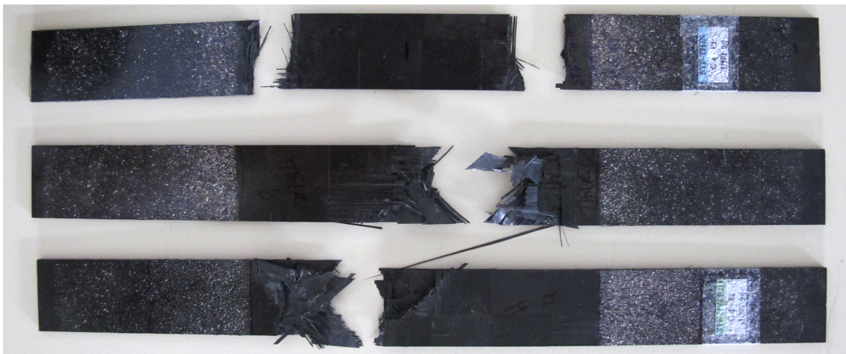

Figure 4.27: Representative STF-THIN (above), STF-THICK (middle) and STF-HYBRID (below) specimens after testing

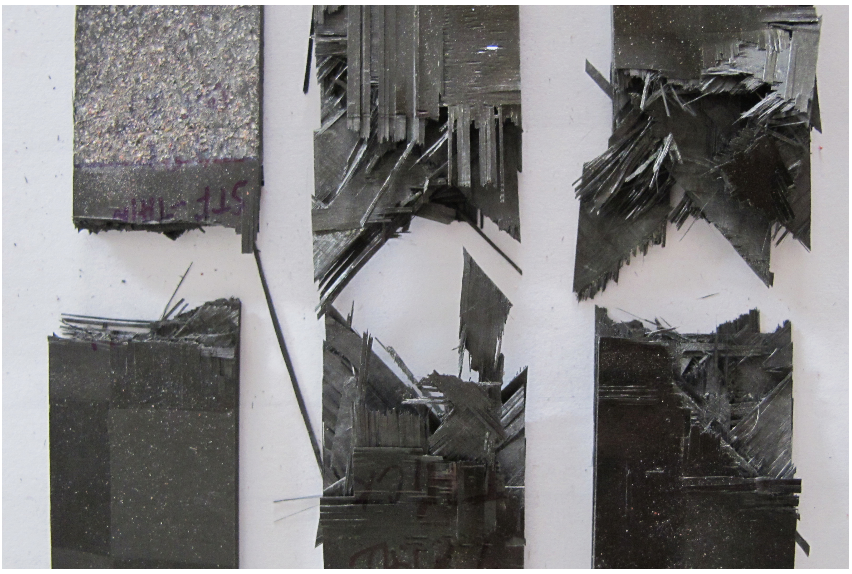

Figure 4.28: Close-up of the fracture plane of representative STF-THIN (left), STF-THICK (middle) and STF-HYBRID (right) specimens after testing

The mean values and standard deviation of the unnotched tension tests for lay-ups STF-THIN, STF-THICK and STF-HYBRID are presented in table 4.2. Even though five tests per laminate configuration were planned, some specimens tested failed within the grips, and were, therefore, not considered valid. STF-THIN specimens presented 1.57% higher unnotched strength than STF-THICK specimens. STF-HYBRID exhibit 1.70% and 0.14% lower unnotched strength than STF-THIN and STF-THICK specimens, respectively.

Table 4.10: Unnotched tension results for lay-ups STF-THIN, STF-THICK and STF-HYBRID

Property	Type	Nr valid tests	Mean Value [MPa]	STDV
X_T^L	STF-THIN	2	887.36	10.79
	STF-THICK	2	873.57	8.30
	STF-HYBRID	2	872.31	20.18

Digital image correlation was during one test per laminate configuration to monitor the longitudinal strain field on the surface of the specimens. Figures 4.29a, 4.29b and 4.29c show the longitudinal strain just before failure on STF-THIN, STF-THICK and STF-HYBRID specimens, respectively. The specimens were loaded in the horizontal direction. Note that, even though the ultimate strength of the specimens presented in figures 4.29a, 4.29b and 4.29c was not considered valid because they failed within the grips (despite being in good agreement with the unnotched strength of the respective laminate), this does not invalidate the comparison between the three laminates.

As explained before, the longitudinal strain along two lines near the specimen's borders are shown in the right bottom images of each figure. Although no transverse cracks appeared in the outer ply of the specimens, the strain field near the free edges is less homogeneous and exhibits more strain concentrations in STF-THICK laminate than in STF-THIN and STF-HYBRID laminates. This suggests that STF-THICK should exhibit a lower unnotched strength than STF-THIN and STF-HYBRID lay-ups since the transverse cracks should be more likely to appear, eventually leading to premature failure of the specimens. However, the experimental results do not corroborate this tendency clearly since, STF-THIN specimens revealed an only slightly higher unnotched tensile strength that STF-THICK specimens. More experimental tests should, therefore, be performed to confirm the unnotched tensile strength of the three laminates. The elastic properties of each laminate were calculated using the Classical Lamination Theory and the results obtained are presented in table 4.3.

Table 4.11: Elastic properties of STF-THIN, STF-THICK and STF-HYBRID calculated using the Classical Lamination Theory

Laminate	E_y [GPa]	E_x [GPa]	ν_{xy}	G_{xy} [GPa]
STF-THIN	49.78	49.78	0.311	18.98
STF-THICK	49.78	49.78	0.311	18.98
STF-HYBRID	49.78	49.78	0.311	18.98

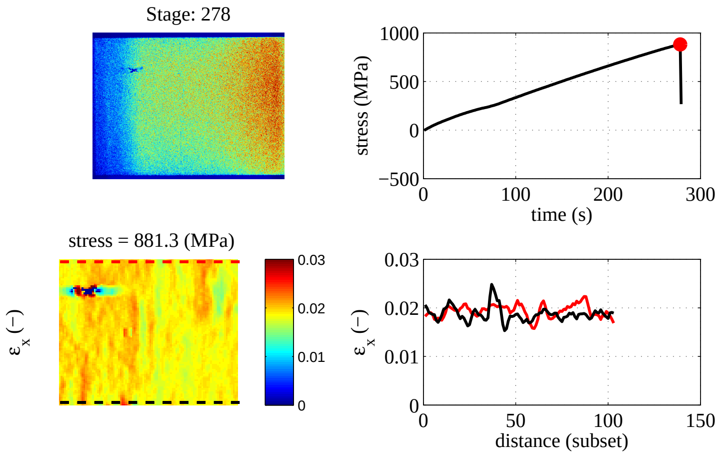

(a) STF-THIN

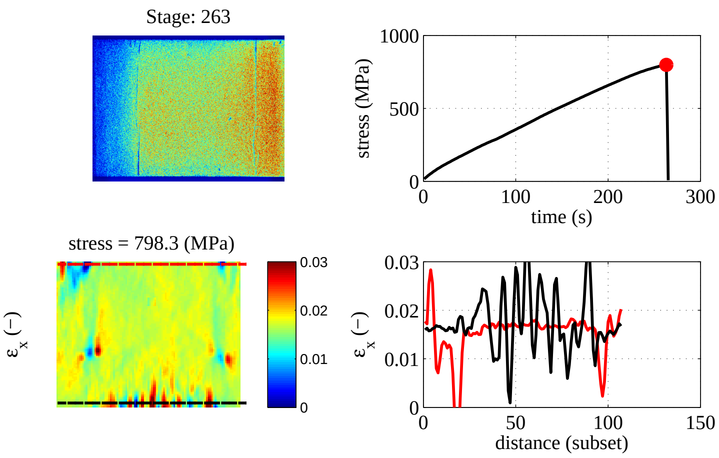

(b) STF-THICK

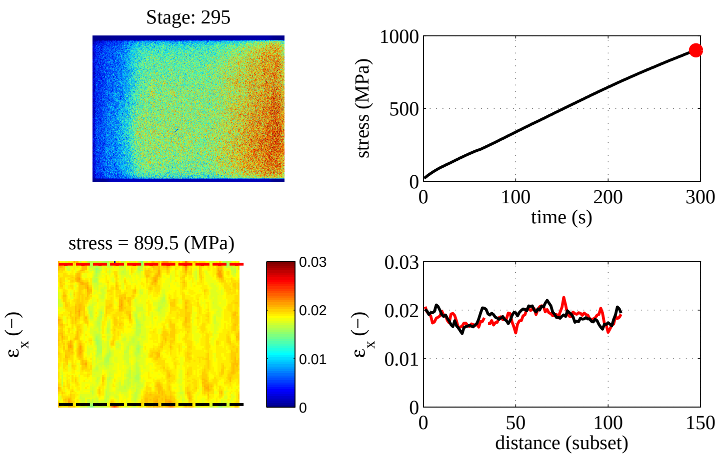

(c) STF-HYBRID

Figure 4.29: Longitudinal strain field for STF T700SC/M21 lay-ups

4.2.2 Open-hole tension test results

In this study, and as mentioned in chapter 3, the notched strength of three lay-ups of STF T700SC/M21 was accessed by testing specimens with hole diameters of $d = 2mm$, $d = 5mm$ and $d = 8mm$ and with hole diameter-to-width ratio of $d/W = 1/6$. The experimental results of the open-hole tension tests performed will be presented hereafter. Although three tests per laminate configuration and per geometry were planned, one STF-THICK specimen failed within the grips and were, for this reason, not considered valid. The results obtained for this specimen will not be addressed.

The remote stress-displacement relations for open-hole tension tests of laminates STF-THIN, STF-THICK and STF-HYBRID are presented in fig. 4.30, 4.31 and 4.32. For open-hole tension tests, all the laminates exhibit almost linear behaviour up to failure. Representative open-hole tension specimens after testing are shown in figs. 4.33a, 4.33b and 4.33c. The failure surface of all specimens is perpendicular to the applied load. STF-THICK and STF-HYBRID specimens exhibit a more irregular fracture surface with some pull-out. No extensive delamination is observed.

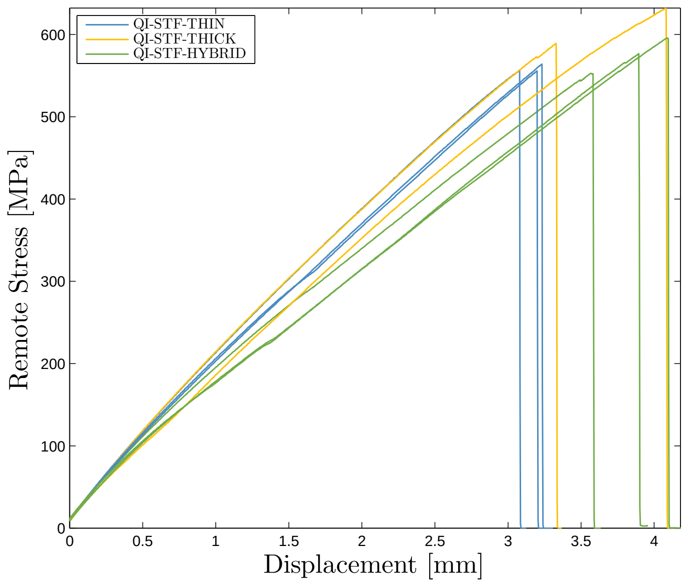

Figure 4.30: Open-hole tension remote stress-displacement relations for $d = 2mm$ for STF-THIN, STF-THIN and STF-HYBRID lay-ups.

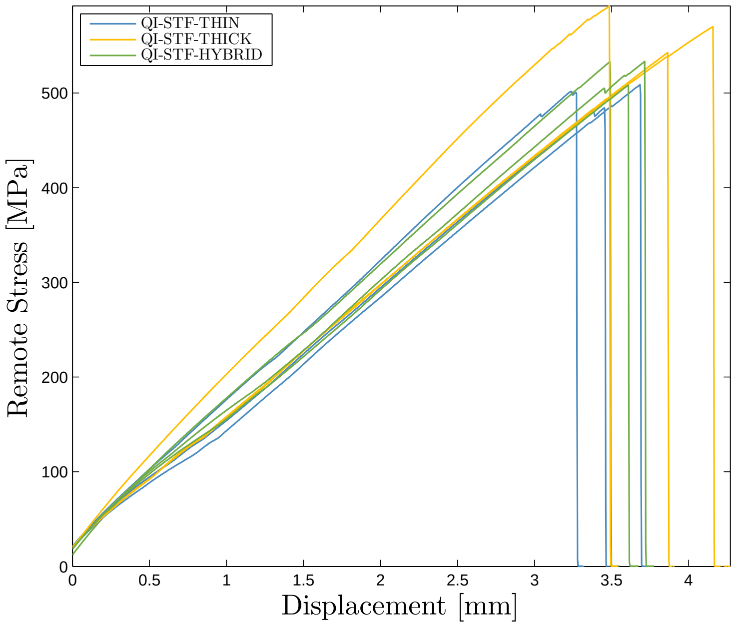

Figure 4.31: Open-hole tension remote stress-displacement relations for d = 5mm for STF-THIN, STF-THIN and STF-HYBRID lay-ups.

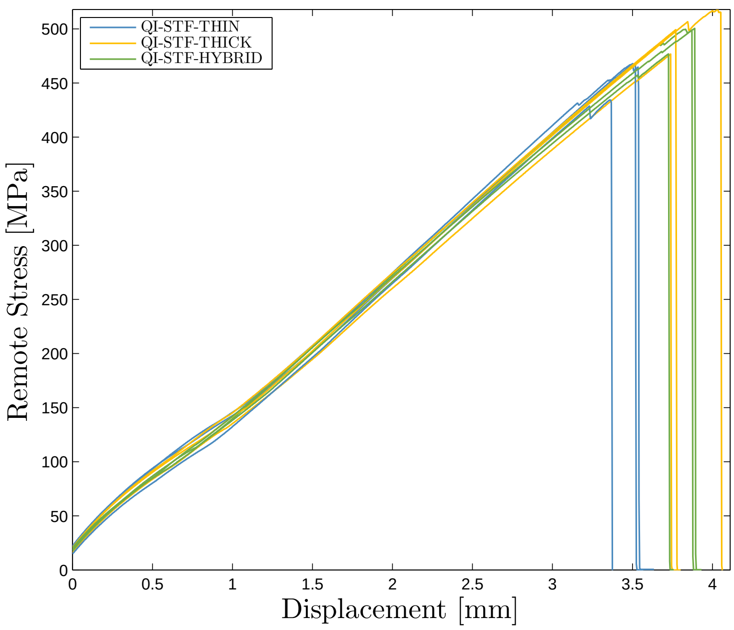

Figure 4.32: Open-hole tension remote stress-displacement relations for d = 8mm for STF-THIN, STF-THIN and STF-HYBRID lay-ups.

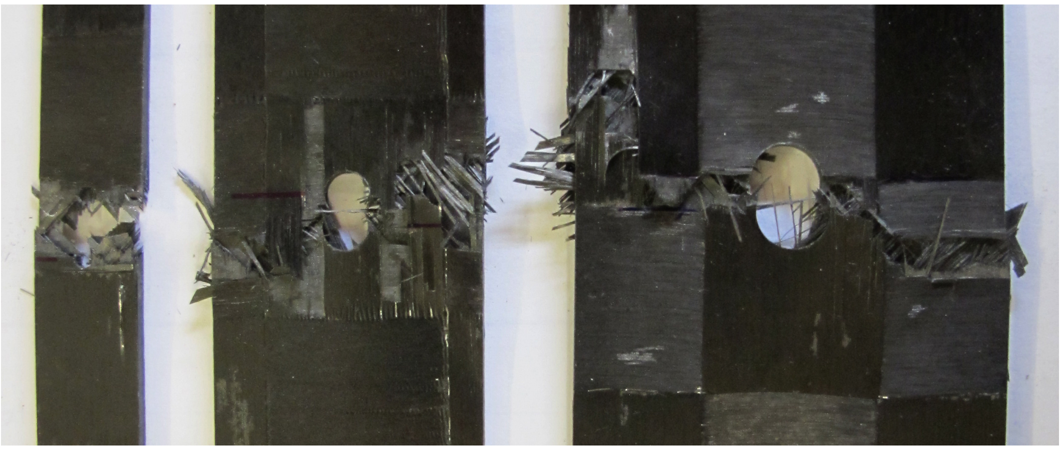

(a) STF-THIN

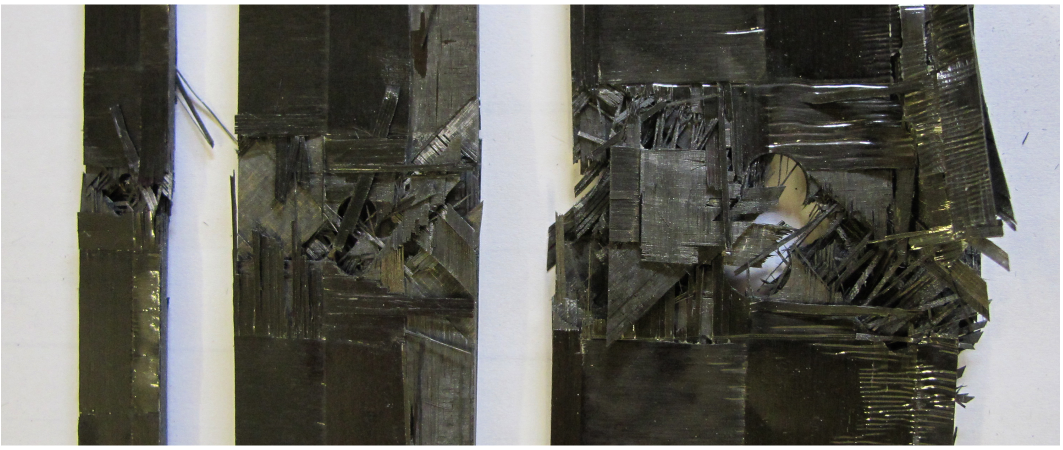

(b) STF-THICK

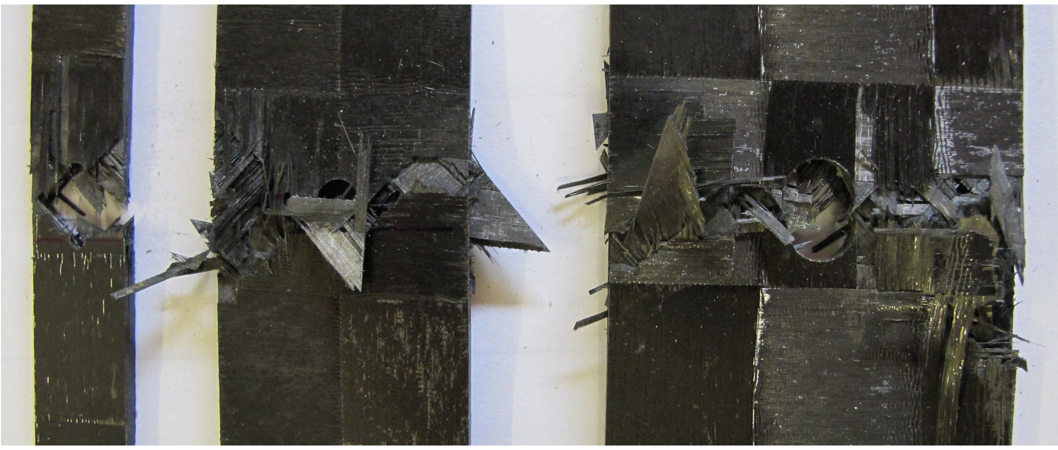

(c) STF-HYBRID

Figure 4.33: Representative STF T700SC/M21 open-hole specimens after testing

The mean values and standard deviation of the open-hole tests are presented in table 4.12 and fig. 4.34. As expected[35] [4], thin-ply structures exhibit lower notched strength than thick-ply structures. In fact, STF-THICK lay-up exhibits 9.3 %, 14.04% and 7.62 % higher notched strength than STF-THIN lay-up for d=2mm, d=5mm and d=8 mm, respectively.

In general, the selected hybrid lay-up revealed to have higher notched strength that STF-THIN lay-up and lower notched strength than STF-THICK lay-up:

- For d=2mm, STF-HYBRID specimens exhibited 2.92% higher notched strength that STF-THIN and 5.84% lower that STF-THICK specimens.
- For d=5mm, STF-HYBRID specimens exhibited 5.35% higher notched strength that STF-THIN and 7.62% lower that STF-THICK specimens.
- For d=8mm, STF-HYBRID specimens exhibited 6.22% higher notched strength that STF-THIN and 1.30% lower that STF-THICK specimens.

This intermediate behaviour can be explained by the type of ply hybridization of STF-HYBRID lay-up. In this lay-up, unlike NCF-HYBRID lay-up where only the 0^o plies had double the thickness of the rest of the laminate, two ($0^o/90^o$) and (45^o/-45^o) plies are made from 240 g/m^2 STF while the rest of the laminate is made from 160 g/m^2 STF. While the "thin" part of the laminate should be able to delay subcritical damage before failure, the "thick" part of the laminate is responsible for redistributing the stresses at the vicinity of the notch, reducing the stress concentration. Its behaviour in the presence of stress concentrations is, therefore, better when compared to a STF-THIN specimens and, as stress redistribution is not as effective, worse than for STF-THICK specimens.

Table 4.12: Open-hole test results for lay-ups STF-THIN, STF-THICK and STF-HYBRID

Property	Type	d [mm]	Nr valid tests	Mean Value [MPa]	STDV
	STF-THIN	2	3	557.73	4.36
$\overline{\sigma}_T^{\infty}$	STF-THICK	2	2	609.6	30.23
	STF-HYBRID	2	3	574.01	21.47
	STF-THIN	5	3	497.68	12.77
$\overline{\sigma}_T^{\infty}$	STF-THICK	5	3	567.92	15.5
	STF-HYBRID	5	3	524.15	14.62
	STF-THIN	8	3	462.68	7.47
$\overline{\sigma}_T^{\infty}$	STF-THICK	8	3	497.92	21.39
	STF-HYBRID	8	3	491.47	13.29

In table 4.12 and fig. 4.34 the same tendency reported in section 4.1.2 can be noted: the notched strength of the specimens increases as the hole diameter decreases. A reduction in hole diameter from 8 mm to 2 mm results in an increase of 20.54%, 22.43 % and 16.79% of the notched strength for STF-THIN, STF-THICK and STF-HYBRID lay-ups, respectively. As explained in section 4.1.2, in smaller specimens the length of the fracture process zone is not negligible when compared

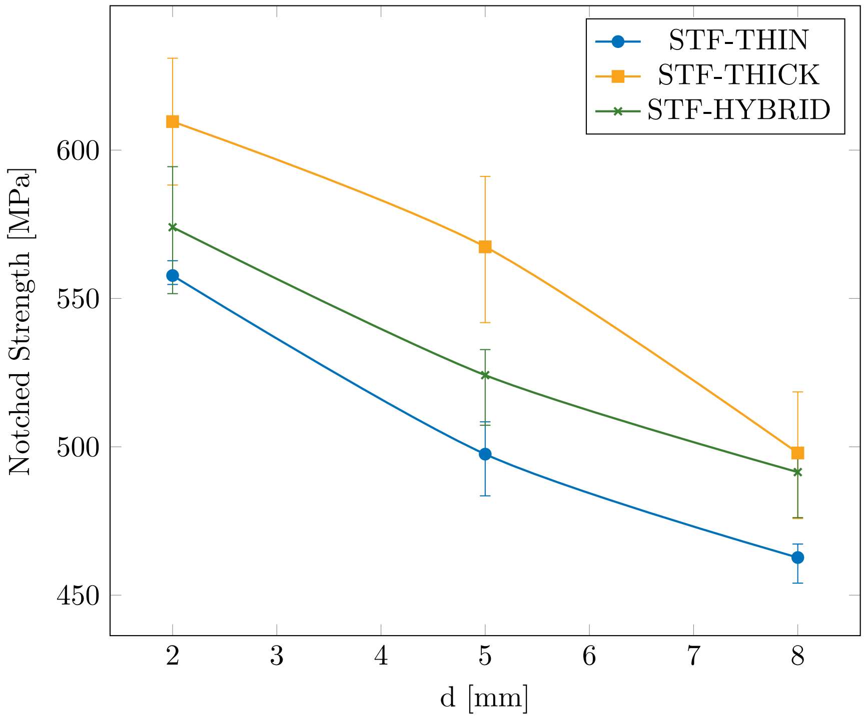

Figure 4.34: Notched strength vs hole diameter for lay-ups STF-THIN, STF-THICK and STF-HYBRID

to the in-plane dimensions of the specimen and therefore, stresses near the hole are redistributed more effectively than in larger specimens. As a consequence, smaller specimens tend to be more notch insensitive than larger specimens.

Digital image correlation was used during one test per geometry and per laminate configuration to monitor the evolution of the strain field and to access the formation of cracks at the vicinity of the holes. The specimens were loaded up to 90% of their notched strength will be inspected using X-ray. Figures 4.35, 4.36 and 4.37 show the strain field on the surface of the specimens when they are loaded at 90% of their notched strength. The bottom right images show the longitudinal strain along two lines positioned near the hole. It was not possible to obtain the strain field of STF-THICK specimens with d=2mm, but the a picture of the vicinity of the hole is shown in figures 4.36a and 4.36b. In STF-THIN specimens no discontinuity of the longitudinal strain along those lines can be identified and therefore, it can be concluded that no cracks appeared at the vicinity of the holes (fig.4.35a, 4.35b and 4.35c). Unlike in STF-THIN specimens, in STF-THICK and STF-HYBRID specimens with d=5mm (fig. 4.36d and 4.37b, respectively), a crack appeared in the vicinity of the hole. As shown in figure in figures 4.36a and 4.36b, a crack also appeared at the vicinity of the hole in STF-THICK specimen with d=2mm. Even though this is only reported for specimens with d=2mm and d=5mm, it suggests that cracks are more likely to appear in STF-THICK and STF-HYBRID specimens which justifies the enhanced notched strengths reported when compared to STF-THIN specimens.

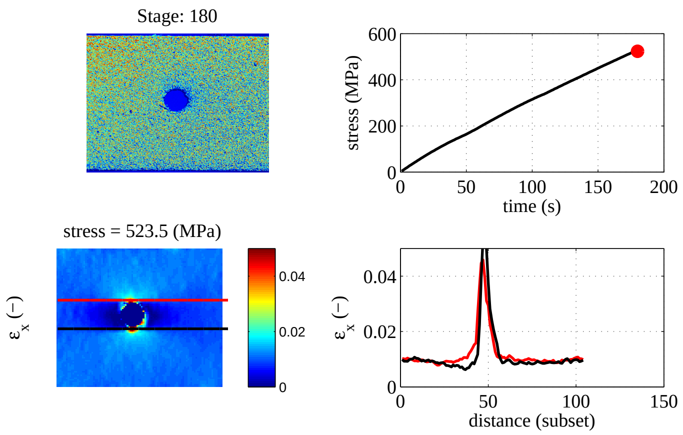

(a) STF-THIN d=2mm

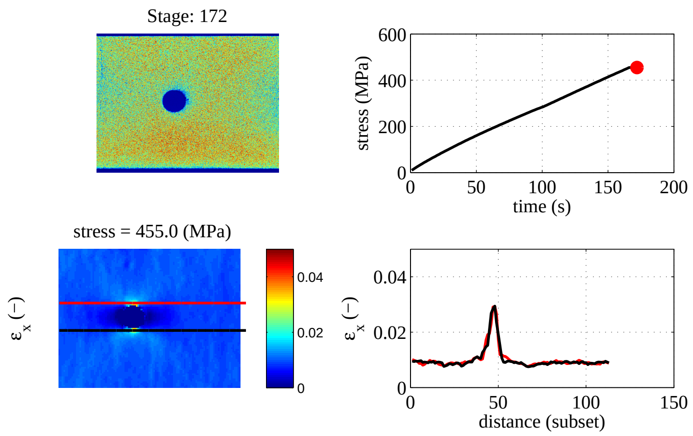

(b) STF-THIN d=5mm

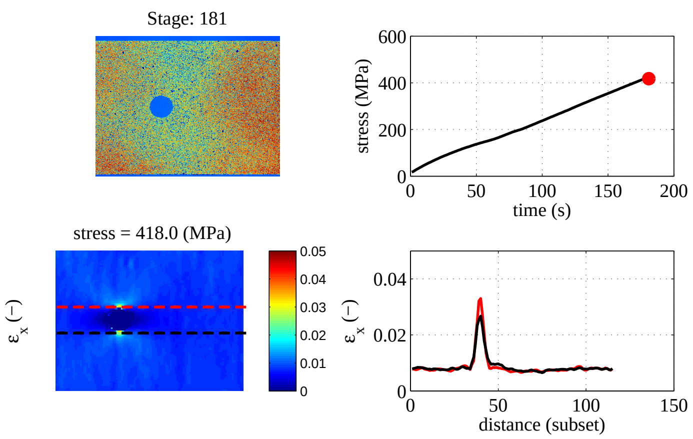

(c) STF-THIN d=8mm

Figure 4.35: Longitudinal strain field of STF-THIN specimens at 90% of their failure stress

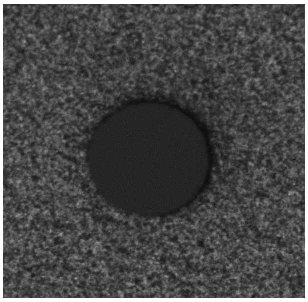

(a) Vicinity of the hole in STF-THICK specimen (d=2mm) before the appearance of a crack

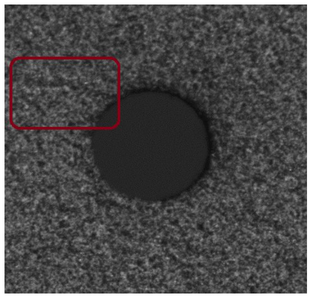

(b) Vicinity of the hole in STF-THICK specimen (d=2mm) after the appearance of a crack

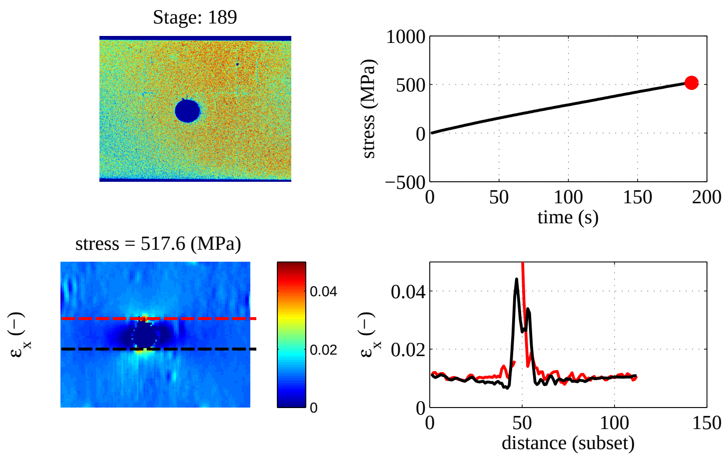

(c) STF-THICK d=5mm

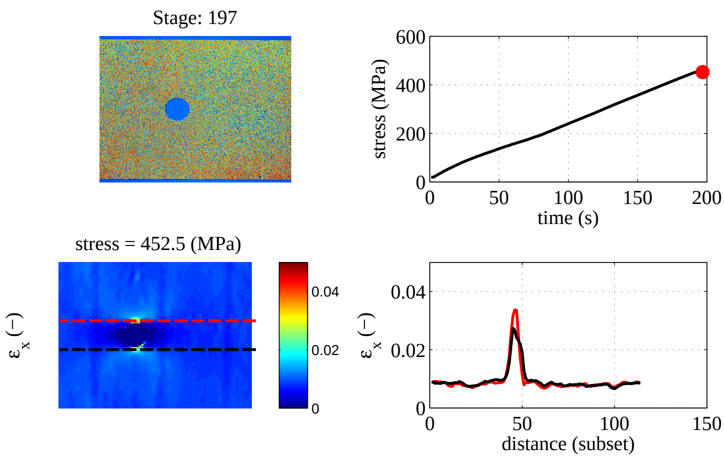

(d) STF-THICK d=8mm

Figure 4.36: Longitudinal strain field of STF-THICK specimens at 90% of their failure stress

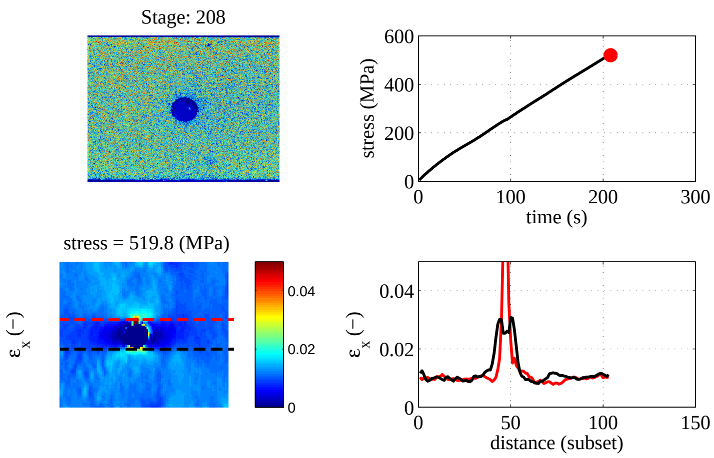

(a) *STF-HYBRID d=2mm*

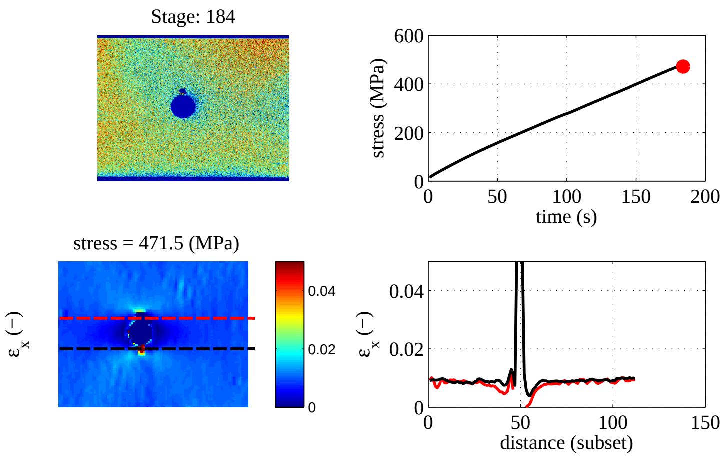

(b) *STF-HYBRID d=5mm*

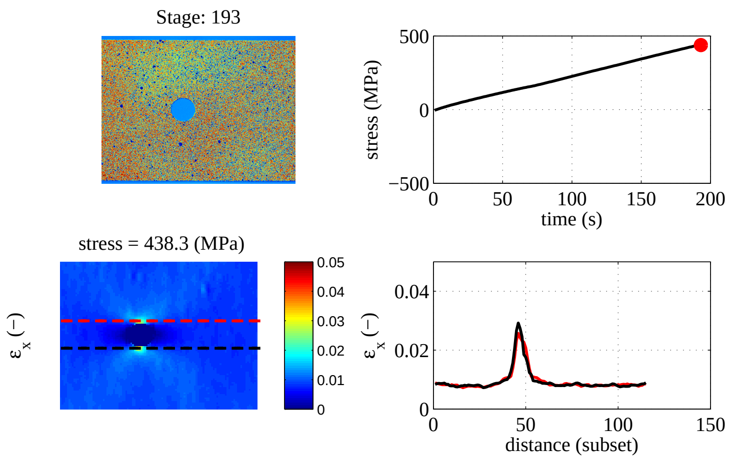

(c) *STF-HYBRID d=8mm*

Figure 4.37: Longitudinal strain field of STF-HYBRID specimens at 90% of their failure stress

In fig. 4.38 the normalized notched strength defined as $\overline{\sigma}_N = \overline{\sigma}_T^{\infty}/X^L$ is presented as a function of the hole diameter for the three STF lay-ups. Allied to the experimental results, two different types of behaviour are are pointed out in black: notch sensitivity which corresponds to a brittle behaviour where the normalized notched strength is defined as $\overline{\sigma}_N = 1/K_T$ and notch insensitivity which corresponds to a ductile behaviour and where the normalized notched strength of the laminate is defined as $\overline{\sigma}_N = 1 - 2R/W$. For diameter-to-width ratio equal to $2R/W = 1/6$, these parameters are the same as the ones presented in section 4.1.2: $\overline{\sigma}_N = 1/K_T = 0.32316$ for notch sensitivity and $\overline{\sigma}_N = 1 - 2R/W = 0.8333$. Analysing fig. 4.38 it can be accessed that STF-THICK lay-up exhibits a more ductile response that both STF-THIN and STF-HYBRID lay-ups. For the geometries studied, it appears that NCF-THICK lay-up is more sensitive to the increase of hole diameter, since its normalized notch strength decreases more rapidly than for the other lay-ups.

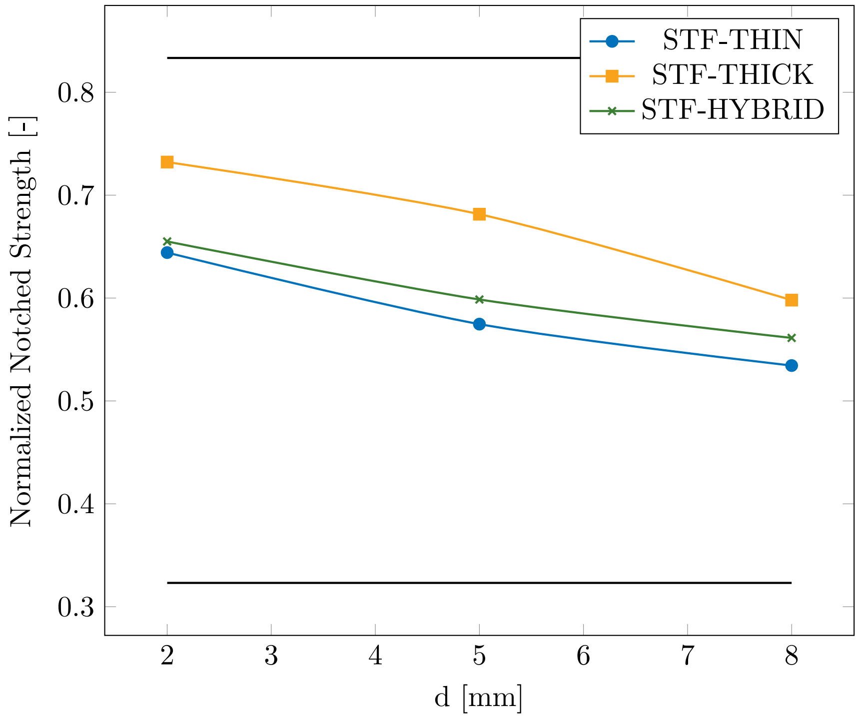

Figure 4.38: Normalized notched strength vs hole diameter for lay-ups STF-THIN, STF-THICK and STF-HYBRID

4.2.3 Open-hole fatigue test results

Open hole fatigue tests were performed to three lay-ups of STF T700SC/M21 to compare the evolution of damage in the three lay-ups. The specimen's hole diameter is $d = 5mm$ and $d/w = 1/6$ as shown in table 3.6. As mentioned in section 4.1.3, although three tests per laminate configuration were planned, only one was performed due to schedule problems. For this reason, the results presented hereafter, serve only as preliminary results.

The reduction of stiffness during the tests is shown in figure 4.39. As presented in table 4.13 STF-THIN, STF-THICK and STF-HYBRID specimens suffered a stiffness reduction of 1.206 %, 6.404 % and 3.286%, respectively.

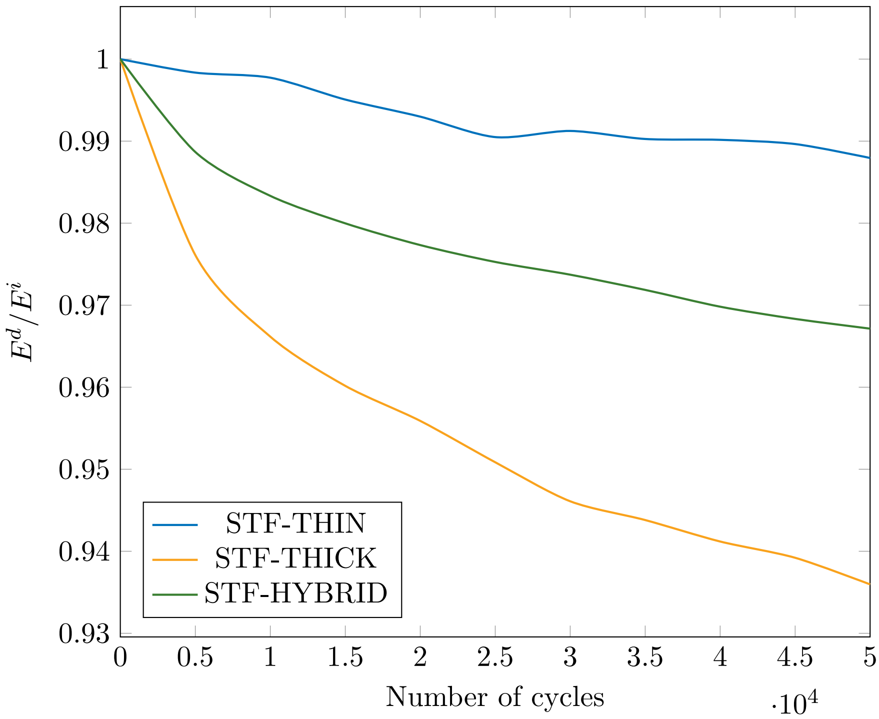

Figure 4.39: Reduction of stiffness during the open-hole fatigue tests to STF-THIN, STF-THICK and STF-HYBRID specimens

Table 4.13: Open-hole fatigue test results for lay-ups STF-THIN, STF-THICK and STF-HYBRID

Type	$\overline{\sigma}_T^\infty$ [MPa]	$\sigma^{max} = 0.7\overline{\sigma}_T^\infty$ [MPa]	Nr valid tests	Modulus reduction after 50k cycles
STF-THIN	497.5	348.3	1	1.206 %
STF-THICK	567.4	397.2	1	6.404%
STF-HYBRID	524.2	366.9	1	3.286%

While there is no visible damage in STF-THIN specimen, STF-THICK and STF-HYBRID specimens show some split cracking near the hole as shown in figures 4.40 and 4.41. The damage is more pronounced in STF-THICK specimen which can explain the less tolerance to fatigue loadings it exhibited. The specimens will be inspected using X-ray, so that, a better insight of the extent and type of damage present in each specimen can be accessed.

As expected, STF-THIN specimen show enhanced resistance to fatigue loadings compared to STF-THICK specimen because they exhibit less subcritical damage prior to failure and therefore, damage propagation is slower and less pronounced. STF-HYBRID, exhibited an intermediate response to fatigue loading.

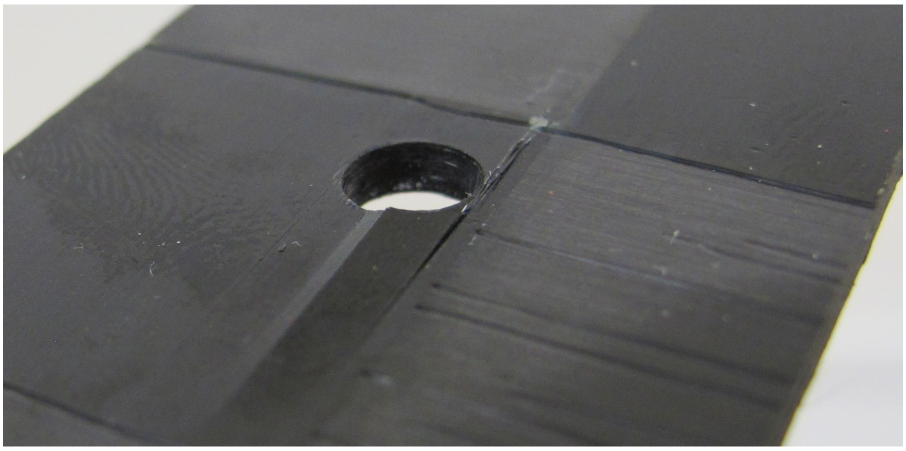

Figure 4.40: STF-THICK specimen after fatigue loading

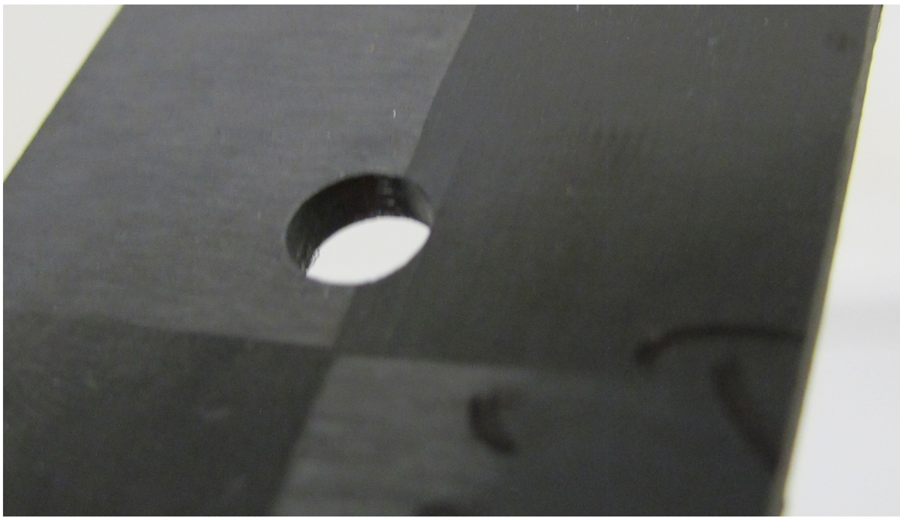

Figure 4.41: STF-HYBRID specimen after fatigue loading

4.2.4 Double edge crack test results

Double edge crack tests with widths of $w = 5mm$, $w = 10mm$, $w = 15mm$, $w = 20mm$ and $w = 25mm$ and notch length-to-width of $a/w = 3/5$ (see table 3.8) were performed to the three STF T700SC/M21 lay-ups in order to characterize the size effect law required to obtain the crack resistance curve of the three lay-ups.

The remote stress-displacement relations for double edge crack tests of laminates STF-THIN, STF-THICK and STF-HYBRID are presented in fig. 4.42, 4.43, 4.44, 4.45 and 4.46. Similarly to NCF T700GC/M21 lay-ups, specimens with $2w = 10mm$, $2w = 20mm$ specimens exhibit linear response up to failure, while specimens with $2w = 30mm$, $2w = 40mm$ and $2w = 50mm$ exhibit linear behaviour with some load drops before final failure.

Representative double edge notch specimens are shown in figures 4.47a, 4.47b and 4.47c.

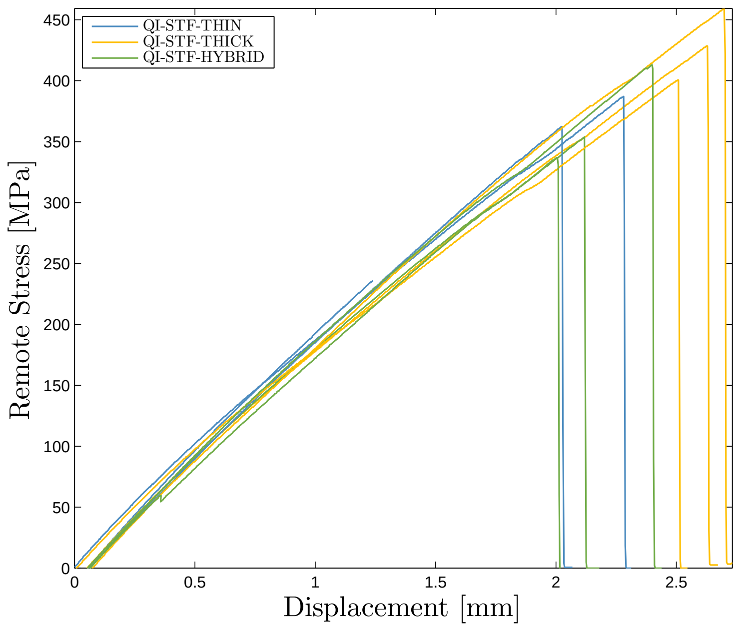

Figure 4.42: Double edge crack remote stress-displacement relations for $2w = 10mm$ for STF-THIN, STF-THIN and STF-HYBRID lay-ups.

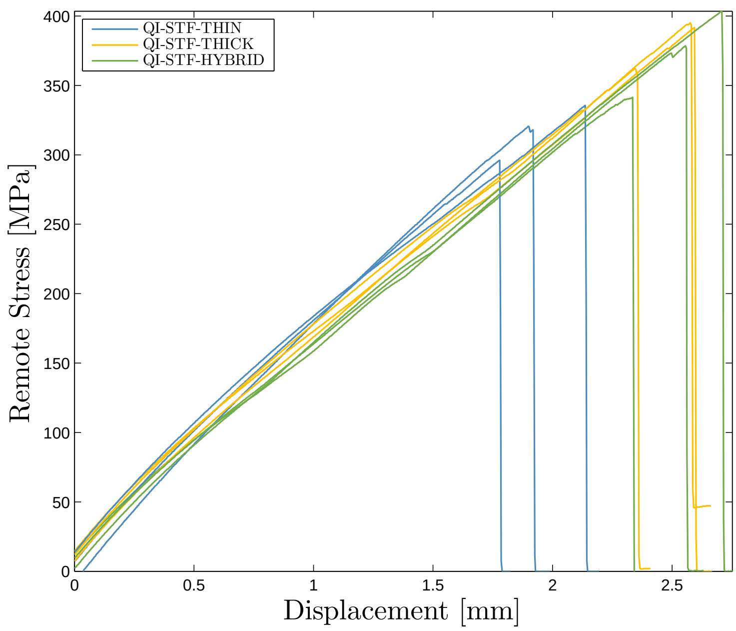

Figure 4.43: Double edge crack remote stress-displacement relations for $2w = 20mm$ for STF-THIN, STF-THIN and STF-HYBRID lay-ups.

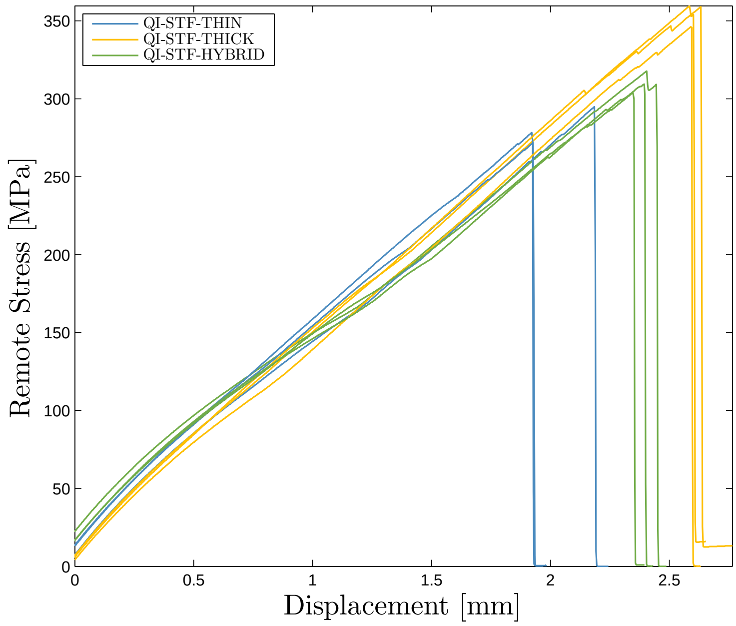

Figure 4.44: Double edge crack remote stress-displacement relations for $2w = 30mm$ for STF-THIN, STF-THIN and STF-HYBRID lay-ups.

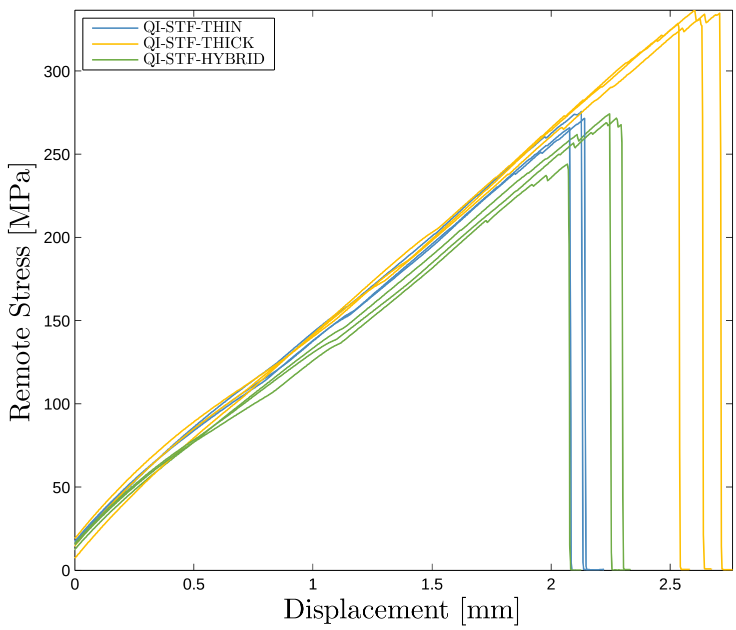

Figure 4.45: Double edge crack remote stress-displacement relations for $2w = 40mm$ for STF-THIN, STF-THIN and STF-HYBRID lay-ups.

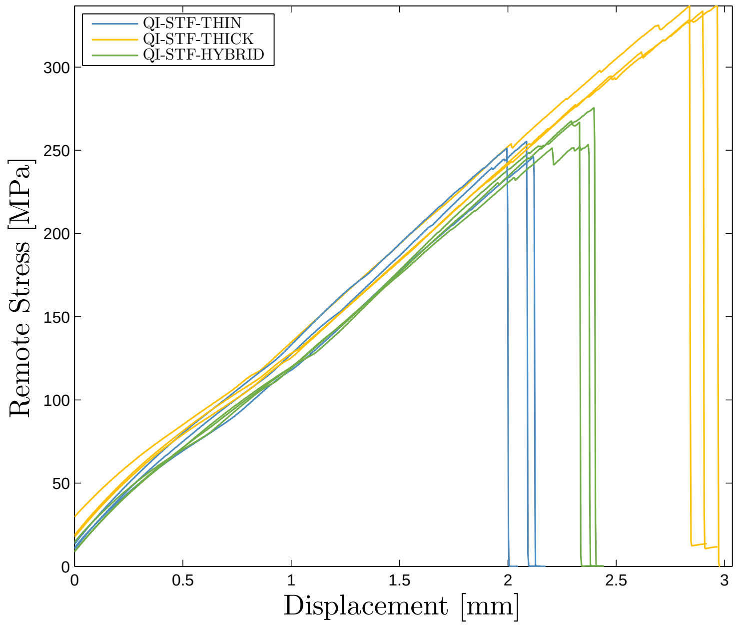

Figure 4.46: Double edge crack remote stress-displacement relations for $2w = 50mm$ for STF-THIN, STF-THIN and STF-HYBRID lay-ups.

The mean values and standard deviation of the double edge crack tests are presented in table 4.14 and fig. 4.48. Between the linear regression I and linear regression II [12] (see section 3.4.4), the regression which best fits the experimental data was determined for each laminate configuration. The three regressions are presented in figures 4.23 and 4.24. The size effect that best fits the experimental data is the linear regression I for STF-THIN and STF-HYBRID lay-ups and linear regression II for STF-THICK lay-up. The fitting parameters are shown in table 4.7. As explained in section 3.4.4, knowing the size effect law and the elastic properties of the laminate, the steady-state value of the R-curve (R_{ss}) and the length of the fracture process zone (l_{fpz}) can be calculated as shown in table 3.7. The elastic properties of the laminate were calculated using the Classical Lamination Theory and are presented in table 4.11. The R-curve parameters R_{ss}, l_{fpz}, γ and β for lay-ups STF-THIN, STF-THICK and STF-HYBRID are shown in table 4.8 and the R-curves are presented in 4.25. Note that the R-curve the analytical expression for the R-curve is:

$$R(\Delta a) = R_{ss}\left[1 - (1 - \gamma\Delta a)^{\beta}\right] \tag{4.2}$$

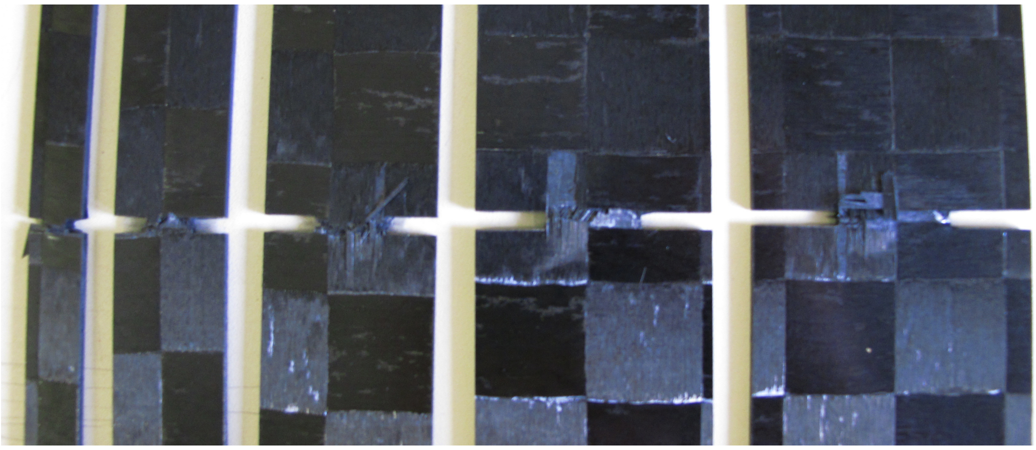

(a) STF-THIN

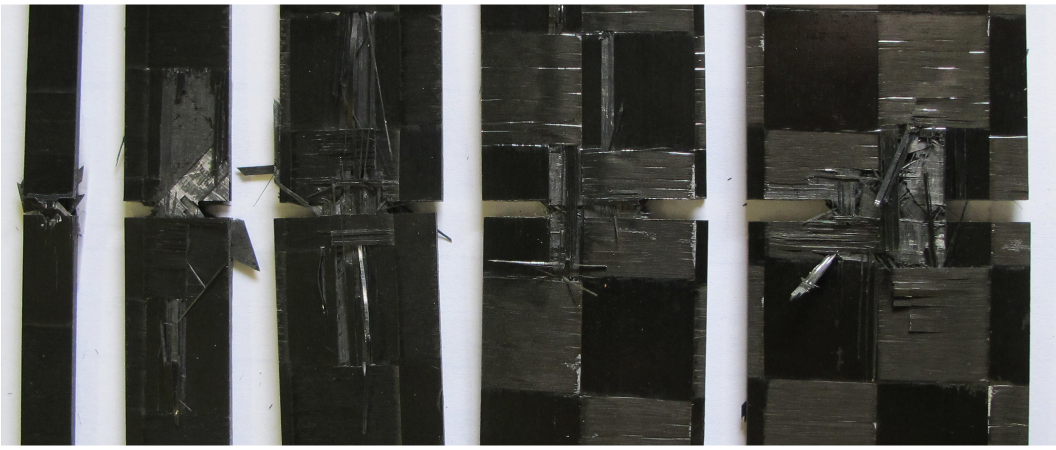

(b) STF-THICK

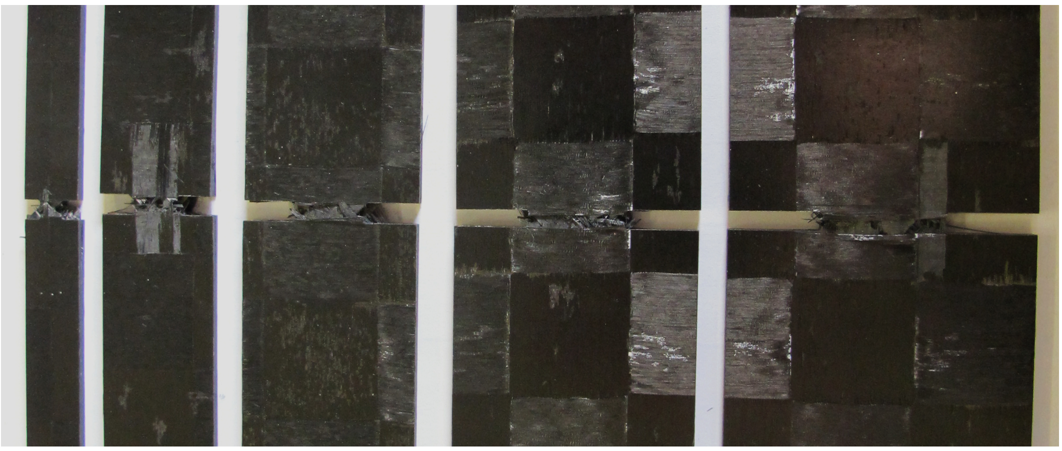

(c) STF-HYBRID

Figure 4.47: Representative STF T700SC/M21 double edge crack specimens after testing

Table 4.14: Double edge crack test results for lay-ups STF-THIN, STF-THICK and STF-HYBRID

Property	Type	2w [mm]	Nr valid tests	Mean Value [MPa]	STDV
$\overline{\sigma}_T^\infty$	STF-THIN	10	3	361.72	24.99
	STF-THICK	10	3	429.22	29.88
	STF-HYBRID	10	3	369.28	37.81
$\overline{\sigma}_T^\infty$	STF-THIN	20	3	317.05	19.99
	STF-THICK	20	3	382.53	17.88
	STF-HYBRID	20	3	377.27	26.42
$\overline{\sigma}_T^\infty$	STF-THIN	30	3	281.66	11.96
	STF-THICK	30	3	354.72	7.44
	STF-HYBRID	30	3	310.28	6.71
$\overline{\sigma}_T^\infty$	STF-THIN	40	3	270.69	4.89
	STF-THICK	40	3	332.98	3.93
	STF-HYBRID	40	3	263.08	16.81
$\overline{\sigma}_T^\infty$	STF-THIN	50	3	250.70	4.47
	STF-THICK	50	3	335.21	1.933
	STF-HYBRID	50	3	265.15	11.16

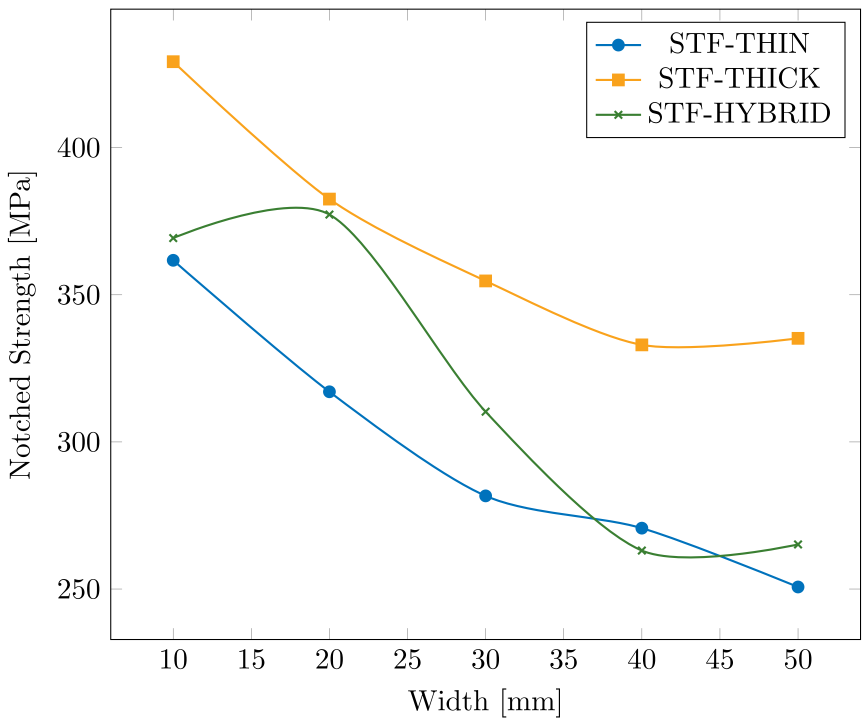

Figure 4.48: Notched strength vs width for for lay-ups STF-THIN, STF-THICK and STF-HYBRID

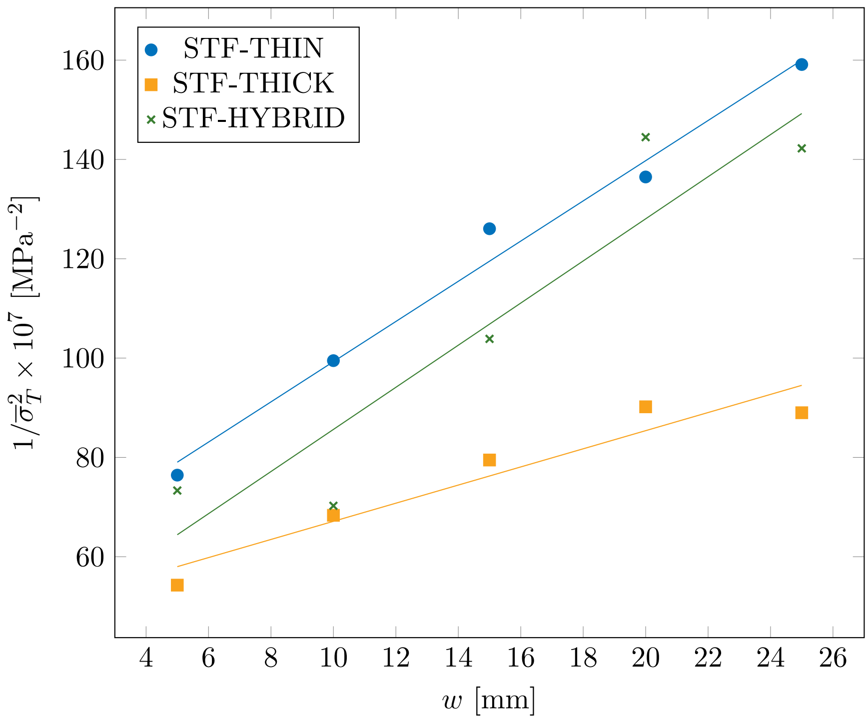

Figure 4.49: Size effect law: Experimental results and linear regression I fitting for STF-THIN, STF-THICK and STF-HYBRID laminates

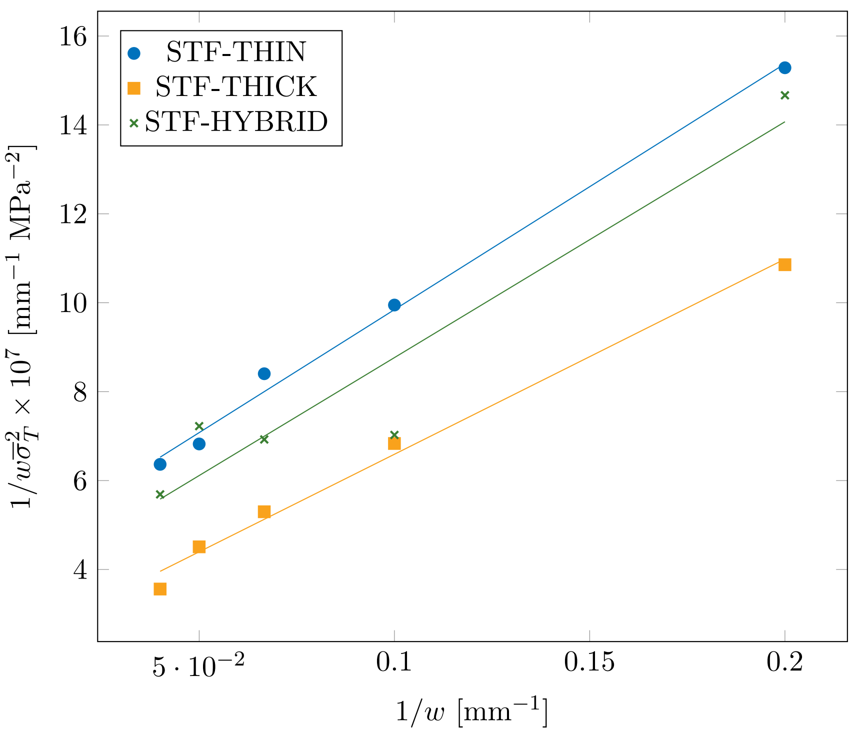

Figure 4.50: Size effect law: Experimental results and linear regression II fitting for STF-THIN, STF-THICK and STF-HYBRID laminates

Table 4.15: Best fitting parameters of the size effect law for STF-THIN, STF-THICK and STF-HYBRID lay-ups

Laminate	Best fitting	A [MPa^{-2} mm^{-1}]	C [MPa^{-2}]	R^2
STF-THIN	LR I	4.0471×10^{-7}	5.8803×10^{-6}	0.9853
STF-HYBRID	LR I	4.2406×10^{-7}	4.3227×10^{-6}	0.8747
Laminate	Best fitting	A [MPa^{-2}]	C [MPa^{-2} mm^{-1}]	R^2
STF-THICK	LR II	4.322×10^{-7}	2.202×10^{-6}	0.9916

Table 4.16: Parameters of the R-curves of STF-THIN, STF-THICK and STF-HYBRID lay-ups

Laminate	R_{ss} [kJ/m^2]	l_{fpz}	γ [mm^{-1}]	β
STF-THIN	140.64	4.756	0.1655	4.156
STF-THICK	258.48	6.425	0.1199	4.268
STF-HYBRID	134.222	3.3367	0.239	4.05

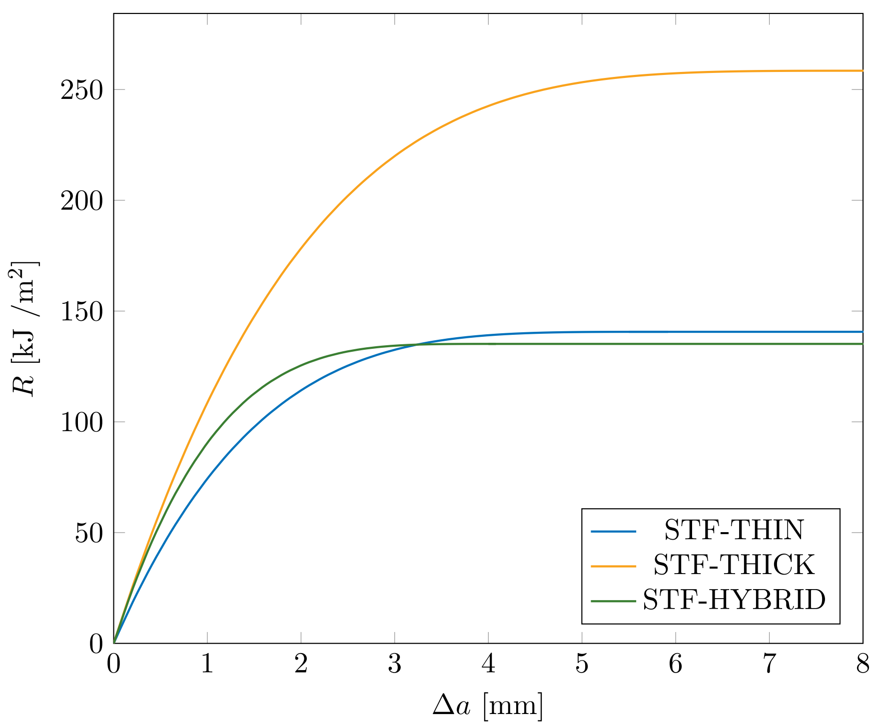

Figure 4.51: R-curves of STF-THIN, STF-THICK and STF-HYBRID lay-ups

4.2.5 Concluding remarks

Analysing the experimental data, it can be concluded that there are no relevant differences between the unnotched tensile strength of the three STF laminates. STF-THICK specimens exhibit a less homogeneous strain field and more strain concentrations near the specimen's free edges which suggests that transverse cracks are more likely to appear in this laminate and, therefore, its unntoched tensile strength should be lower than those of STF-THIN and STF-HYBRID lay-ups. Since only 2 specimens per laminate configuration were considered valid, more unnotched tensile tests should be performed to confirm the values obtained.

When loaded in tension, STF-THICK notched specimens show enhanced resistance when compared to STF-THIN and STF-HYBRID specimens since they are more likely to develop subcritical damage near the notches. While the appearance of damage near the hole will allow the redistribution of stresses and the reduction of stress concentrations in static loadings, it will hasten damage propagation in fatigue loadings.

STF-HYBRID structure is more notch tolerant than STF-THIN but less than STF-THICK structures. This intermediate behaviour can be explained by the type of ply hybridization of STF-HYBRID lay-up: it has 66.6% of 0.160 mm thick plies and 33.3% of 0.240 mm plies. While the "thin" part of the laminate should be able to delay subcritical damage before failure, the "thick" part of the laminate is responsible for redistributing the stresses at the vicinity of the notch, reducing the stress concentrations. This is valid for both static and fatigue loadings. In fact, STF-HYBRID showed 48.69% higher and 172.56% lower resistance to stiffness reduction than STF-THICK and STF-THIN specimens, respectively. Open-hole fatigue tests results serve as preliminary results for the same reasons presented in section 4.1.5.

Chapter 5

Analysis Methods

The process of selecting the material, geometry and lay-up of composite structures with stress concentrations requires the prediction of their notched strength. This prediction needs to be physically-based, accurate and, so that the process is effective, fast. Especially during preliminary design and optimization, the predictions should be obtained fast and rely as little as possible on experimental tests, since they are costly and time-consuming. Non-linear finite elements method can be used to predict notched strength of composite laminates, however, the process is time consuming and, therefore, avoided as a preliminary design and sizing tool. The Point Stress model and the Average Stress model [27] and the Inherent Flaw model [40] are predictions methods used to calculate notched strength of laminates composites and come as an alternative to FE models. The Point Stress model, the Average Stress model are stress-based criteria: the first one predicts failure when the stress in a point at a given distance from the notch reaches the material's unnotched strength, and the second predicts failure when the average stress from the notch tip up to a characteristic distance reaches the material's unnotched strength. These models flaw because they all rely on calibration from a baseline specimen to calculate the "characteristic distance", thus adding unnecessary costs to the predictions. Moreover, since this calibration is not physically based, the predictions tend to be inaccurate for geometries different from the one used for calibration. The Finite Fracture Mechanics model [17] enriches the Average Stress model, including a energy-based criteria to the stress criteria already defined, thus, not requiring model calibration. In this chapter, the Finite Fracture Mechanics Model is explained with more detail. Predictions using the IFM, PS, AS and FFM models are made and the values obtained are compared with the available experimental results of open-hole strength for NCF T700GC/M21 lay-ups (NCF-THIN, NCF-THICK and NCF-HYBRID) and STF T700SC/M21 lay-ups (STF-THIN, STF-THICK and STF-HYBRID).

5.1 Finite Fracture Mechanics Model

Using the finite fracture mechanics model proposed by Camanho et al. [17] the fracture strength of notched composites that exhibits brittle or pull-out failure can be predicted fast and accurately. If the main failure mechanism is delamination, the model cannot be applied.

Fracture mechanics models assume that crack propagation is predicted when both stress-based and energy-based criteria are satisfied and that failure occurs by the propagation of kinematically admissible cracks with finite length, i.e. failure is predicted if when two conditions are simultaneous met:

1. The average stress ahead of the crack tip until the crack length l reaches the material unnotched strength

2. The energy needed to propagate the crack the distance l is equal to the fracture toughness of the material.

Other analytical models able to predict the notched strength of composite structures can be used, such as the Point Stress model [27], the Average Stress model [27] and the Inherent Flaw model [40]. Even tough these models appear to give good predictions of the remote failure stress of the laminate, they require calibration from a baseline specimen. In fact, a "characteristic distance" l^* , incorrectly identified exclusively as a material property, has to be determined experimentally which adds unnecessary costs to the predictions and will lead to inaccurate predictions since it is ill-defined as a geometry independent property.

The Finite Fracture Mechanics model has been used to predict the failure stress of composite structures with open-holes or cracks loaded in tension [17] and compression and to predict the large damage capability of notched composites [8]. The extensions of the Finite Fracture Mechanics Model to predict open-hole strength with ant without taking the R-curve into account will be presented hereafter.

5.1.1 Finite Fracture Mechanics for the prediction of open-hole strength

The failure criterion for composite structures with open holes loaded in tension as shown in fig.5.1 reads

$$\begin{cases} \frac{1}{l}\int\limits_{R}^{R+l} \sigma_{yy}(x,0)\,dx = X_T^L \\ \frac{1}{l}\int\limits_{R}^{R+l} K_I^2(a)\,da = K_{Ic}^2 \end{cases} \tag{5.1}$$

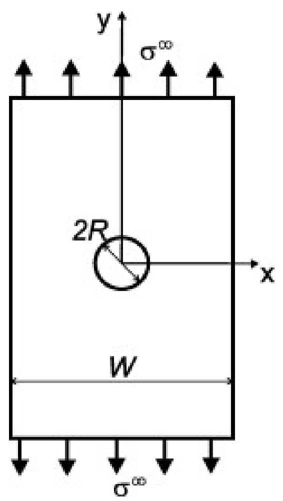

Figure 5.1: Notched laminate under tensile loading [17]

The first and second equations are the stress-based and energy-based criteria respectively. l is the crack length at failure, X_T^L is the unnotched strength of the laminate and K_{Ic} is the mode I fracture toughness of the laminate. The system of equations 5.1 has two equations and two unknowns (the crack length at failure l and the remote stress at failure $\overline{\sigma}^{\infty}$) and, therefore, unlike other models used to predict laminate failure ([27] and [40]), the model presented does not require the determination of a "characteristic distance" l^*.

1. **Stress-based criterion**

The stress distribution in the center of the laminate along the x direction reads:

$$\sigma_{yy}(x,0) = R_k \frac{\sigma^{\infty}}{2}\left[2 + \xi^2 + 3\xi^4 - (K_T^{\infty} - 3)(5\xi^6 - 7\xi^8)\right] \tag{5.2}$$

where $\xi = \frac{R}{x}$, σ^{∞} is the remote stress applied, K_T^{∞} is the stress concentration factor of an infinity plane with hole in the center and R_K is a finite width correlation factor. They read:

$$K_T^{\infty} = 1 + \sqrt{\frac{2}{A_{22}}\left(\sqrt{A_{11}A_{22}} - A_{12} + \frac{A_{11}A_{22} - A_{12}^2}{2A_{66}}\right)} \tag{5.3}$$

$$R_K = \frac{K_T}{K_T^{\infty}} = \left\{\frac{3(1-2R/W)}{2+(1-2R/W)^3} + \frac{1}{2}\left(\frac{2R}{W}M\right)^6 (K_T^{\infty} - 3)\left[1 - \left(\frac{2R}{W}M\right)^2\right]\right\}^{-1} \tag{5.4}$$

where A_{ij} are the elements of the in-plane stiffness matrix that can be calculated using the Classical Lamination Theory (section 6.1) and M is a parameter defined as:

$$M^2 = \frac{\sqrt{1 - 8\left[\frac{3(1-2R/W)}{2+(1-2R/W)^3} - 1\right]} - 1}{2(2R/W)^2} \tag{5.5}$$

2. **Energy-based criterion**

   The stress intensity factor for two symmetrical cracks that appear in the edges of the hole in a rectangular isotropic plate loaded in tension (figure 5.1) is given by

$$K_I = \sigma^{\infty} F_h F_w \sqrt{\pi a} \tag{5.6}$$

where,

$$F_w = \sqrt{\sec\left(\frac{\pi R}{W}\right)\sec\left(\frac{\pi a}{W}\right)} \tag{5.7}$$

$$F_h = \sqrt{1 - \frac{R}{a} f_n} \tag{5.8}$$

$$f_n = 1 + 0.358\lambda + 1.425\lambda^2 - 1.579\lambda^3 + 2.156\lambda^4 \tag{5.9}$$

with $\lambda = R/a$

In fact, laminates are not isotropic, but if the stacking sequence is such that the laminate exhibits a quasi-isotropic behaviour, equation 5.6 can be used.

The crack extension at failure l can be calculated solving the non-linear equation 5.10 that results from dividing the second equation of 5.1 by the square of the first one:

$$\frac{4l\pi \int\limits_{R}^{R+l} (F_h F_w)^2 a\, da}{R_K^2 \left\{ \int\limits_{R}^{R+l} \left[2+\xi^2+3\xi^4-(K_T^\infty-3)(5\xi^6-7\xi^8)\right]\, dx \right\}^2} = \left(\frac{K_{Ic}}{X_T^L}\right)^2 \tag{5.10}$$

Once l is determined, $\overline{\sigma}^\infty$ can be calculated using eq. 5.1.

5.1.2 Finite Fracture Mechanics for the prediction of open-hole strength (with R-curve)

Based on the finite fracture model proposed by Camanho et al. [17] and explained in section 5.1 a model do predict the residual strength of laminates with large though-thickness cracks is defined. As explained in 5.1, according to the finite fracture model proposed in [17], failure of composite structures with stress concentrations is predicted when an energy-based and a stress-based criterion are satisfied simultaneously. To predict the large damage capability of a material, the energy-based criterion should account for its R-curve [8] and, therefore, the failure criteria yields

$$\begin{cases} \frac{1}{l} \int\limits_{R}^{R+l} \sigma_{yy}(x,0)\, dx = X_T^L \\ \int\limits_{R}^{R+l} G_I(a)\, da = \int\limits_{0}^{l} R(\Delta a)\, d\Delta a \end{cases} \tag{5.11}$$

The first and second equations are the stress-based and energy-based criteria respectively. l is the crack length at failure, X_T^L is the unnotched strength of the laminate, $G_I(a)$ is the energy release rate and $R(\Delta a)$ is the R-curve, expressed in terms of the critical energy release rate. Both criteria will be explained with more detail hereafter.

1. **Stress-based criterion**

   The stress-based criterion suffers no modifications from the one explained in section 5.1.1.

2. **Energy-based criterion**

   According to [9] and [41] the energy release rate in mode I of a two-dimensional orthotropic body for a crack propagating in the x direction is given by:

$$G_I = \frac{1}{\acute{E}} K_I^2 \tag{5.12}$$

   where K_I is the stress intensity factor for two symmetrical cracks that appear in the edges of the hole in a rectangular isotropic plate loaded in tension given by 5.6 and $\acute{E}$ is the laminate's equivalent modulus given by

$$\acute{E} = \left(\frac{1+\rho}{2E_x E_y}\right)^{-1/2} \mu^{1/4} \tag{5.13}$$

with ρ and μ is given by

$$\rho = \frac{(E_x E_y)^{1/2}}{2G_{xy}} - (\nu_{xy}\nu_{yx})^{1/2} \tag{5.14}$$

and

$$\mu = \frac{E_y}{E_x} \tag{5.15}$$

Finally, the energy-based criterion of the finite fracture mechanics model (first member of the second equation of 5.11) reads

$$\int_R^{R+l} G_I(a)da = \frac{1}{\acute{E}}(\sigma^\infty)^2 \pi \int\limits_R^{R+l} (F_h F_w)^2 a\, da \tag{5.16}$$

To define the second member of the energy-based criterion, the R-curve of the material has to be determined. It reads

$$R(\Delta a) = \begin{cases} R_{SS}\left[1-(1-\zeta\Delta a)^\eta\right] & ,\Delta a \leq l_{fpz} \\ R_{SS} & \Delta a > l_{fpz} \end{cases} \tag{5.17}$$

where R_{SS}, l_{fpz}, ζ and η have to be determined experimentally as explained in section 3.4.4. After integration, 5.17 reads

$$\int_0^l R(\Delta a)d\Delta a = R_{0-l} = \begin{cases} R_{SS}\frac{\zeta l+\eta\zeta l+(1-\zeta l)^\eta-(1-\zeta l)^\eta\zeta l-1}{\zeta(\eta+1)} & ,l \leq l_{fpz} \\ R_{SS}\left[\frac{\zeta l_{fpz}+\eta\zeta l_{fpz}+(1-\zeta l_{fpz})^\eta-(1-\zeta l_{fpz})^\eta\zeta l_{fpz}-1}{\zeta(\eta+1)}+l-l_{fpz}\right] & ,l > l_{fpz} \end{cases} \tag{5.18}$$

Using equations 5.2, 5.16 and 5.18 in 5.11 and diving the second equation by the square of the first one it yields:

$$\frac{4l^2\pi \int\limits_R^{R+l} (F_h F_w)^2 a\, da}{\acute{E}R_K^2\left\{\int\limits_R^{R+l}\left[2+\xi^2+3\xi^4-(K_T^\infty-3)(5\xi^6-7\xi^8)\right]dx\right\}^2} = \frac{R_{0-l}}{(X_T^L)^2} \tag{5.19}$$

which has only one unknown l. Having determined l, the remote stress at failure can be determined using one of the equations in 5.11.

5.1.3 Material properties

The model proposed in [17] requires only the material's ply elastic properties (E_1, E_2, G_{12}, ν_{12}), which can be obtained following the ASTM D-3039 [1] and D-3518 standard [2] or calculated using the Classical Lamination Theory, the laminate unnotched strength (X_T^L) which can be obtained following the ASTM D-3039 [1] standard and the mode I fracture toughness (K_{IC}) or, to predict large damage capability, the material's R-curve. There are no standard methods to determine neither the mode I fracture toughness nor the R-curve of composite laminates, however, some methods are proposed.

An extension of the finite fracture mechanics model for specimens with central cracks can be used to calculate the material's fracture toughness. For this geometry the failure criteria reads

$$\begin{cases} \frac{1}{l}\int\limits_a^{a+l} \sigma_{yy}(x,0)\,dx = X_T^L \\ \frac{1}{l}\int\limits_a^{a+l} K_I^2(a)\,da = K_{Ic}^2 \end{cases} \tag{5.20}$$

The W/a ratio of the specimen should be large enough so that

$$\sigma_{yy}(x,0) = \frac{\sigma^{\infty} x}{\sqrt{x^2 - a^2}} \tag{5.21}$$

and

$$K_I = \sigma^{\infty}\sqrt{\pi a} \tag{5.22}$$

The remote stress at failure $\overline{\sigma}^{\infty}$ is measured and replaced in 5.21 and 5.22. These equations can now be used in 5.20, allowing the determination of both the crack length at failure l and the mode I laminate fracture toughness K_{IC}.

The fracture toughness can also be determined by inverse identification of an open-hole tension test result: an open-hole tensile test is performed, the remote stress obtained at failure and the unnotched tensile strength are then replaced in equation 5.1, allowing the determination of both the crack length at failure l and the mode I laminate fracture toughness K_{IC}.

The R-curve of a given laminate can be determined as proposed by Catalanotti et al. [18] and explained in section 3.4.4.

5.2 Open-hole tensile strength predictions

The experimental notched strength for ratio d/W=1/6 and d=2mm, d=5mm and d=8mm and the predictions obtained using the Point Stress, Average Stress, Inherent Flaw model and the Finite Fracture Mechanics models for NCF-THIN, NCF-THICK, NCF-HYBRID, STF-THIN, STF-THICK and STF-HYBRID lay-ups are presented in tables 5.1, 5.2 and 5.3, 5.4 and 5.5 and 5.6, respectively. The corresponding prediction curves are shown in figure 5.2 and 5.3.

Point Stress, Average Stress and Inherent Flaw models require calibration from a baseline specimen. The specimen used for calibration was the specimen with hole diameter equal to 5mm and, for this reason, the errors obtained for this geometry are either small or zero. However, for different geometries, the relative errors increase substantially, because this models wrongly assume that the "characteristic distance" l^* obtained for the baseline specimen is a geometry independent property. Based on the experimental data, in general, for smaller hole diameters, the notch strength is overpredicted and underpredicted for larger hole diameters.

Predictions based on the Finite Fracture Mechanics model were made with and without taking the R-curve into account. The traditional FFMs model requires the material's fracture toughness, which can be obtained from inverse identification of an experimental open-hole tension test result. Predictions using the both extensions of the model were performed:

- **Inverse identification of the material's fracture toughness using the experimental test results of open-hole tension tests with d=5mm:** in general, the predictions are in good agreement with the experimental results (relative errors below 11% for all lay-ups and geometries). For specimens with small in-plane dimensions as the ones tested, the errors associated with the predictions obtained using this method are within the range of what these models can usually deliver. Note that, even though this particular methodology might seem to lose its interest compared to PS, AS and IFM models because the fracture toughness is obtained by inverse identification of an open-hole test specimen, this serves, not as model calibration, but only as an alternative to determining the fracture toughness using a center crack or double edge crack specimen, which are usually more difficult to machine given the geometry of the notch.

- **Taking the R-curve into account:** This model is more physically accurate that the traditional one because it accounts for the bridging effect that delays unstable crack propagation and accounts for the variation of fracture toughness during the fracture process, rather than taking the fracture toughness as a constant material property. The errors of the predictions obtained accounting for the R-curve are below 14% for all specimen geometries and lay-ups, except for STF-THICK lay-up. For this lay-up the model seams to overpredict the notch strength (errors up to 16.25%), which might be caused by overprediction of the R-curve (note that R_{ss} for STF-THICK is 45 % and 48% higher than for STF-THIN and STF-HYBRID lay-ups, respectively). However, no anomalies were reported in the experimental results obtained for double edge crack specimens for STF-THICK lay-up , and therefore, up to date, there is no reason to consider its R-curve invalid. The material's R-curve is useful to predict large damage capability of composite laminates without loss of accuracy in predictions for smaller specimens and should, therefore, be a included in the experimental characterization programs. However, as the R-curve varies with the laminate's lay-up, as shown in chapter 4 and because obtaining the size effect law needed to calculate the R-curve requires a very extensive and costly set of experimental tests, preliminary lay-up selection should not rely on the its determination, unless the prediction of the notched strength of large specimens is a relevant requirement. Having selected the lay-up, preliminary optimization and design should be made taking the material's R-curve into account, because they allow obtaining accurate predictions within a few second, avoiding the time consuming and the computational effort of Finite Elements analysis.

Figures 5.4a and 5.4b show the normalized notched strength predictions and experimental results for diameter-to-width ratio of d/w=1/6 as a function of the hole diameter for NCF T700GC/M21 and STF T700SC/M21 lay-ups, respectively. The predictions were obtained using the the Finite Fracture Mechanics Model accounting for the R-curve and the normalized notched strength is defined as $\overline{\sigma}_N = \overline{\sigma}_T^{\infty}/X^L$. Two different types of behaviour are pointed out in black:

1. **Notch sensitivity**: the normalized notched strength of the laminate $\overline{\sigma}_N$ is a function only of the stress concentration factor K_T. It corresponds to a brittle behaviour. It reads

$$\overline{\sigma}_N = \frac{1}{K_T} \tag{5.23}$$

For $d/W = 1/6$, and for a quasi-isotropic lay-ups ($K_T^{\infty} = 3$), K_T yields:

$$K_T = K_T^{\infty} R_K = 3\left(\frac{3(1-d/W)}{2+(1-d/W)^3}\right)^{-1} = 3.0944$$

The normalized notch strengths is therefore $\overline{\sigma}_N = 1/K_T = 0.32316$ for notch sensitivity.

2. **Notch insensitivity**: the normalized notched strength of the laminate $\overline{\sigma}_N$ is a function of the geometry. It corresponds to a ductile behaviour. It reads

$$\overline{\sigma}_N = 1 - \frac{2R}{W} \tag{5.24}$$

For $d/W = 1/6$, $\overline{\sigma}_N = 1 - 2R/W = 0.8333$ for notch insensitivity.

The experimental data suggests that NCF-THIN, NCF-HYBRID and NCF-THICK lay-ups show increasing notch sensitivity and the predictions are able to capture this tendency, even if the errors associated with the predictions might be as high as 11%. The same tendency is reported for STF lay-ups: STF-THIN, STF-HYBRID and STF-THICK lay-ups show increasing notch sensitivity, even though the values obtained for STF-THICK lay-up seam to be overpredicted. This tendency is also captured by the FFM model. Finite fracture mechanics models are, therefore, able to capture subtle differences is laminate configuration for the same material system, if the material's R-curve, unnotched strength and elastic properties are known.

Table 5.1: Predictions for NCF-THIN lay-up with d/W=1/6, obtained using IFM, PS, AS and FFM model with and without taking the R-curve into account. IFM, PS and AS models were calibrated using the experimental result for d=5mm.

d		Exp.	IFM	PS	AS	FFM	FFM (R-curve)
2 mm	$\overline{\sigma}^{\infty}$ [MPa]	530.68	627.48	617.09	590.65	571.93	590.14
	Error	-	18.24%	16.28%	11.30%	9.66%	11.20%
5 mm	$\overline{\sigma}^{\infty}$ [MPa]	479.76	479.76	459.74	479.76	479.76	508.81
	Error	-	0.00%	-4.17%	0.00%	0.00%	6.06%
8 mm	$\overline{\sigma}^{\infty}$ [MPa]	444.76	406.91	390.33	421.66	422.58	453.02
	Error	-	-8.51%	-12.24%	-5.19%	-4.99%	1.86%

Table 5.2: Predictions for NCF-THICK lay-up with d/W=1/6, obtained using IFM, PS, AS and FFM model with and without taking the material's R-curve into account. IFM, PS and AS models were calibrated using the experimental result for d=5mm.

d		Exp.	IFM	PS	AS	FFM	FFM (R-curve)
2 mm	$\overline{\sigma}^{\infty}$ [MPa]	564.25	607.01	598.03	575.86	558.97	569.10
	Error	-	7.58%	5.99%	2.06%	-0.94%	0.86%
5 mm	$\overline{\sigma}^{\infty}$ [MPa]	490.62	490.62	470.15	490.62	490.63	529.61
	Error	-	0.00%	-4.17%	0.00%	0.00%	7.95%
8 mm	$\overline{\sigma}^{\infty}$ [MPa]	472.68	419.21	397.63	437.39	440.47	491.29
	Error	-	-11.31%	-15.88%	-7.47%	-6.81%	3.94%

Table 5.3: Predictions for NCF-HYBRID lay-up with d/W=1/6, obtained using IFM, PS, AS and FFM model with and without taking the material's R-curve into account. IFM, PS and AS models were calibrated using the experimental result for d=5mm.

d		Exp.	IFM	PS	AS	FFM 1	FFM (R-curve)
2 mm	$\overline{\sigma}^{\infty}$ [MPa]	584.48	659.57	650.04	624.71	608.44	610.37
	Error	-	12.85%	11.22%	6.88%	4.10%	4.43%
5 mm	$\overline{\sigma}^{\infty}$ [MPa]	526.92	526.92	504.94	526.92	526.93	541.04
	Error	-	0.00%	-4.17%	0.00%	0.00%	2.68%
8 mm	$\overline{\sigma}^{\infty}$ [MPa]	495.41	448.91	426.77	467.87	509.90	487.66
	Error	-	-9.39%	-13.86%	-5.56%	-5.04%	-1.56%

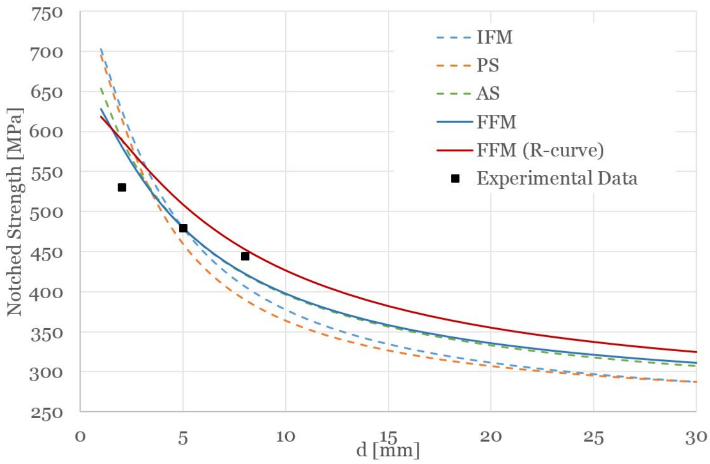

(a) NCF-THIN

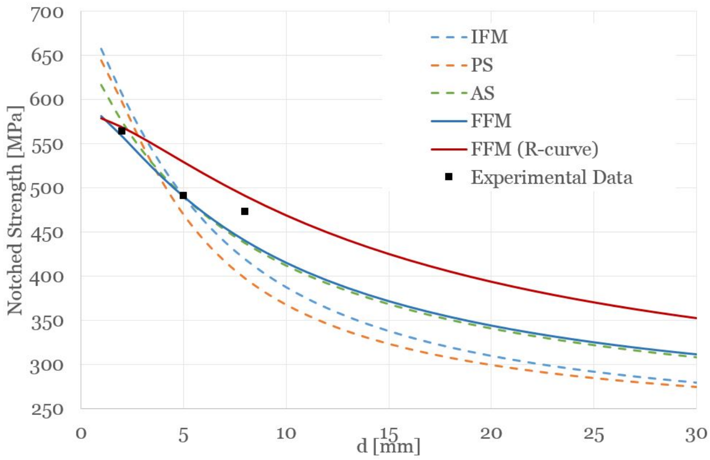

(b) NCF-THICK

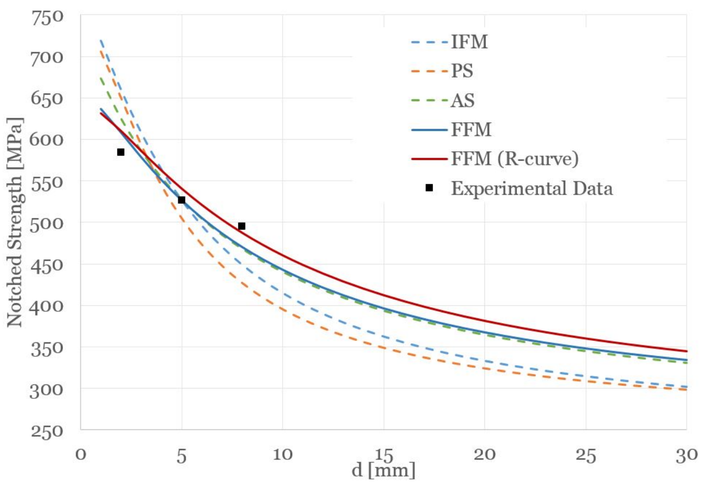

(c) NCF-HYBRID

Figure 5.2: Predictions for NCF T700GC/M21 lay-ups with d/W=1/6, obtained using IFM, PS, AS and FFM model with and without taking the material's R-curve into account.

Table 5.4: Predictions for STF-THIN lay-up with d/W=1/6, obtained using IFM, PS, AS and FFM model with and without taking the material's R-curve into account. IFM, PS and AS models were calibrated using the experimental result for d=5mm.

d		Exp.	IFM	PS	AS	FFM	FFM (R-curve)
2 mm	$\overline{\sigma}^{\infty}$ [MPa]	557.73	665.58	651.46	-	618.71	635.45
	Error	-	19.34%	16.81%	-	10.93%	13.97%
5 mm	$\overline{\sigma}^{\infty}$ [MPa]	497.53	497.53	476.77	-	497.53	536.80
	Error	-	0.00%	-4.17%	-	0.00%	7.89%
8 mm	$\overline{\sigma}^{\infty}$ [MPa]	462.68	423.31	408.19	-	437.58	474.87
	Error	-	-8.51%	-11.78%	-	-5.42%	2.64%

Table 5.5: Predictions for STF-THICK lay-up with d/W=1/6, obtained using IFM, PS, AS and FFM model with and without taking the material's R-curve into account. IFM, PS and AS models were calibrated using the experimental result for d=5mm.

d		Exp.	IFM	PS	AS	FFM	FFM (R-curve)
2 mm	$\overline{\sigma}^{\infty}$ [MPa]	609.60	718.51	708.14	679.42	663.86	683.01
	Error	-	17.87%	16.16%	11.45%	8.90%	12.04%
5 mm	$\overline{\sigma}^{\infty}$ [MPa]	567.40	567.40	543.73	567.40	567.41	628.82
	Error	-	0.00%	-4.17%	0.00%	0.00%	10.83%
8 mm	$\overline{\sigma}^{\infty}$ [MPa]	497.92	482.32	459.59	502.06	504.21	578.85
	Error	-	-3.13%	8.34%	0.83%	1.26%	16.25%

Table 5.6: Predictions for STF-HYBRID lay-up with d/W=1/6, obtained using IFM, PS, AS and FFM model with and without taking the material's R-curve into account. IFM, PS and AS models were calibrated using the experimental result for d=5mm.

d		Exp.	IFM	PS	AS	FFM	FFM (R-curve)
2 mm	$\overline{\sigma}^{\infty}$ [MPa]	574.01	685.45	674.12	-	635.70	648.95
	Error	-	19.41%	17.44%	-	10.75%	13.06%
5 mm	$\overline{\sigma}^{\infty}$ [MPa]	524.15	524.15	502.28	-	524.15	555.09
	Error	-	0.00%	-4.17%	-	0.00%	5.90%
8 mm	$\overline{\sigma}^{\infty}$ [MPa]	491.47	444.55	426.43	-	461.69	493.07
	Error	-	-9.55%	-13.23%	-	-6.06%	0.33%

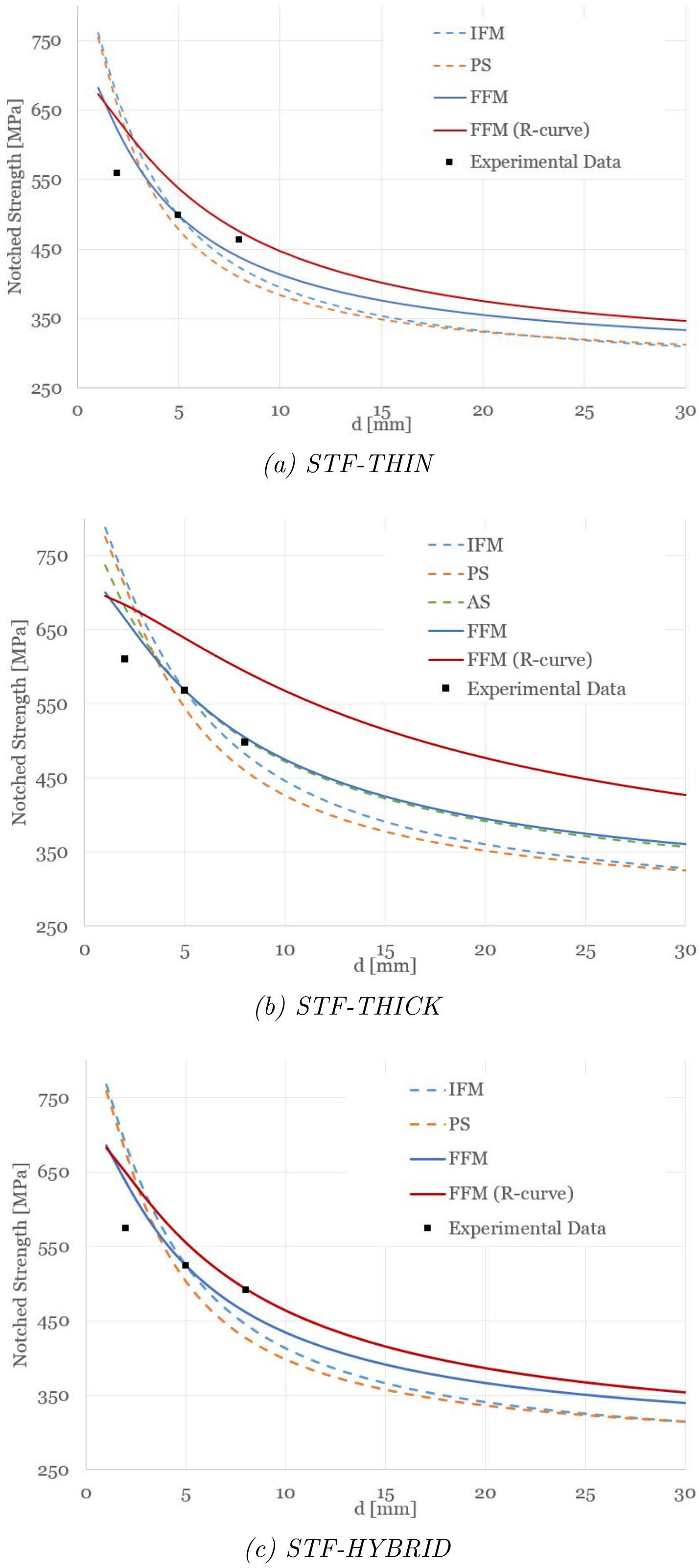

(a) STF-THIN

(b) STF-THICK

(c) STF-HYBRID

Figure 5.3: Predictions for STF T700SC/M21 lay-ups with d/W=1/6, obtained using IFM, PS, AS and FFM model with and without taking the material's R-curve into account.

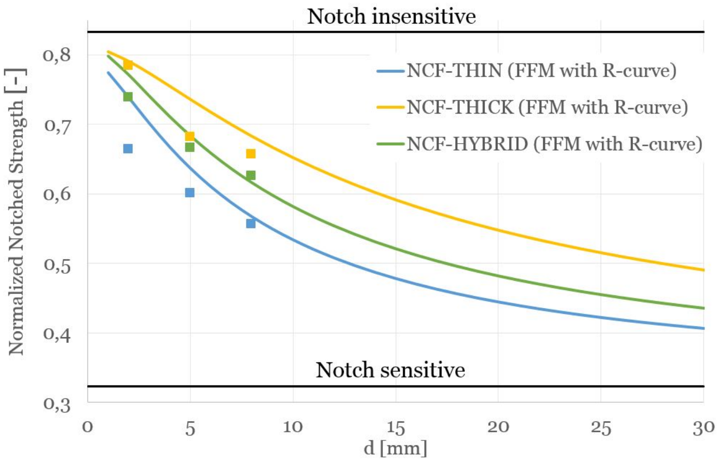

(a)

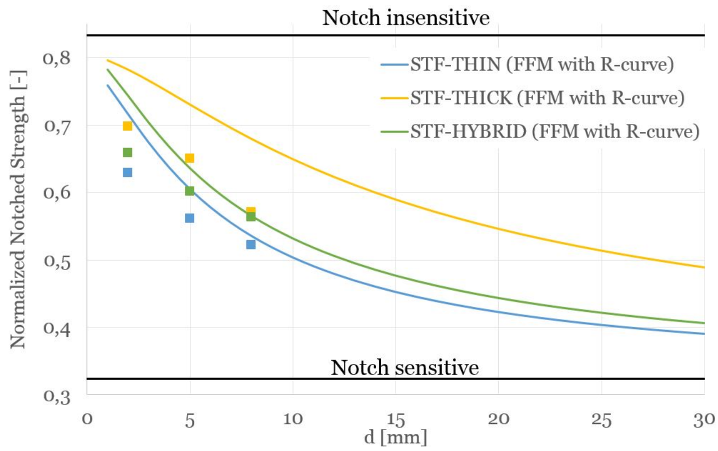

(b)

Figure 5.4: Normalized notched strength vs hole diameter for NCF T700GC/M21 (reffig:NCF-with-Rcurve) STF T700SC/M21 (5.4b) lay-ups and d/w=1/6: Experimental data and predictions using the FFM model taking the R-curve into account

5.3 Design Charts

As the finite fracture mechanics model is able to predict the remote stress fast and accurately, it can be used to produce design charts for a certain material and lay-up relying only on information about the material's elastic properties, unnotched strength and fracture toughness (or R-curve). In such design charts the normalized notch strength $\overline{\sigma}_N$ is given as a function of the hole diameter-to-width ratio d/W. Two limits are pointed out: notch sensitivity given by $\overline{\sigma}_N = \frac{1}{K_T}$ and notch insensitivity $\overline{\sigma}_N = 1 - \frac{2R}{W}$. The laminate behaviour and, therefore, the predictions obtained with the finite fracture mechanics model will be between the two limits.

The design charts for NCF-THIN, NCF-THICK, NCF-HYBRID, STF-THIN, STF-THICK and STF-HYBRID lay-ups together with the available experimental data (see chapter 4) are presented in figure 5.5. The predictions were obtained using the finite fracture mechanics model accounting for the R-curve of each laminate since it is the more physically accurate as it accounts for the increase of fracture toughness during the fracture process and, except for STF-THICK laminate, provided the more accurate predictions when compared to the available experimental data. It is not possible to make design charts made using IFM, PS and AS models because they require calibration from a baseline specimen for each diameter-to-width ratio, thus invalidating the purpose of the design tool.

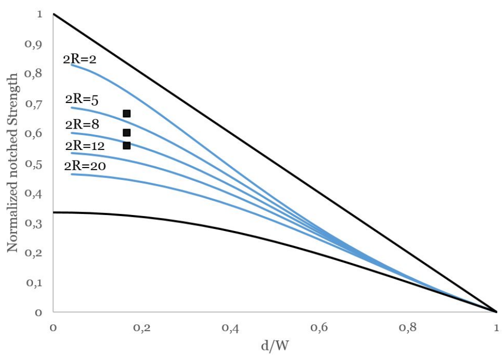

(a) NCF-THIN

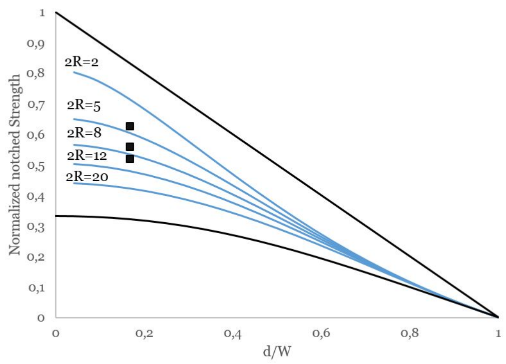

(b) STF-THIN

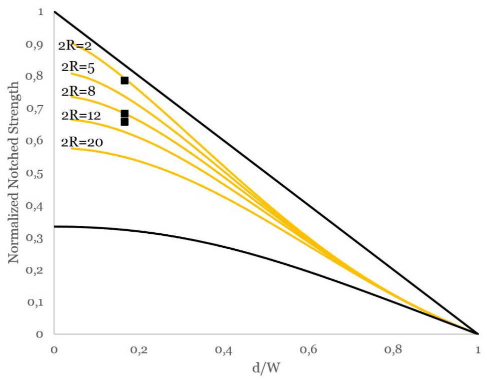

(c) NCF-THICK

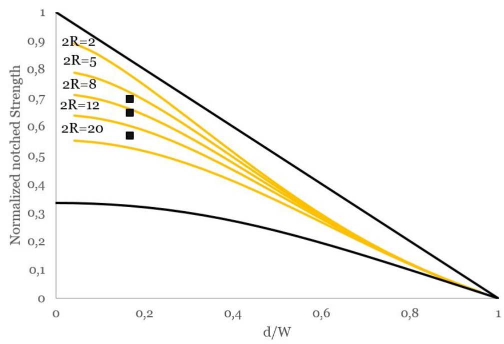

(d) STF-THICK

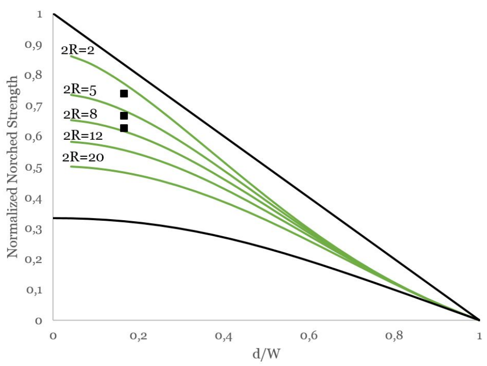

(e) NCF-HYBRID

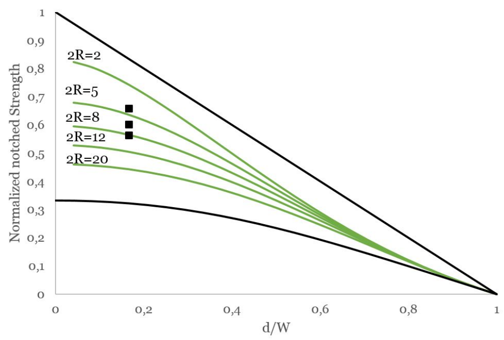

(f) STF-HYBRID

Figure 5.5: Design Charts for open-hole tensile strength for NCF T700GC/M21 and STF T700SC/M21 lay-ups

Chapter 6

Mechanical behaviour of composite laminates - Literature review

In this chapter, some relevant aspects and some analytical models used to predict the mechanical properties of laminates composites will be explained in detail, since they were used and/or implemented in this thesis. This includes, the Classical Lamination Theory, failure criteria commonly used and analytical models able to predict the *in-situ* properties of composite laminae and the fracture toughness of laminated composites.

6.1 Classical Lamination Theory

A laminated plate is composed by a N stacked orthotropic layers with the thickness given by h. There are two coordinate systems: the material and the problem coordinates systems. The coordinate system used in the problem formulation, in general, does not coincide with the principal material coordinate system, unless there is only 1 ply and the its angle is zero. Usually, the composite has several layers with different orientations of their material coordinates with respect to the laminate coordinates. (figure 6.1)

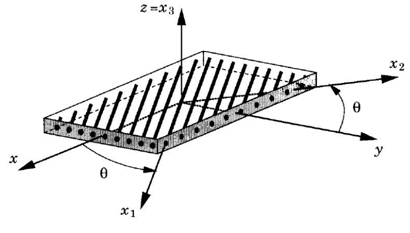

Figure 6.1: Material and problem coordinates systems [34]

The Classical Lamination theory follows the following assumptions [26]:

- The layers of the laminate are perfectly bonded.

- Each layer is a homogeneous material with known properties.
- The plies can be isotropic, transversely isotropic or orthotropic.
- Each layer is in a state of plane stress
- It follows the Kirchoff assumptions for thin plates:
  - Normals to the midplane remain straight normal to the deformed midplane, which means that $\gamma_{zx} = \gamma_{zy} = 0$
  - The length of the normals to the midplane do not change length, which means that $\epsilon_{zz} = 0$

Displacement field
The displacement field in any point of the laminate $u(x,y)$, $v(x,y)$, $w(x,y)$ reads

$$\begin{aligned} u(x,y) &= u^0 - z\frac{\partial w}{\partial x} \\ v(x,y) &= v^0 - z\frac{\partial w}{\partial y} \\ w(x,y) &= w^0 \end{aligned} \tag{6.1}$$

where u^0, v^0 and w^0 are the displacements along the coordinate lines of a material point on the xy-plane.

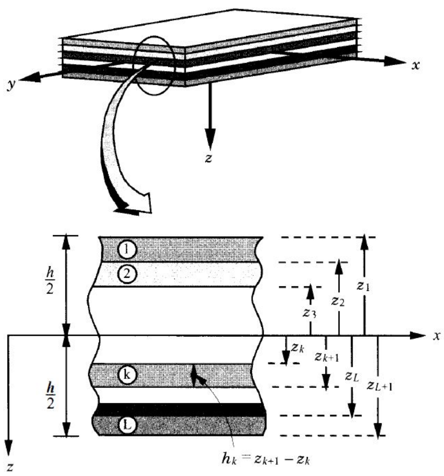

Figure 6.2: Coordinate syst.em and layer numbering used for a laminated plate [34]

Strain Field
The strain field reads

$$\{\epsilon\}_x = \left\{ \begin{array}{c} \epsilon_x \\ \epsilon_y \\ \gamma_{xy} \end{array} \right\} = \left\{ \begin{array}{c} \frac{\partial u}{\partial x} \\ \frac{\partial y}{\partial v} \\ \frac{\partial u}{\partial y} + \frac{\partial v}{\partial x} \end{array} \right\} = \left\{ \begin{array}{c} \frac{\partial u^0}{\partial x} \\ \frac{\partial y^0}{\partial v} \\ \frac{\partial u^0}{\partial y} + \frac{\partial v^0}{\partial x} \end{array} \right\} + z \left\{ \begin{array}{c} -\frac{\partial^2 w}{\partial x^2} \\ -\frac{\partial^2 w}{\partial y^2} \\ -2\frac{\partial^2 w}{\partial x \partial y} \end{array} \right\} = \{\epsilon^0\} + z\{\kappa\} \tag{6.2}$$

Stress Field
The stiffness of each layer Q^k is calculated as:

$$[\overline{Q}]^k = [T]^T[Q][T] \tag{6.3}$$

where $[Q]$ is the stiffness matrix of a layer in the material coordinate system, $[\overline{Q}]^k$ is the stiffness matrix of a layer in the global coordinate system and $[T]$ is the transformation matrix. For a transversely isotropic material, $[Q]$ reads

$$[T] = \begin{bmatrix} \frac{1}{E_1} & -\frac{\nu_{12}}{E_1} & 0 \\ -\frac{\nu_{12}}{E_1} & \frac{1}{E_2} & 0 \\ 0 & 0 & \frac{1}{G_{12}} \end{bmatrix}^{-1} \tag{6.4}$$

where E_1, E_2 are the axial Young's modulus respectively, ν_{12} is the axial Poisson coefficient and G_{12} is the axial shear modulus in the material coordinate system. The transformation matrix $[T]$ reads

$$[T] = \begin{bmatrix} m^2 & n^2 & -2mn \\ n^2 & m^2 & 2mn \\ 2mn & -2mn & m^2 - n^2 \end{bmatrix} \tag{6.5}$$

where $m = \cos(\theta)$ and $n = \sin(\theta)$.

Each layer k has the following stress-strain relation:

$$\{\sigma\}_x^k = [\overline{Q}]^k\{\epsilon\}_x = [\overline{Q}]^k\{\epsilon^0\} + z[\overline{Q}]^k\{\kappa\} \tag{6.6}$$

In-plane forces per unit length

The in-plane forces per unit length read

$$\{N\} = \int_{-h/2}^{h/2} \{\sigma\}_x \, dz = \int_{-h/2}^{h/2} [\overline{Q}]^{(k)}\{\epsilon\}_x \, dz = [A]\{\epsilon^0\} + [B]\{\kappa\} \tag{6.7}$$

where $[A]$ is the in-plane stiffness of the laminate and is defined as

$$[A] = \int_{-h/2}^{h/2} [\overline{Q}]^{(k)} \, dz = \sum_{k=1}^{N} \int_{z_k}^{z_{k+1}} [\overline{Q}]^{(k)} \, dz = \sum_{k=1}^{N} [\overline{Q}]^{(k)}(z_{k+1} - z_k) \tag{6.8}$$

and $[B]$ is the in-plane/bending coupling stiffness of the laminate and is defined as

$$[B] = \int_{-h/2}^{h/2} [\overline{Q}]^{(k)} z \, dz = \sum_{k=1}^{N} \int_{z_k}^{z_{k+1}} [\overline{Q}]^{(k)} z \, dz = \frac{1}{2} \sum_{k=1}^{N} [\overline{Q}]^{(k)}(z_{k+1}^2 - z_k^2) \tag{6.9}$$

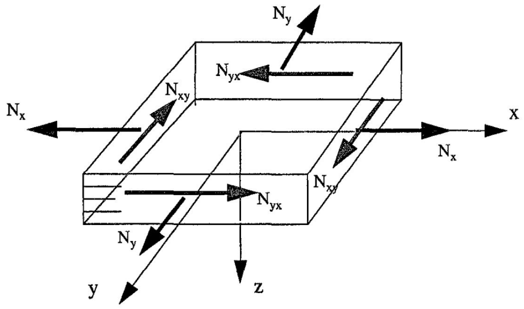

Figure 6.3: In-plane forces per unit length [26]

Moments per unit length

The moments per unit length read

$$\{M\} = \int_{-h/2}^{h/2} \{\sigma\}_x \; z, dz = \int_{-h/2}^{h/2} [\overline{Q}]^{(k)} \{\epsilon\}_x z \, dz = [B]\{\epsilon^0\} + [D]\{\kappa\} \tag{6.10}$$

where $[B]$ is the in-plane/bending coupling stiffness defined in 6.9 and $[D]$ is the bending stiffness of the laminate and is defined as

$$[D] = \int_{-h/2}^{h/2} [\overline{Q}]^{(k)} z^2 \, dz = \sum_{k=1}^{N} \int_{z_k}^{z_{k+1}} [\overline{Q}]^{(k)} z^2 \, dz = \frac{1}{3} \sum_{k=1}^{N} [\overline{Q}]^{(k)} (z_{k+1}^3 - z_k^3) \tag{6.11}$$

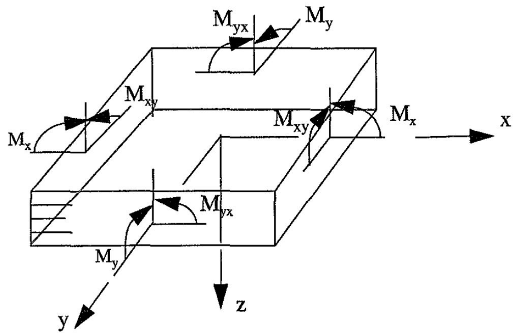

Figure 6.4: Moments per unit length [26]

6.2 Failure criteria for laminated composites

The effective use of laminated composites in structural applications relies on the ability to predict its strength. Stress- [20] [29] [25] [36] [28] and strain-based [25] failure criteria are simple and easy to implement, however, lack accuracy as they are purely empirical. For this reason, the definition of more physically-based and accurate failure criteria have been an important investigation subject over the last few years [33] [22] [21] [31] [19] [15]. An appropriate failure criteria should be applicable at the ply, laminate and structural level, yet simple enough so that it can be used in engineering applications. [15]. In this section, the stress-based Tsai-Hill and a three-dimensional invariant-based failure criteria for fibre-reinforced composites proposed by Camanho et al. [15] will be explained with detail.

6.2.1 Tsai-Hill criterion

The Tsai-Hill failure criterion is a interactive stress-based criterion, but it does not distinguish different failure modes, i.e. does not identify if the composite is failing due to matrix cracking or fibre failure. It reads

$$\frac{\sigma_{11}^2}{S_{11}^2} - \frac{\sigma_{11}\sigma_{22}}{S_{11}^2} + \frac{\sigma_{22}^2}{S_{22}^2} + \frac{\sigma_{12}^2}{S_{12}^2} > 0 \tag{6.12}$$

where S_{11} is the ultimate longitudinal tensile strength (X_T) if $\sigma_{11} > 0$ and the ultimate longitudinal compressive strength (X_C) if $\sigma_{11} < 0$, S_{22} is the ultimate transverse tensile strength (Y_T) if $\sigma_{22} > 0$ and the ultimate transverse compressive strength (Y_C) if $\sigma_{22} < 0$ and S_{12} is the in-plane shear stress S.

6.2.2 Three-dimensional invariant-based failure criteria for fibre-reinforced composites

This failure criteria is a combination of an invariant-based failure criterion for transverse failure and a failure criterion for longitudinal failure of unidirectional composites, i.e. a combination of criteria that predict matrix dominated failure and criteria that can predict fibre dominated failure. This results in failure criteria that are able to distinguish matrix and fibre failure, which is quite relevant for, e.g. damage models. The schematic representation of the failure criteria is presented in figure 6.5 and it will be explained hereafter.

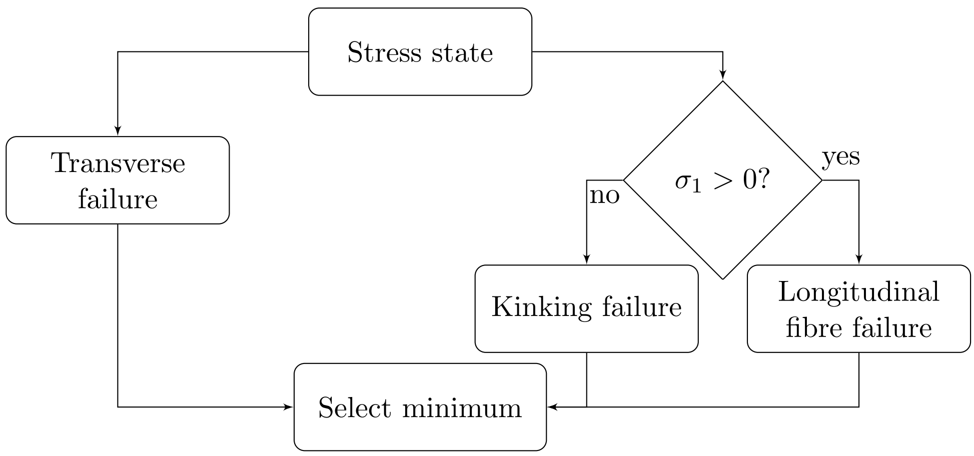

Figure 6.5: Schematic representation of the three-dimensional invariant-based failure criteria for fiber-reinforced composites

6.2.2.1 Invariant-based failure criterion for transverse failure of unidirectional composites

The three-dimensional invariant-based failure criteria for fibre-reinforced composites proposed by Camanho et al. [15] is formulated from the invariant based yield function for transversely isotropic materials proposed by Vogler et al. [39]

Transversely isotropic materials have a preferred direction **a** which, for UD composite materials is the direction of the fibres. The material's characteristic direction is defined by the structural tensor **A**. It reads

$$\mathbf{A} = \mathbf{a} \otimes \mathbf{a} \tag{6.13}$$

The invariants used to define de failure function f_M were formulated using linear combinations of the functional basic invariants for transverse isotropy by argument tensors A and σ and linear decomposition of the stress tensor in order to consider certain specific properties and to decouple the stress states which is useful to simplify the determination of the yield function parameters. The basic invariants, presented below could have been used to define the yield surface, however, the determination of the material parameters would be more difficult.

These basic invariants are: $tr[\sigma]$, $tr[\sigma^2]$, $tr[\sigma^3]$, $tr[A\sigma]$ and $tr[A\sigma^2]$.

The stress tensor can be decomposed in a plasticity inducing (σ^p) and reaction σ^{reac} part:

$$\sigma = \sigma^{reac} + \sigma^p \tag{6.14}$$

with

$$\sigma^r = \frac{1}{2}(tr\sigma - a\sigma a)1 - \frac{1}{2}(tr\sigma - 3a\sigma a)A \tag{6.15}$$

$$\sigma^p = \sigma - \sigma^r \tag{6.16}$$

The proposed invariants are:

- $I_1 = \frac{1}{2}tr(\sigma^p)^2 - a(\sigma^p)^2 a$
- $I_2 = a(\sigma^p)^2 a$
- $I_3 = tr\sigma - a\sigma a$

The failure function reads:

$$f_M = \alpha_1 I_1 + \alpha_2 I_2 + \alpha_3 I_3 + \alpha_{32} I_3^2 - 1 \tag{6.17}$$

with

$$\alpha_3 = \alpha_3^t \quad and \quad \alpha_{32} = \alpha_{32}^t \quad if \quad I_3 > 0$$

$$\alpha_3 = \alpha_3^c \quad and \quad \alpha_{32} = \alpha_{32}^c \quad if \quad I_3 \leq 0$$

The invariants and α parameters are activated in different stress states such as in-plane shear, transverse shear, uniaxial tension/compression and biaxial tension and compression as shown in table 6.1. The six α parameters can be determined activating this types of loading, yielding:

$$\alpha_1 = \frac{1}{S_T^2} \tag{6.18}$$

$$\alpha_2 = \frac{1}{S_L^2} \tag{6.19}$$

$$\alpha_{32}^t = \frac{1 - \frac{Y_T}{2Y_{BT}} - \alpha_1 \frac{Y_T^2}{4}}{Y_T^2 - 2Y_{BT}Y_T} \tag{6.20}$$

$$\alpha_3^t = \frac{1}{2Y_{BT}} - 2\alpha_{32}^t Y_{BT} \tag{6.21}$$

$$\alpha_{32}^c = \frac{1 - \frac{Y_C}{2Y_{BC}} - \alpha_1 \frac{Y_C^2}{4}}{Y_C^2 - 2Y_{BC}Y_C} \tag{6.22}$$

$$\alpha_3^c = \frac{1}{2Y_{BC}} - 2\alpha_{32}^c Y_{BC} \tag{6.23}$$

where S_T and S_L are the transverse and in-plane shear strengths, Y_T ans Y_C are the transverse tension and transverse compression strengths and Y_{BT} and Y_{BC} are the biaxial transverse tensile and compressive strengths.

Table 6.1: Invariants activated and α parameters that can be determined in each stress state

Stress state	Symbol	α	Invariant I	Strength
Transverse Shear	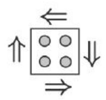	α_1	I_1	S_T
In-plane Shear	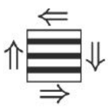	α_2	I_2	S_L
Transverse Uniaxial Tension	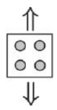	α_3^t , α_{32}^t, α_1	I_1 and I_3	Y_T
Transverse Biaxial Tension	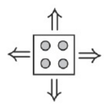	α_3^t and α_{32}^t	I_3	Y_{BT}
Transverse Uniaxial Compression	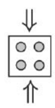	α_3^c , α_{32}^c, α_1	I_1 and I_3	Y_C
Transverse Biaxial Compression	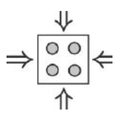	α_3^c and α_{32}^c	I_3	Y_{BC}

6.2.2.2 Failure criteria for longitudinal failure of unidirectional composites

Longitudinal fibre failure

Tensile failure in the fibre direction ($\sigma_1 > 0$) can be predicted using the maximum allowable strain criterion:

$$f_F = \frac{\epsilon_{11}}{\epsilon_1^T} \leq 1 \tag{6.24}$$

Invariant-based criterion for kinking failure

Longitudinal compressive failure of composite laminates is a fibre dominated failure that occurs due to damage in the surrounding matrix. Camanho et al. [15] propose a three dimensional kinking failure criterion based on the invariant-based criterion explained in section 6.2.2.1 that will be explained hereafter.

It is assumed that the fibres are misaligned and, when the material is loaded, this misalignment is aggravated until the material fails. The model simulates this by considering an initial fibre misalignment which will result in shearing stresses between the fibres and that will eventually lead to the formation of a kink band.

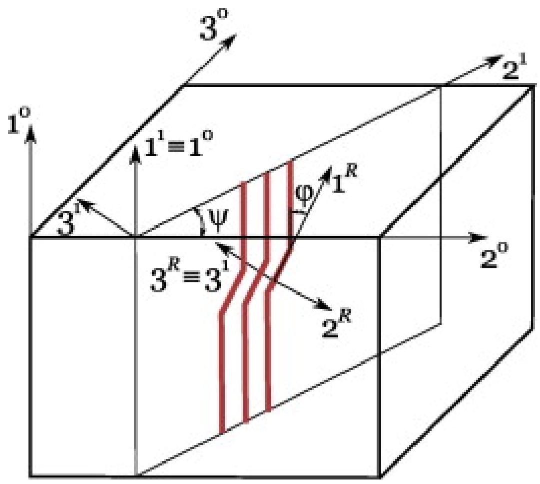

Figure 6.6: 3D kinking model [15]

Figure 1 shows the kinking plane in the kinking model. Three coordinates system are represented:

- $1^0 2^0 3^0$ - coincident with the material axes of the composite
- $1^1 2^1 3^1$ - coordinate system of the kinking plane. It is obtained by rotating $1^0 2^0 3^0$ by an angle of ψ around the axis 1^0
- $1^R 2^R 3^R$ - coordinate system coincident with the misaligned fibres material axes. It is obtained by rotating $1^1 2^1 3^1$ by an angle of φ around the axis 3^1

The preferred direction in the material coordinate system, i.e. the direction of the misaligned fibres written in the $1^0 2^0 3^0$ coordinate system yields:

$$
\begin{aligned}
a^{(0)} &= T_{10} \cdot a^1 = T_{10} \cdot T_{R1} \cdot a^{(R)} = \\
&= \begin{bmatrix} 1 & 0 & 0 \\ 0 & \cos\psi & -\sin\psi \\ 0 & \sin\psi & \cos\psi \end{bmatrix} \begin{bmatrix} \cos\varphi & -\sin\varphi & 0 \\ \sin\varphi & \cos\varphi & 0 \\ 0 & 0 & 1 \end{bmatrix} \begin{bmatrix} 1 \\ 0 \\ 0 \end{bmatrix} = \begin{bmatrix} \cos\varphi \\ \cos\psi\sin\varphi \\ \sin\psi\sin\varphi \end{bmatrix}
\end{aligned}
\tag{6.25}
$$

The stress state for a given situation can be calculated and once the preferred direction $\mathbf{a}$ is known, the invariants I_1, I_2 and I_3 can be calculated and the failure criterion in eq. 6.17 can be applied. However, to do so, the angle of the kinking plane ψ and the the initial misalignment φ_0 have to be determined. Catalanotti et al. [19] suggests that the angle of the kinking plane can be calculated as function of the stress state. It reads:

$$\psi = \arctan\frac{\sigma_{13}}{\sigma_{12}} \tag{6.26}$$

unless σ_{12} and σ_{13} are both zero, in which case, the angle of the kinking plane reads [19]:

$$\psi = \frac{1}{2}\arctan\left(\frac{2\sigma_{23}}{\sigma_{22} - \sigma_{33}}\right) \tag{6.27}$$

The total misalignment φ is the sum of an initial misalignment φ^0 and the misalignment originated by the applied shear loading. If the material exhibits a linear shear response:

$$\varphi' = \varphi_0 + \varphi^R = \varphi_0 + \frac{\left|\sigma_{12}^{(R)}(\varphi_0, \psi)\right|}{G_{12}} \quad \mathit{and} \quad \varphi = \begin{cases} \varphi' & if \quad \sigma_{12}^{(R)}(\varphi_0, \psi) \geq 0 \\ -\varphi' & if \quad \sigma_{12}^{(R)}(\varphi_0, \psi) < 0 \end{cases} \tag{6.28}$$

where G_{12} is the shear modulus and $\sigma_{12}^{(R)}$ is the applied shear stress in the misaligned frame given by:

$$
\begin{aligned}
\sigma_{12}^{(R)}(\varphi_0, \psi) = &\frac{1}{2}\left[-\sigma_{11} + \sigma_{22}\cos^2\psi + \sigma_{33}\sin^2\psi + \sigma_{23}\sin 2\psi\right]\sin 2\varphi_0 \\
&+ (\sigma_{12}\cos\psi + \sigma_{13}\sin\psi)\cos 2\varphi_0
\end{aligned}
\tag{6.29}
$$

The initial misalignment φ_0 can be calculated for the particular case of pure compression. If the material exhibits non-linear shear response a parameter that regards the nonlinearity of the stress-shear strain relation β has to be taken into account. In this case, the initial misalignment yields:

$$\varphi_C = \varphi_0 + \varphi_C^R \Leftrightarrow \varphi_0 = \varphi_C - \varphi_C^R \Leftrightarrow \varphi_0 = \varphi_C - \left|\frac{X_C \sin 2\varphi_0}{2G_{12}} + \beta\frac{X_C^3 \sin^3 2\varphi_0}{8}\right| \tag{6.30}$$

If the nonlinear shear behaviour can be neglected $\beta = 0$ and the previous equation yields:

$$\varphi_0 = \varphi_C - \frac{|X_C \sin 2\varphi_0|}{2G_{12}} \tag{6.31}$$

In both cases, this results in a non-linear equation that can be solved numerically to find the initial misalignment. In the case of linear behaviour (eq. 6.31) and assuming that the initial misalignment is small, the following expression can be used:

$$\varphi_0 = \varphi_C \left(1 + \frac{|X_C|}{G_{12}}\right)^{-1} \tag{6.32}$$

The total misalignment for the case of pure compression φ_C reads:

$$\begin{aligned}\varphi_C =& \frac{1}{2}\arccos\{[4\sqrt{\alpha_1 - 4\alpha_2 + \alpha_2^2 X_C^2 + (\alpha_3^c)^2 + 2\alpha_2\alpha_3^c X_C + 4\alpha_{32}^c} \\ &+ (\alpha_1 + 4\alpha_{32}^c)\, X_C + 4\alpha_3^c]\,[(\alpha_1 - 4\alpha_2 + 4\alpha_{32}^c)\, X_C]^{-1}\}\end{aligned} \tag{6.33}$$

6.3 *In-situ* properties

The transverse and shear strengths of a given laminae embedded in a multidirectional laminate are a function of its ply thickness and of the ply's position in the laminate. This is a deterministic size effect that should be accounted for, otherwise, if the strengths used to design a given component are the strengths of a unidirectional laminate, the resulting design will be very conservative. [13]

Camanho et al. [13] proposed an analytical model to predict the in-situ transverse tension Y_T^{is} and in-plane shear S_L^{is} strengths using Fracture Mechanics models to relate the in-situ properties with the fracture toughness of the material. In general, the in-situ strength increases with the reduction of the ply thickness. If the ply is embedded between two plies the in-situ strengths are greater than if it is an outer ply since outer plies are not constrained and therefore more likely to develop surface cracks.

6.3.1 Transverse tensile and in-plane shear strengths

Three ply configurations are considered to calculate the transverse tensile and in-plane shear strengths: thick, thin inner and thin outer plies.

6.3.1.1 Thick plies

In a thick plies embedded in a multidirectional laminate, a slit crack such as the one shown in figure 6.7 will propagate firstly in the transverse direction, and therefore the mode I and mode II energy release rate read:

$$G_I(T) = \frac{\pi a_0}{2}\Lambda_{22}^o \sigma_{22}^2 \tag{6.34}$$

$$G_I I(T) = \frac{\pi a_0}{2}\chi(\gamma_{12}) \tag{6.35}$$

where $2a_0$ is the slit crack lengths along the thickness, $\chi(\gamma)$ is given by

$$\chi(\gamma_{12}) = 2\int_0^{\gamma_{12}} \sigma_{12} d\gamma_{12} \tag{6.36}$$

and Λ_{22}^o is given by [23]:

$$\Lambda_{22}^o = 2(\frac{1}{E_2} - \frac{\nu_{12}^2}{E_1}) \tag{6.37}$$

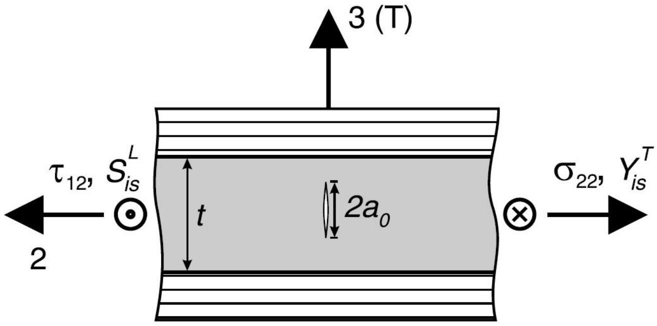

Figure 6.7: Thick embedded ply [13]

Dvorak and Laws [23] proposed that the transverse tensile *in-situ* strength can be obtained by solving equation 6.34 for Y_{is}^T yielding

$$Y_{is}^T = \sqrt{\frac{2G_{Ic}(T)}{\pi a_0 \Lambda_{22}^0}} \tag{6.38}$$

Hahn and Tsai proposed that the shear response of a given laminated composite could be approximated by the following polynomial [24]

$$\gamma_{12} = \frac{1}{G_{12}}\sigma_{12} + \beta\sigma_{12}^3 \tag{6.39}$$

where β defines the non-linear behaviour of the shear stress. Having defined γ_{12}, the mode II fracture toughness can be calculated replacing 6.39 in equation 6.35, yielding:

$$G_{IIc}(T) = \pi a_0 \left[\frac{(S_L^{is})^2}{2G_{12}} + \frac{3}{4}\beta(S_L^{is})^4\right] \tag{6.40}$$

Dvorak and Laws [23] also proposed that the a unidirectional laminate can be considered a special case of a thick ply with unconstrained outer surfaces and, therefore, the *in-situ* strengths of a thick ply can be related to the those of an unidirectional thick ply. Using the classical solutions for stress intensity factors of surface cracks in unidirectional laminates [37], the mode I and mode II components of fracture toughness can also be calculated as

$$G_{Ic} = 1.12^2 \pi a_0 \Lambda_{22}^0 (Y^T)^2 \tag{6.41}$$

and

$$G_{IIc} = 2\pi a_0 \left[\frac{(S_L)^2}{2G_{12}} + \frac{3}{4}\beta(S_L)^4\right] \tag{6.42}$$

Combining equations 6.38 and 6.41, the transverse tensile in-situ strength for a thick ply yields:

$$Y_{is}^{T} = 1.12\sqrt{2}Y^{T} \tag{6.43}$$

Combining equations 6.40 and 6.42, the in-plane shear strength can be obtained solving the following equation for S_L^{is}

$$\frac{(S_L)^2}{G_{12}} + \frac{6}{4}\beta(S_L)^4 = \frac{(S_L^{is})^2}{2G_{12}} + \frac{3}{4}\beta(S_L^{is})^4 \tag{6.44}$$

6.3.1.2 Thin inner plies

In a thin plies embedded in a multidirectional laminate, a slit crack such as the one shown in figure 6.8 will propagate in the longitudinal direction since it is already extends through the ply thickness and, therefore the mode I and mode II energy release rate read [23]:

$$G_I(L) = \frac{\pi t}{8}\Lambda_{22}^{o}\sigma_{22}^{2} \tag{6.45}$$

$$G_{II}(T) = \frac{\pi t}{8}\chi(\gamma_{12}) \tag{6.46}$$

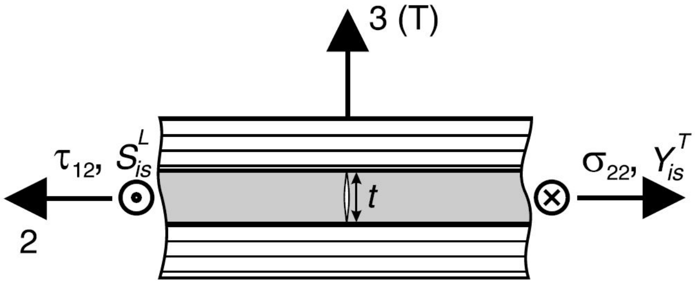

Figure 6.8: Thin embedded ply [13]

The transverse tensile *in-situ* strength can be obtained by solving equation 6.45 for Y_{is}^T yielding

$$Y_{is}^{T} = \sqrt{\frac{8G_{Ic}(L)}{\pi t \Lambda_{22}^{0}}} \tag{6.47}$$

Replacing equation 6.39 in equation 6.46 yields

$$\frac{(S_{is}^L)^2}{8G_{12}} + \frac{3}{16}\beta(S_{is}^L)^4 = \frac{G_{IIc}(L)}{\pi t} \tag{6.48}$$

which can be solved for the *in-situ* in-plane shear strength S_{is}^L.

6.3.1.3 Thin outer plies

A thin outer ply is a special case of the thin ply for which the energy release rate is larger because the slit crack is closer to the laminate's surface.

The mode I fracture toughness reads

$$G_{IIc} = \frac{\pi t}{2} \int_0^{\gamma_{12}} \sigma_{12} d\gamma_{12} \tag{6.49}$$

Replacing equation 6.39 in 6.49, it yields:

$$\frac{(S_o^L)^2}{4G_{12}} + \frac{3}{8}\beta(S_o^L)^4 = \frac{G_{IIc}}{\pi t} \tag{6.50}$$

The *in-situ* in-plane shear strength is obtained solving equation 6.50 for S_o^L.

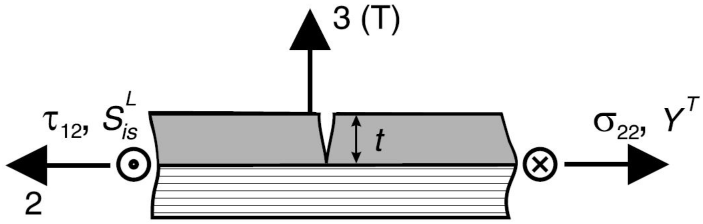

Figure 6.9: Thin outer ply [13]

6.3.1.4 General expression for the transverse tensile and in-plane shear strengths

For an inner ply:

- the transverse tensile strength is the maximum between the transverse tensile strength of a thin embedded ply and a thick embedded ply, i.e.,

$$Y_{is}^T = \sqrt{\frac{8G_{Ic}}{\pi t \Lambda_{22}^o}} \text{ and } Y_{is}^T = 1.12\sqrt{2}Y^T$$

- the in-plane shear strength is the maximum between the in-plane shear strength of a thin embedded ply and a thick embedded ply, i.e., the maximum of

$$S_{is}^L = \sqrt{\frac{(1+\beta\phi G_{12}^2)^{1/2} - 1}{3\beta G_{12}}} \tag{6.51}$$

obtained with

$$\phi = \frac{48G_{IIc}}{\pi t} \text{ and } \phi = \frac{12(S^L)^2}{G_{12}} + \frac{72}{4}\beta(S^L)^4$$

For an outer ply:

- the transverse tensile strength is the maximum between

$$Y_{is}^T = 1.78\sqrt{\frac{G_{Ic}}{\pi t \Lambda_{22}^o}} \text{ and } Y_{is}^T = Y^T$$

- The in-plane shear strength is the maximum between the in-plane shear strength of a UD ply and a thin outer ply, i.e.,

$$S_{is}^{L} = S^{L} \text{ and } S_{is}^{L} = \sqrt{\frac{(1+\beta\phi G_{12}^{2})^{1/2}-1}{3\beta G_{12}}}$$

with

$$\phi = \frac{24 G_{IIc}}{\pi t} \tag{6.52}$$

6.3.2 Compressive transverse, biaxial transverse tensile and transverse shear strengths

The *in situ* transverse shear strength, S_T^{is}, and the *in-situ* biaxial transverse tensile strength, Y_{BT}^{is}, are calculated imposing that the slope in the σ_{22}-σ_{12} failure envelope when $\sigma_{22}=0$, η_L, and that the slope in the σ_{22}-σ_{23} failure envelope when $\sigma_{22}=0$, η_T, are equal to the slope of the envelopes obtained with the *in-situ* properties (see figure 6.10):

$$\begin{cases} \eta_L^{(+)} = \eta_{L,is}^{(+)} \\ \eta_T^{(+)} = \eta_{T,is}^{(+)} \end{cases} \tag{6.53}$$

The slopes depend on the sign of σ_{22}. In the tensile range, they read:

$$\eta_L^{(+)} = \left.\frac{\partial \sigma_{12}}{\partial \sigma_{22}^{(+)}}\right|_{\sigma_{22}=0^+} = -\frac{1}{2}\frac{\alpha_3^t}{\sqrt{\alpha_2}} \tag{6.54}$$

$$\eta_L^{(+)} = \left.\frac{\partial \sigma_{23}}{\partial \sigma_{22}^{(+)}}\right|_{\sigma_{22}=0^+} = -\frac{1}{2}\frac{\alpha_3^t}{\sqrt{\alpha_1}} \tag{6.55}$$

where α_1, α_2 and α_3^t are defined in equations 6.18, 6.19 and 6.21, respectively. The *in-situ* transverse shear strength, S_T^{is}, and the *in-situ* biaxial transverse tensile strength, Y_{BT}^{is}, can now be calculated solving the system of equations 6.53.

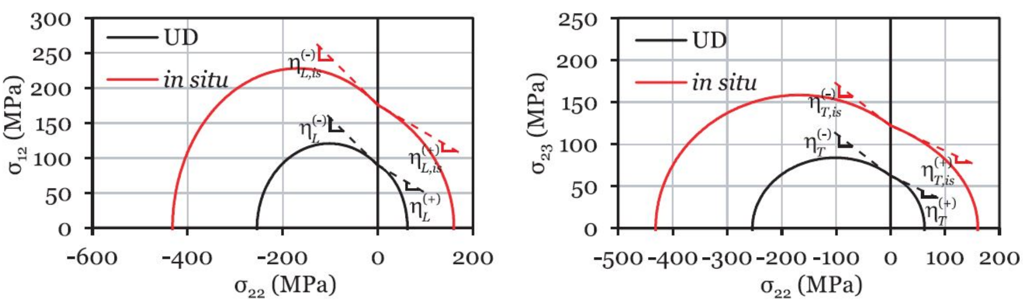

(a) $\sigma_{22}-\sigma_{12}$ failure envelope.

(b) $\sigma_{22}-\sigma_{23}$ failure envelope.

Figure 6.10: Definition of η_L and η_T [32]

It is assumed that the biaxial transverse compressive strength is constant which means that $Y_{BC}^{is} = Y_{BC}^{ud}$. The transverse compressive stress Y_C^{is} can therefore, be calculated imposing that

$$\eta_L^{(-)} = \eta_{L,is}^{(-)} \tag{6.56}$$

or

$$\eta_T^{(-)} = \eta_{T,is}^{(-)} \tag{6.57}$$

with

$$\eta_L^{(-)} = \left.\frac{\partial \sigma_{12}}{\partial \sigma_{22}^{(-)}}\right|_{\sigma_{22}=0^-} = -\frac{1}{2}\frac{\alpha_3^c}{\sqrt{\alpha_2}} \tag{6.58}$$

$$\eta_L^{(-)} = \left.\frac{\partial \sigma_{23}}{\partial \sigma_{22}^{(-)}}\right|_{\sigma_{22}=0^-} = -\frac{1}{2}\frac{\alpha_3^c}{\sqrt{\alpha_1}} \tag{6.59}$$

where α_3^c are defined in equation 6.23. The *in-situ* transverse compressive strength, Y_{BT}^{is}, can now be calculated solving equations 6.56 or 6.57.

6.4 Fracture Toughness

Camanho et al. [16] proposed an analytical model to calculate the mode I fracture toughness of multidirectional laminates, K_{Ic}^L, from the fracture toughness of the 0º plies, K_{Ic}^0. The presence of a notch in a composite laminate will result in a complex three dimensional stress field that will trigger complex damage mechanisms such as delamination. In the model proposed, the effect of the three dimensional stress field is neglected and the damage mechanisms are assumed to result in a though-the-thickness macro-crack. For this reason, as the Finite Fracture mechanics model [17] presented in section 5.1, if the main failure mechanism it delamination, the model cannot be applied.

For a given laminate, the ratio between the mean remote failure stress of a group of plies that represent the balanced sub-laminate (i) and the remote failure stress of the a sub-laminate with all plies with the fibres aligned with the loading direction proposed by Vaidya and Sun [38] can be calculated using the Classical Lamination Theory since it only requires the ply elastic properties and the lay-up as input vaariables. The ratio reads:

$$\Omega_0^{(i)} = \frac{\bar{\sigma}^{(i)}}{\bar{\sigma}^0} \tag{6.60}$$

$\bar{\sigma}^{(i)}$ and $\bar{\sigma}^{(0)}$ can be also be calculated from Linear-Elastic Fracture Mechanics:

$$\bar{\sigma}^{(i)} = \frac{K_{Ic}^{(i)}}{\chi^{(i)} Y \sqrt{\pi a}} \tag{6.61}$$

$$\bar{\sigma}^{(0)} = \frac{K_{Ic}^{(0)}}{\chi^{(0)} Y \sqrt{\pi a}} \tag{6.62}$$

where χ accounts for the laminate's orthotropy [11] and is given by:

$$\chi = 1 + 0.1(\rho - 1) - 0.016(\rho - 1)^2 + 0.002(\rho - 1)^3 \tag{6.63}$$

and ρ is given by

$$\rho = \frac{(E_x E_y)^{1/2}}{2G_{xy}} - (\nu_{xy}\nu_{yx})^{1/2} \tag{6.64}$$

where E_x and E_y are the laminate's Young Modulus in the orthotropy axes (x being is the loading direction), G_{xy} is the laminate shear modulus in the orthotropy axes and ν_{xy} and ν_{yx} are the Poisson ratios. $K_{Ic}^{(i)}$ and $K_{Ic}^{(0)}$ are the fracture toughness of the sub-laminate (i) and of the 0^{o} plies. Combining equations (6.60), (6.61) and (6.62), the fracture toughness of sub-laminate (i) yields:

$$K_{Ic}^{(i)} = \frac{\chi^{(i)}\Omega_0^{(i)}}{\chi^0} K_{Ic}^0 \tag{6.65}$$

Assuming a self-similar crack propagation along all plies, the laminate's fracture toughness K_{Ic}^L is calculated as

$$K_{Ic}^L = \frac{\sum_{(i)}^N K_{Ic}^{(i)} t^{(i)}}{t^L}, (i) \neq 90^{o} \tag{6.66}$$

where t^L is the thickness of the laminate, $t^{(i)}$ it the thickness of the sub-laminate (i) and N is the number of sub-laminates considered.

Chapter 7

Modeling and performance prediction

A algorithm capable of determining the notched strength of laminated composites using only the ply elastic, strength and fracture properties as input variables is presented in this chapter. Such an algorithm lays on two hypothesis:

- delamination is suppressed and, therefore, unnotched tensile and compressive strength can be predicted using the Classical Lamination theory allied with an appropriate failure criteria. The failure criteria is a function of the in-situ properties, which can also be calculated analytically.

- the effect of a three dimensional stress field at the vicinity of notches, which can trigger delamination, can be neglected and that the damage mechanisms can be lumped up into a through the thickness macrocrack.

Since it has only ply properties as input variables, such a model would avoid the need of extensive and, therefore, costly and time-consuming experimental programs to determine properties for different lay-ups of the same material system and could possible be used as a preliminary design and optimization tool.

For conventional and thick laminates, the effect of delamination cannot be neglected and, therefore, analytical models that discard its effect are not sophisticated enough to be able to predict their notched strength and cannot serve as an alternative to Finite Elements analysis.

However, as shown in chapters 2 and 4 and reported in [4] [35] [6], thin-ply laminates are able to suppress delamination onset, and therefore, such a model could eventually be used. It could also be the base of an optimization algorithm capable of selecting an optimal lay-up of thin-ply laminates having open-hole tension and plain strength as design drivers.

The model will be explained with more detail hereafter. It was only partially implemented and, therefore, no results will be presented in this stage of the work.

7.1 Unnotched tensile and compressive strength

As explained in chapter 2, quasi-isotropic thin-ply composites loaded in tension and compression show little severe damage such as transverse cracking and delamination prior to failure and, therefore, Amacher et al. [4] suggests that the unnotched tensile and compressive strength of these kind of materials can be predicted combining the Classical Lamination Theory presented in 6.1 and a failure criteria as the ones presented in 6.2. The failure criteria is a function of each ply's in-situ strengths, which can be determined as explained in 6.3. This means that, if there is in fact no severe delamination prior to failure, the unnotched strength can be predicted using analytical models having only the laminate lay-up and ply thickness, the ply elastic properties of the material and the ply strengths as input variables (see table 7.1). This avoids the expensive and time consuming process of experimental testing to obtain properties of different lay-ups of the same material system and will potentially allow the selection of a optimal lay-up for a specific application.

For a plate loaded in tension or compression, some simplifications can be made to the Classical Lamination Theory. They will be presented hereafter.

For a plate loaded in tension, the in-plane forces per unit length reads

$$\{N\} = \begin{Bmatrix} N_x \\ N_y \\ N_{xy} \end{Bmatrix} = \begin{Bmatrix} N \\ 0 \\ 0 \end{Bmatrix} = [A]\{\epsilon^0\} + [B]\{\kappa\} = [A]\{\epsilon^0\} \tag{7.1}$$

because $\{\kappa\} = \{0\}$ since $w = 0$ (see eq. 6.2).

The stress distribution in a ply k reads

$$\{\sigma\}_x^k = \begin{Bmatrix} \sigma_x \\ \sigma_y \\ \sigma_{xy} \end{Bmatrix}^k = [\overline{Q}]^k\{\epsilon^0\} = [\overline{Q}]^k[A]^{-1}\{N\} \tag{7.2}$$

If the ply elastic properties E_1, E_2, G_{12} and ν_{12} and the stacking sequence and ply thickness are known, $[\overline{Q}]^k$ and $[A]$ can be computed, and therefore, the stresses in each ply for a given load N can be determined.

Amacher et al. [4] applied the classical lamination theory allied with the Tsai-Hill criterion. In both cases, a virtual tensile test was performed, i.e. the applied remote stress was increased in 1 MPa per cycle, and the stress state for each ply was calculated. Two different hypothesis were followed:

- In the first one, no damage is considered. In this case, the failure stress is the stress for which the Tsai-Hill failure criterion is met for 0° plies. This model revealed more accurate for thin-ply (30 g/m^2) as shown in figure 7.1 since delamination and transverse cracking is suppressed until the point just before failure, which indicated that all the plies are able to carry load until the 0° plies fail.
- In the second, damage is taken into account. In this case, when a ply's stress state reaches the Tsai-Hill failure criteria, their elastic properties were reduced

to 0.0001 of their initial value and the test continues until the 0^o plies fails. This model proved more accurate for thick-ply composites (300 g/m^2) as shown in figure 7.1 since delamination and transverse cracking are able to spread through the whole specimen, leaving the 0^o plies to carry the load.

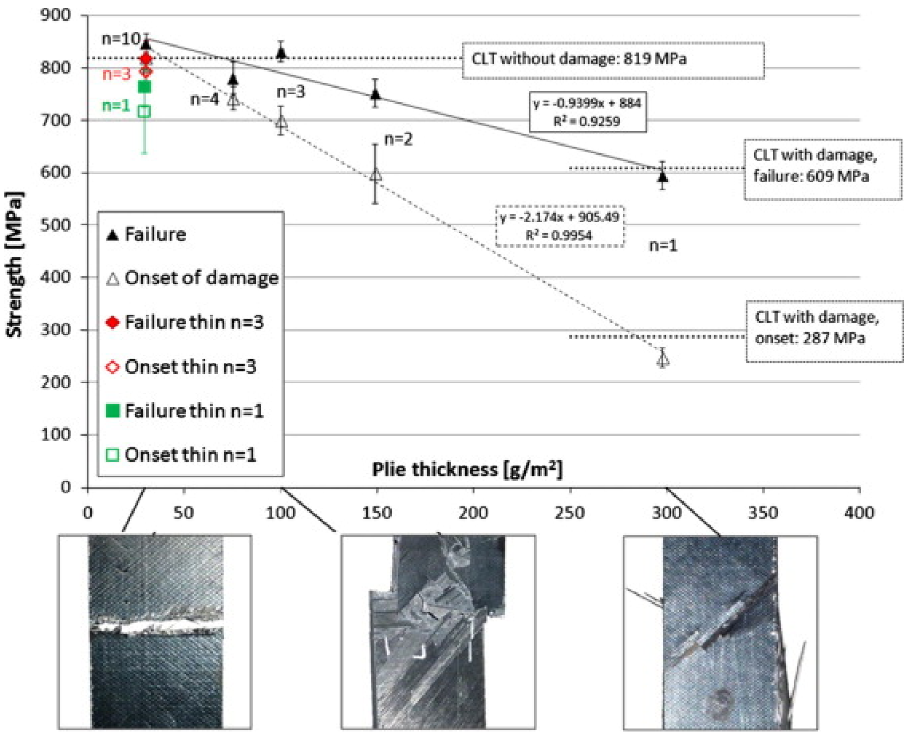

Figure 7.1: Ultimate strength and onset of damage with respect to ply thickness in unnotched quasi-isotropic tests, and failure modes observed for thick, intermediate and thin-ply laminates [4]

In the present work, the Classical lamination theory model was implemented in a Matlab code but, since the final goal of this code is to be the basis of an optimization algorithm that is able to select lay-ups of a given material system for a specific application, a different approach that was believed to be less time consuming than that described above was used. Instead of increasing the applied remote stress until a given ply failed, the stresses in each ply were calculated as a function of the applied load N (eq. 7.2). The failure criterion is then applied to each ply which also yields a function of N. Solving this equation for N, the remote load required for each ply to fail can be calculated. The ply that actually fails is the one for which the remote load is minimum. The remote stress at failure is calculated dividing the load N by the total thickness of the laminate h. Two different models were implemented:

- In the first, no damage is considered. In this case, the final failure is considered when the first ply fails. This model was implemented using the Tsai-Hill (hereafter referred to as TsHi. model) and the invariant-based criteria proposed by Camanho et al. [15] and explained in chapter 6.2.2 (hereafter referred to as Inv. model). The results obtained with both should be compared so that advantages of using a more complex criterion that is able to distinguish matrix and fibre failure could be accessed. A schematic representation of the TsHi and Inv. models are shown in figures 7.2 and 7.3 respectively.

- In the second, damage is considered. In this case, if a ply fails due to matrix cracking (which can only be accessed if the invariant-based criteria proposed by Camanho et al.[15] and explained in chapter 6.2.2 is used) the transverse and shear elastic properties of that ply are reduced to 0.0001 of its original value, i.e. $G'_{12} = 0.0001G_{12}$ and $E'_{12} = 0.0001E_{12}$ and the process is repeated until the ply that fails fails due to fibre failure (kinking or maximum strain). A schematic representation of the model is shown in figure 7.4. Hereafter, this model will be referred to as as INV-D model.

Any failure criteria is a function of the *in-situ* properties of the plies, that can be calculated using the analytical model presented in 6.3 [13] [32]. The *in-situ* properties are calculated using the required elastic, strength and fracture properties: the Young Moduli E_1, E_2, the Poisson coefficient ν_{12}, the shear modulus G_{12}, the mode I and II interlaminar fracture toughness, G_I and G_{II}, and the UD strengths X_T, X_C, Y_T, Y_C, Y_{BT}, Y_{BC}, S_L and S_T.

Table 7.1: Input variables required by the model

	Sym.	Property
Ply elastic properties	E_1	Longitudinal Young's modulus
	E_2	Transverse Young's modulus
	ν_{12}	Poisson coefficient
	G_{12}	Shear Modulus
Unidirectional strengths	X_T	Longitudinal tensile strength
	X_C	Longitudinal compressive strength
	Y_T^{ud}	Uniaxial transverse tensile strength
	Y_{BT}^{ud}	Biaxial transverse tensile strength
	Y_C^{ud}	Uniaxial transverse compressive strength
	Y_{BC}^{ud}	Biaxial transverse compressive strength
	S_L^{ud}	In-plane shear strength
	S_T^{ud}	Transverse shear strength
Fracture toughness	G_{Ic}	Mode I interlaminar fracture toughness
	G_{IIc}	Mode II interlaminar fracture toughness
	K_{Ic}^0	Fracture toughness of the 0° plies
Lay-up	-	Ply orientations and thicknesses
Geometry	d/W	Hole diameter-to-width ratio
	d	Hole diameter

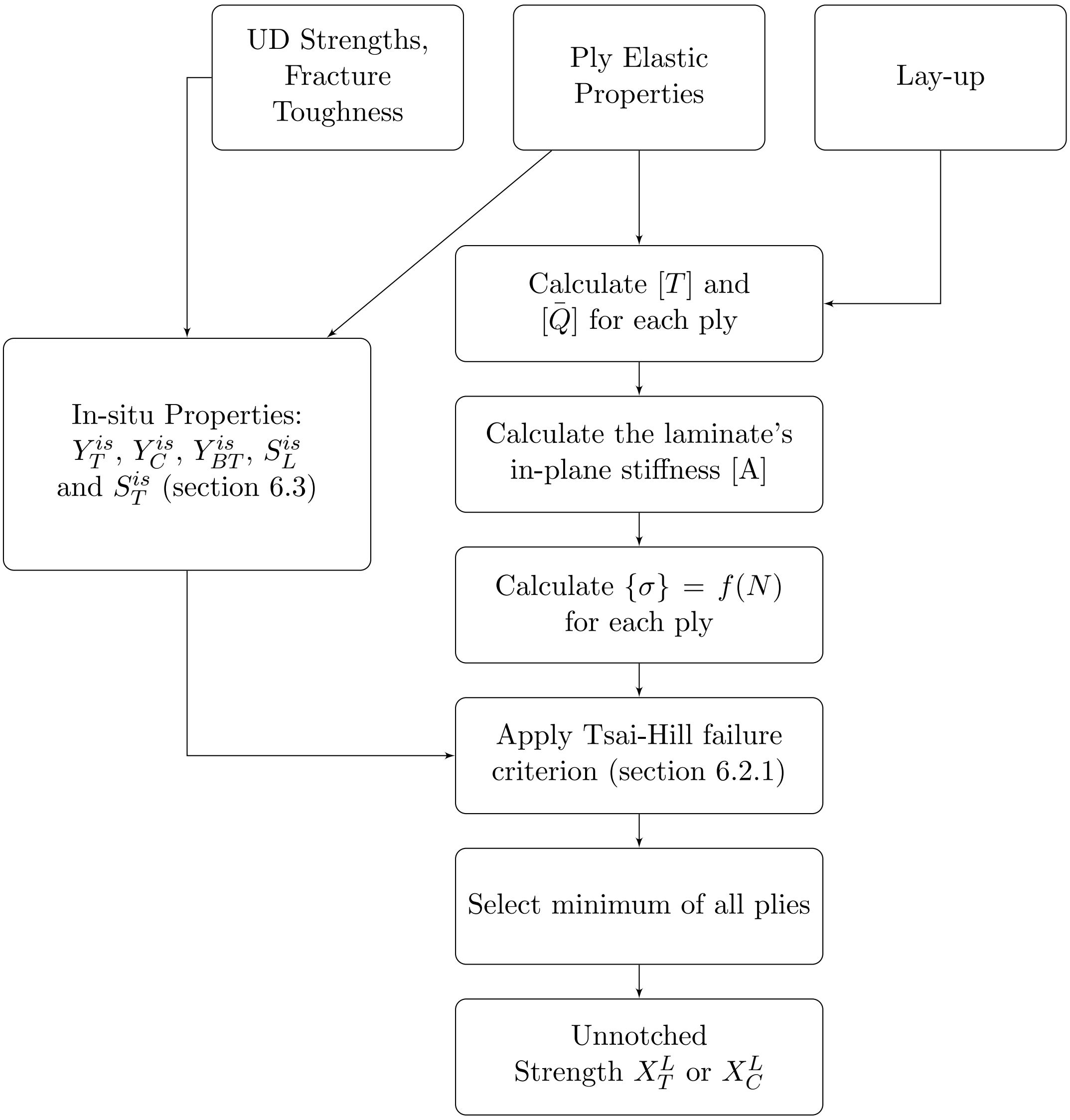

Figure 7.2: Schematic representation of the TsHi model: CLT model using the Tsai-Hill failure criterion and not considering damage progression.

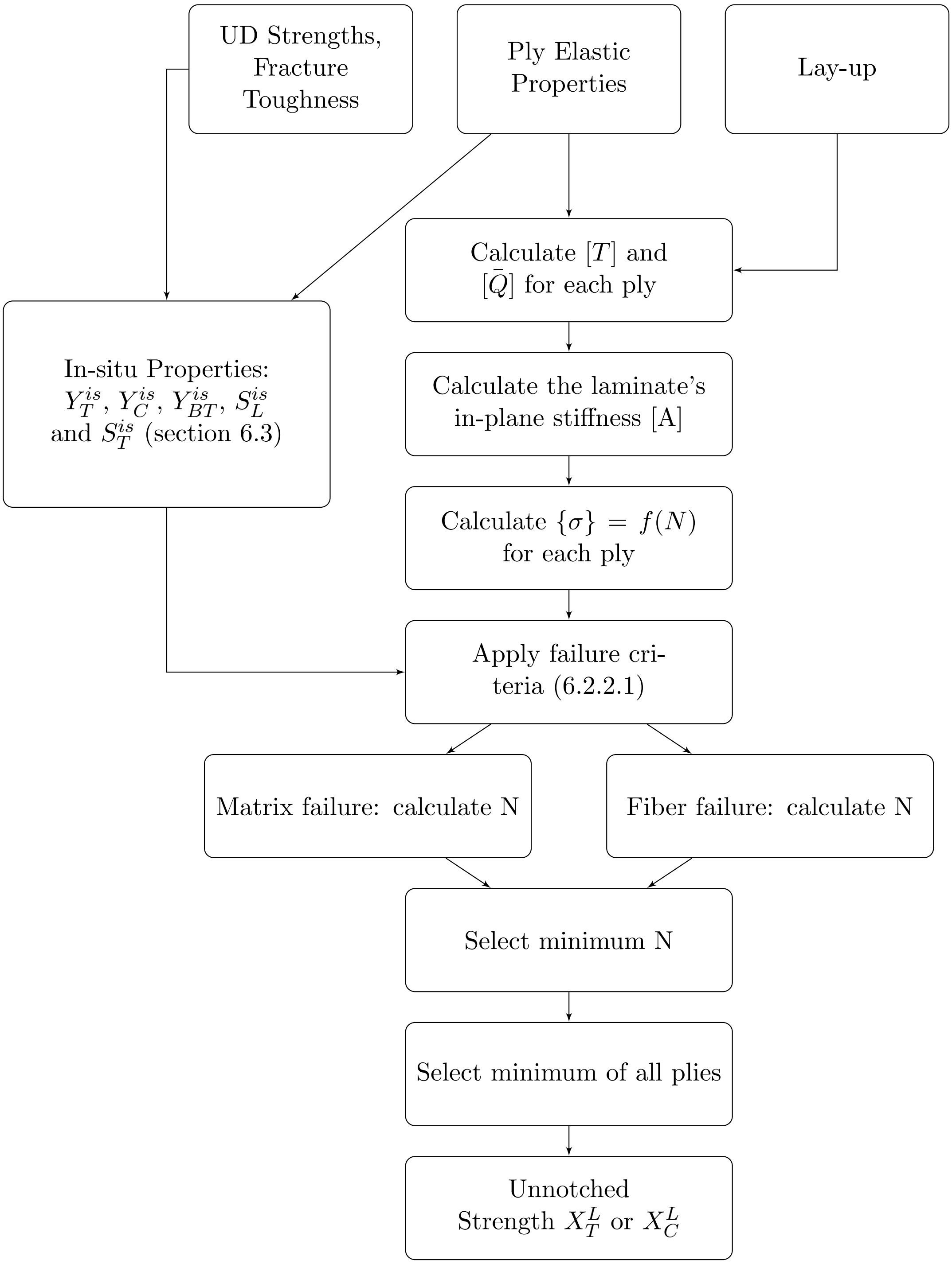

Figure 7.3: Schematic representation of the INV model: CLT model using the three-dimensional invariant-based failure criteria for fiber-reinforced composites and without considering damage progression.

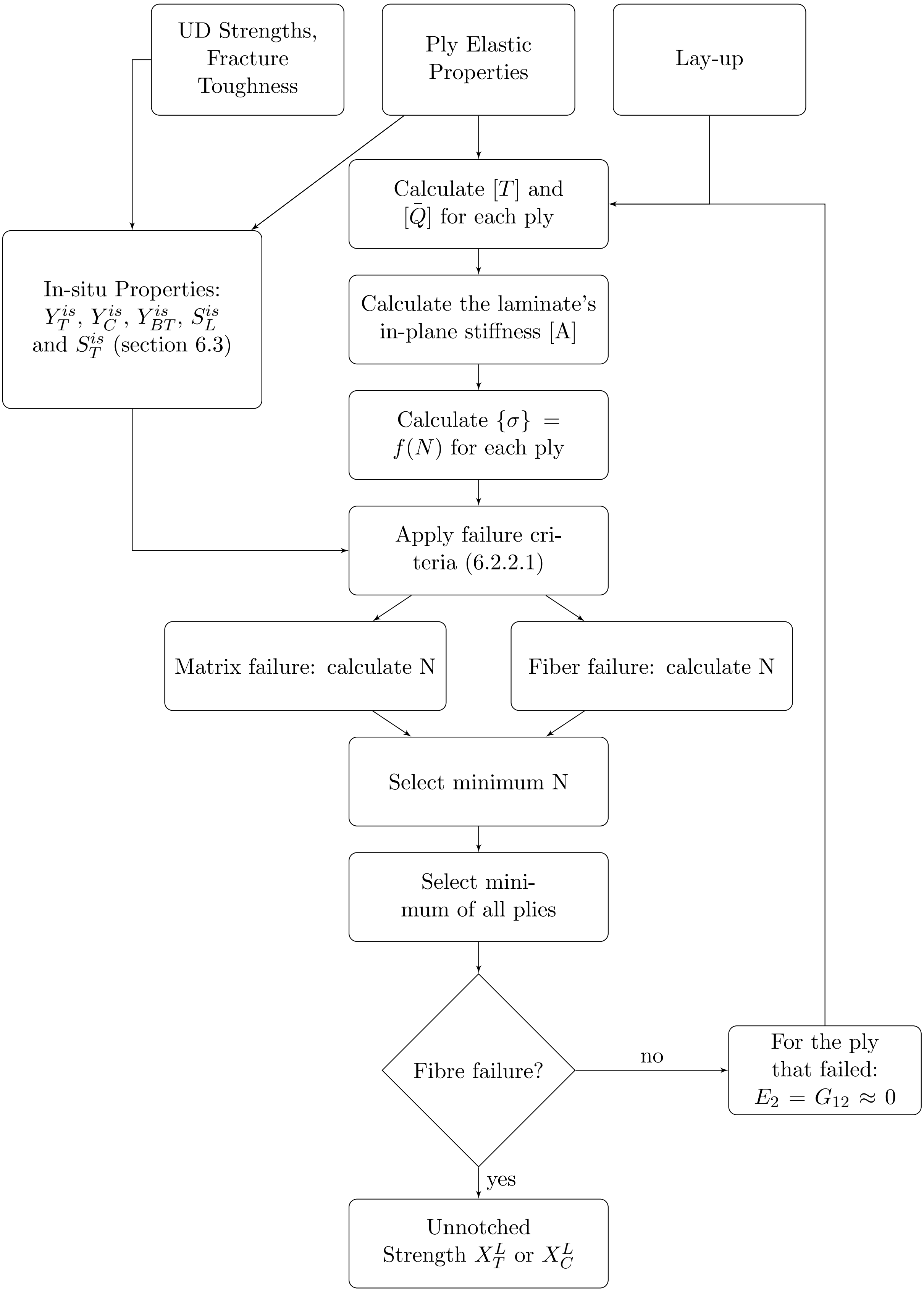

Figure 7.4: Schematic representation of the INV-D model: CLT model using the three-dimensional invariant-based failure criteria for fiber-reinforced composites and considering damage progression.

7.2 Notched tensile and compressive strength

As explained in section 5.1, the notched strength of a composite laminate can be predicted using Finite Fracture Mechanics if the geometry, laminate fracture toughness (or R-curve for large damage capability) and laminate unnotched strength are known, given the composites exhibits brittle or pull-out failure. Taking into account that:

- the unnotched tensile or compressive strength can be calculated analytically as explained in section 7.1 and

- for quasi-isotropic laminates, the mode I fracture toughness of a laminate can be predicted analytically from the one of the 0^o ply as explained in section 6.4 [16]

the notched strength of a given laminate and geometry can be predicted having only the laminate lay-up, the ply elastic properties, the ply strengths and fracture toughness and the fracture toughness of the 0^o ply as input variables (see table 7.1)

A schematic representation of the whole model, i.e., unnotched strength predicted using the CLT model and notched strength predicted using the Finite Fracture Mechanics model, is shown in figure 7.5

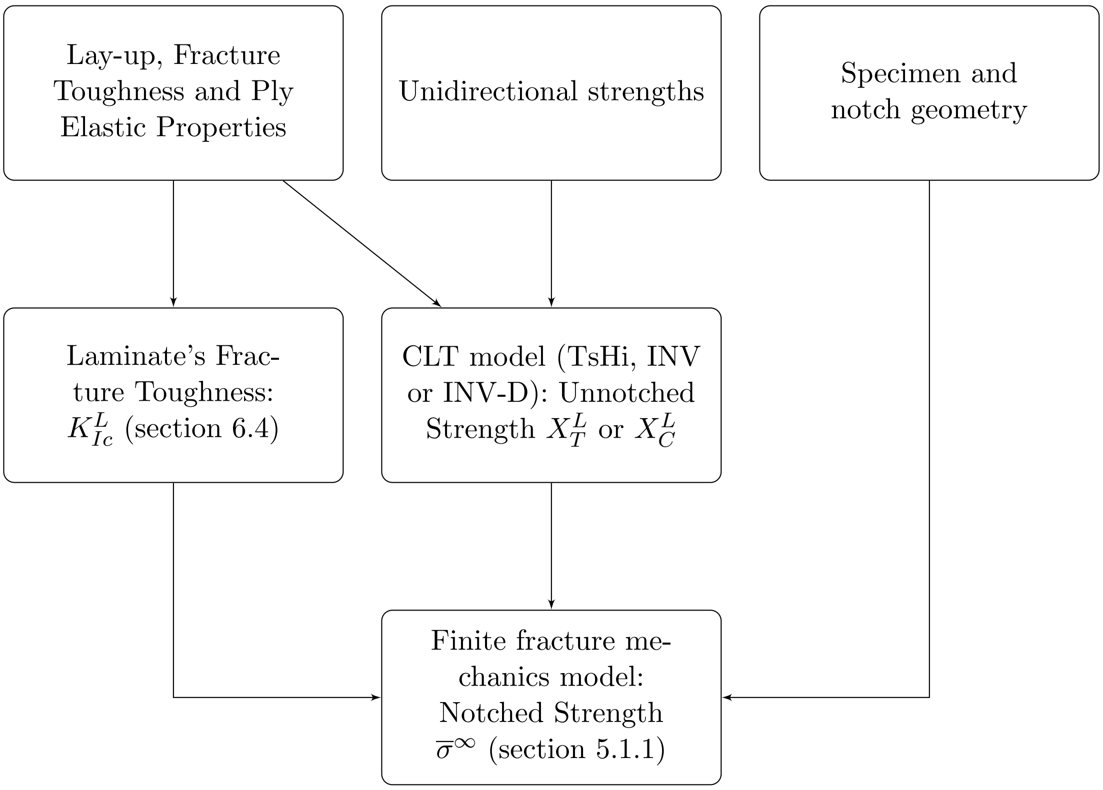

Figure 7.5: Schematic representation of model to predict the notched strength of laminated composites

7.3 Concluding remarks

The model presented in this chapter should be able to predict the notched strength of composite laminates for which the effect of delamination can be neglected (such as thin-ply laminates) having only the ply elastic, strength and fracture properties as input variables. The model is only partially implemented and, up to date, its accuracy could not be accessed. Since it only requires the ply properties as input variables, proven it can predict notched strength of thin-ply laminates, such a model would avoid the need of extensive and, therefore, costly and time-consuming experimental programs to determine properties for different lay-ups of the same material system and could possible be used as a preliminary design and optimization tool.

Chapter 8

Conclusion and Future Work

8.1 Conclusion

The objective of this work was to study how thin-ply laminates can be used to their full potential. Two lines of research were followed: the first was ply hybridization, which is the combination of both thin and thick plies of the same material in the same lay-up. To understand the consequences of ply hybridization, an experimental study was conducted where unnotched tension, open-hole tension, open-hole fatigue and double edge crack tests were performed to thin, thick and hybrid quasi-isotropic laminates of the same material system. Priority was given to studying the tensile response of hybrid laminates in comparison to thin and thick laminates, since one of the major disadvantages of the thin-ply technology is the worse response of notched thin-ply structures loaded in tension.

Comparing thin and thick lay-ups of the same material system the same tendency described in other experimental works was reported:

- thin-ply lay-ups exhibited higher unnotched tensile strength than thick laminates due to the delayed onset of damage;
- thin-ply laminates exhibit lower notched strength because they inhibit local stress distribution at the vicinity of the notch leading to premature brittle failure of the specimens;
- thin-ply lay-ups exhibited enhanced fatigue resistance because they exhibit less subcritical damage prior to failure and therefore, damage propagation is slower and less pronounced.

Two types of ply hybridization were studied:

- **combining thin plies with thicker 0^{o} plies**. The experimental study conducted showed that, this type of ply-hybridization, results in enhanced notched tensile resistance. The hybrid lay-up exhibited:
  - equivalent unnotched tension strength to the thin lay-up. The ply's tensile strength in the direction of the fibres, X^T, is not a function of the ply thickness and, since, ply blocking is limited to 0^{o} plies only, the *in-situ* strengths of the plies are not significantly affected when compared

to the thin lay-up which explains the similar unnotched tension strength between the two lay-ups.

  - higher notched strength when compared with the thick lay-up. The experimental study suggests that, by ply-blocking the 0^o plies, fibre splitting is triggered while damage in the 45^o and 90^o plies is suppressed. This type of damage allows the redistribution of stresses near the hole, which reduces the stress concentration and, at the same time, as the damage is aligned with the loading direction, limits the damage to vicinity of the notch, which explains the enhanced notched strength in open-hole tension tests.
  - intermediate fatigue resistance. There is more extensive subcritical damage than in the thin laminated but, since the damage is aligned with the loading direction, its propagation will be slower and less pronounced than in thick laminates.

- **combining thick and thin plies of all fibre orientations (0^o, -45^o, 45^o and 90^o) in the same lay-up**: this type of hybrid lay-up is more notch tolerant than thin but less tolerant than thick lay-ups. This intermediate behaviour can be explained by the type of ply hybridization: while the "thin" part of the laminate should be able to delay subcritical damage before failure, the "thick" part of the laminate is responsible for redistributing the stresses at the vicinity of the notch, reducing the stress concentrations. This is valid for both static and fatigue loadings.

The fact that combining thin plies with thicker 0^o plies increases the notched strength compared to thick laminates while maintaining the unnotched strength of thin laminates might be the solution to overcoming one of the main obstacle to market penetration thin-ply composites: their reduced tensile strength in the presence of stress concentrations.

The process of selecting the material, geometry and lay-up of composite structures with stress concentrations requires the fast and accurate prediction of their notched strength which can be obtained using closed-form analytical models. In this work, the experimental open-hole tension test results were compared with predictions obtained using the Inherent flaw , the Point stress, the Average stress and the Finite Fracture Mechanics models with and without taking the material's R-curve into account. The IFM, PS and AS models require model calibration from a baseline specimen, which is a clear limitation as re-calibration is required for different geometries. The predictions obtained using the FFM model are in good agreement with the experimental results and are able to capture subtle differences is laminate configuration for the same material system. The material's R-curve is useful to predict large damage capability of composite laminates without loss of accuracy in predictions for smaller specimens and should, therefore, be a included in the experimental characterization programs. However, as the R-curve varies with the laminate's lay-up and because obtaining the size effect law needed to calculate the R-curve requires a very extensive and costly set of experimental tests, preliminary lay-up selection should not rely on the its determination, unless the prediction of the notched strength of large specimens is a relevant requirement. Having selected the lay-up, preliminary optimization and design should be made taking the material's R-curve into account, because this method results in accurate predictions within a few seconds, avoiding the time consuming and the computational effort of Finite Element analysis.

The second research line was based on the development of an algorithm that could serve as the base of an optimization algorithm capable of selecting an optimal lay-up of thin-ply laminates having open-hole tension and plain strength as design drivers. The model presented should be able to predict:

- unnotched strength of laminated composites using a combination of the classical lamination theory, an anallytical model to calculate the ply's *in-situ* properties and a failure criteria. Three models were proposed:
  - **TsHi** - Combination of the CLT with the Tsai-Hill failure criterion. In this model, no damage is considered, and, therefore, failure is predicted when the first ply fails.
  - **INV** - Combination of the CLT with a three-dimensional invariant-based failure criteria for fibre-reinforced composites. In this model, no damage is considered, and, therefore, failure is also predicted when the first ply fails.
  - **INV-D** - Combination of the CLT with a three-dimensional invariant-based failure criteria for fibre-reinforced composites. In this model, damage is considered and failure is predicted when a ply fails due to fibre failure (fibre kinking or maximum strain).
- notched strength of laminated composites using the finite fracture mechanics model. The fracture toughness of the laminate is be predicted analytically from the fracture toughness of the 0^o plies and the unnotched strength is predicted using the TsHi, INV or INV-D models.

The model was only partially implemented and, up to date, its accuracy could not be accessed. Since it only requires the ply properties as input variables, proven it can predict notched strength of thin-ply laminates, such a model would avoid the need of extensive and, therefore, costly and time-consuming experimental programs to determine properties for different lay-ups of the same material system and could possible be used as a preliminary design and optimization tool.

8.2 Future Work

Some aspects of the experimental work carried out should be addressed with more detail. Firstly, since only one specimen per laminate configuration was tested due to schedule problems, more open-hole fatigue tests should be performed to confirm the results obtained. These specimens should be subjected to fatigue loading until the defined failure criteria is reached (reduction of 10% in the specimen's stiffness), so that a more valid comparison between lay-ups can be made. Moreover, the remaining open-hole fatigue specimens should be instrumented with strain gages rather than using the information provided by the testing machine's LVDT, so that, the test results are more accurate.

Secondly, the R-curve of the STF-THICK laminate appears to be overpredicted, which results in overprediction of open-hole tensile strengths using the finite fracture mechanics model. Even though, no anomalies were reported during double edge crack tests, and therefore, up to date, there is no reason to consider the R-curve invalid, it is important to understand if the results are in fact valid or not.

Thirdly, since only 2 specimens per laminate configuration were considered valid, more unnotched tensile tests of STF T700SC/M21 lay-ups should be performed to confirm the values obtained.

In the experimental work carried out, priority was given to studying the tensile response of hybrid laminates in comparison to thin and thick laminates. However, an experimental study to evaluate the consequences of ply hybridization when the laminates are loaded in compression should also be conducted. This experimental work should include unnotched compression, open-hole compression, open-hole fatigue tests and the determination of the laminate's R-curve.

The algorithm to calculate the notched strength having only the ply elastic, strength and fracture properties as input variables should be fully implemented and the predictions should be compared with available experimental results so that its accuracy can be accessed. Proven it can predict the notched strength accurately, it should be allied with an optimization algorithm so it becomes able to select an optimal lay-up of thin-ply laminates for a specific application having open-hole tension and plain strength as design drivers.

Finally, advanced damage models whose formulation accounts for the particular response of thin-ply laminates should be developed and implemented in non-linear Finite Element codes.

Bibliography

[1] ASTM D 3039 / D 3039M-14. Standard Test Method for Tensile Properties of Polymer Matrix Composite Materials. ASTM International, West Conshohocken, PA, 2014, www.astm.org.

[2] ASTM D 3518 / D 3518M-13. Standard Test Method for In-Plane Shear Response of Polymer Matrix Composite Materials by Tensile Test of a $\pm$ 45 Laminate. ASTM International, West Conshohocken, PA, 2013, www.astm.org.

[3] ASTM D 5766/ D 5766M-02a. Open hole tensile strength of polymer composite laminates. ASTM International, West Conshohocken, PA, 2014, www.astm.org.

[4] R. Amacher, J. Cugnoni, J. Botsis, L. Sorensen, W. Smith, and C. Dransfeld. Thin ply composites: Experimental characterization and modeling of size-effects. Composites Science and Technology, 101:121–132, September 2014.

[5] a. Arteiro, G. Catalanotti, a.R. Melro, P. Linde, and P.P. Camanho. Micromechanical analysis of the in situ effect in polymer composite laminates. Composite Structures, 116:827–840, September 2014.

[6] a. Arteiro, G. Catalanotti, J. Xavier, and P.P. Camanho. Notched response of non-crimp fabric thin-ply laminates. Composites Science and Technology, 79:97–114, April 2013.

[7] a. Arteiro, G. Catalanotti, J. Xavier, and P.P. Camanho. Notched response of non-crimp fabric thin-ply laminates: Analysis methods. Composites Science and Technology, 88:165–171, November 2013.

[8] a. Arteiro, G. Catalanotti, J. Xavier, and P.P. Camanho. Large damage capability of non-crimp fabric thin-ply laminates. Composites Part A: Applied Science and Manufacturing, 63:110–122, August 2014.

[9] G Bao, S Ho, Z Suo, and B Fan. The role of material orthotropy in fracture specimens for composites. International Journal of Solids and Structures, 29(9):1105–1116, 1992.

[10] G Bao, S Ho, Z Suo, and B Fan. The role of material orthotropy in fracture specimens for composites. International Journal of Solids and Structures, 29(9):1105–1116, 1992.

[11] G Bao, S Ho, Zhigang Suo, and B Fan. The role of material orthotropy in fracture specimens for composites. International Journal of Solids and Structures, 29(9):1105–1116, 1992.

[12] Zdenek P Bazant and Jaime Planas. Fracture and size effect in concrete and other quasibrittle materials, volume 16. CRC press, 1997.

[13] Pedro P. Camanho, Carlos G. Dávila, Silvestre T. Pinho, Lorenzo Iannucci, and Paul Robinson. Prediction of in situ strengths and matrix cracking in composites under transverse tension and in-plane shear. Composites Part A: Applied Science and Manufacturing, 37(2):165–176, February 2006.

[14] Pedro Ponces Camanho, Pere Maimí, and CG Dávila. Prediction of size effects in notched laminates using continuum damage mechanics. Composites Science and Technology, 67(13):2715–2727, 2007.

[15] P.P. Camanho, a. Arteiro, a.R. Melro, G. Catalanotti, and M. Vogler. Three-dimensional invariant-based failure criteria for fibre-reinforced composites. International Journal of Solids and Structures, 55:92–107, March 2015.

[16] P.P. Camanho and G. Catalanotti. On the relation between the mode I fracture toughness of a composite laminate and that of a 0 ply: Analytical model and experimental validation. Engineering Fracture Mechanics, 78(13):2535–2546, August 2011.

[17] P.P. Camanho, G.H. Erçin, G. Catalanotti, S. Mahdi, and P. Linde. A finite fracture mechanics model for the prediction of the open-hole strength of composite laminates. Composites Part A: Applied Science and Manufacturing, 43(8):1219–1225, August 2012.

[18] G. Catalanotti, a. Arteiro, M. Hayati, and P.P. Camanho. Determination of the mode I crack resistance curve of polymer composites using the size-effect law. Engineering Fracture Mechanics, 118:49–65, March 2014.

[19] G. Catalanotti, P.P. Camanho, and A.T. Marques. Three-dimensional failure criteria for fiber-reinforced laminates. Composite Structures, 95:63–79, January 2013.

[20] R.M. Christensen. Stress based yield/failure criteria for fiber composites. International Journal of Solids and Structures, 34(5):529–543, February 1997.

[21] Carlos G Dávila and Pedro P Camanho. Failure criteria for frp laminates in plane stress. NASA TM, 212663(613), 2003.

[22] Carlos G Davila, Pedro P Camanho, and Cheryl A Rose. Failure criteria for frp laminates. Journal of Composite materials, 39(4):323–345, 2005.

[23] George J Dvorak and Norman Laws. Analysis of progressive matrix cracking in composite laminates ii. first ply failure. Journal of Composite Materials, 21(4):309–329, 1987.

[24] Hong T Hahn and Stephen W Tsai. Nonlinear elastic behavior of unidirectional composite laminae. Journal of Composite Materials, 7(1):102–118, 1973.

[25] L Hart-Smith. Predictions of the original and truncated maximum-strain failure models for certain fibrous composite laminates. Composites Science and Technology, 58(7):1151–1178, July 1998.

[26] C T Herakovich. Mechanics of Fibrous Composites. Wiley, 1997.

[27] Whitney JM and RJ Nuismer. Stress fracture criteria for laminated composites containing stress concentrations. J Compos Mater, (8):253–65, 1974.

[28] Akira Kuraishi, Stephen W Tsai, and Kevin K.S Liu. A progressive quadratic failure criterion, part B. Composites Science and Technology, 62(12-13):1683–1695, September 2002.

[29] K Liu. A progressive quadratic failure criterion for a laminate. Composites Science and Technology, 58(7):1023–1032, July 1998.

[30] Fabrice Pierron, Ben Green, and Michael R Wisnom. Full-field assessment of the damage process of laminated composite open-hole tensile specimens. part i: Methodology. Composites Part A: Applied Science and Manufacturing, 38(11):2307–2320, 2007.

[31] S.T. Pinho, L. Iannucci, and P. Robinson. Physically-based failure models and criteria for laminated fibre-reinforced composites with emphasis on fibre kinking: Part I: Development. Composites Part A: Applied Science and Manufacturing, 37(1):63–73, January 2006.

[32] M. Vogler P.P. Camanho, A. Arteiro, G. Catalanotti,A.R. Melro. Three-dimensional invariant-based failure criteria for transversely isotropic fibre-reinforced composites. 2014.

[33] A Puck. Failure analysis of FRP laminates by means of physically based phenomenological models. Composites Science and Technology, 58(7):1045–1067, July 1998.

[34] J N Reddy. Mechanics of Laminated Composite Plates and Shells: Theory and Analysis, Second Edition. Taylor & Francis, 2004.

[35] S Sihn, R Kim, K Kawabe, and S Tsai. Experimental studies of thin-ply laminated composites. Composites Science and Technology, 67(6):996–1008, May 2007.

[36] C.T Sun, J Tao, and A.S Kaddour. The prediction of failure envelopes and stress/strain behavior of composite laminates: comparison with experimental results. Composites Science and Technology, 62(12-13):1673–1682, September 2002.

[37] Hiroshi Tada, Paul C Paris, and George R Irwin. The stress analysis of cracks handbook. the american society of mechanical engineers. New York, 2000.

[38] Rajesh S Vaidya and CT Sun. Fracture criterion for notched thin composite laminates. AIAA journal, 35(2):311–316, 1997.

[39] M. Vogler, R. Rolfes, and P.P. Camanho. Modeling the inelastic deformation and fracture of polymer composites – Part I: Plasticity model. Mechanics of Materials, 59:50–64, April 2013.

[40] Eisenmann J. R. Waddoups, M. E. and B. E. Kaminski. Macroscopic fracture mechanics of advanced composite materials. J Compos Mater, (5):446–54, 1971.

[41] D.L. Chen B. Weiss and R. Stickler. A new geometric factor formula for a center cracked plate tensile specimen of finite width. Int J Fract, 55:R3–R8, 1992.